FINAL REPORT

Actively Shaken *In-Situ* Passive Sampler Platform for Methylmercury and Organics

SERDP Project ER-2540

FEBRUARY 2016

Upal Ghosh
Mehregan Jalalizadeh
James Sanders
University of Maryland Baltimore County

Cynthia C. Gilmour
Smithsonian Environmental Research Center

SERDP
DOD ▪ EPA ▪ DOE

Page Intentionally Left Blank

	REPORT DOCUMENTATION PAGE		Form Approved OMB No. 0704-0188

The public reporting burden for this collection of information is estimated to average 1 hour per response, including the time for reviewing instructions, searching existing data sources, gathering and maintaining the data needed, and completing and reviewing the collection of information. Send comments regarding this burden estimate or any other aspect of this collection of information, including suggestions for reducing the burden, to Department of Defense, Washington Headquarters Services, Directorate for Information Operations and Reports (0704-0188), 1215 Jefferson Davis Highway, Suite 1204, Arlington, VA 22202-4302. Respondents should be aware that notwithstanding any other provision of law, no person shall be subject to any penalty for failing to comply with a collection of information if it does not display a currently valid OMB control number.
PLEASE DO NOT RETURN YOUR FORM TO THE ABOVE ADDRESS.

1. REPORT DATE (DD-MM-YYYY)	2. REPORT TYPE		3. DATES COVERED (From - To)
12/30/2016	Final Report		9/29/2014 to 2/29/2016

4. TITLE AND SUBTITLE	5a. CONTRACT NUMBER
Actively Shaken In-Situ Passive Sampler Platform for Methylmercury and Organics	W912HQ-14-P-0111
	5b. GRANT NUMBER
	5c. PROGRAM ELEMENT NUMBER

6. AUTHOR(S)	5d. PROJECT NUMBER
Upal Ghosh, Mehregan Jalalizadeh, James Sanders, Cynthia C. Gilmour	ER2540
	5e. TASK NUMBER
	5f. WORK UNIT NUMBER

7. PERFORMING ORGANIZATION NAME(S) AND ADDRESS(ES)	8. PERFORMING ORGANIZATION REPORT NUMBER
University of Maryland Baltimore County, Baltimore, MD Smithsonian Environmental Research Center, Edgewater, MD	

9. SPONSORING/MONITORING AGENCY NAME(S) AND ADDRESS(ES)	10. SPONSOR/MONITOR'S ACRONYM(S)
Strategic Environmental Research and Development Program	SERDP
	11. SPONSOR/MONITOR'S REPORT NUMBER(S)

12. DISTRIBUTION/AVAILABILITY STATEMENT
Public

13. SUPPLEMENTARY NOTES

14. ABSTRACT
This 1-year SEED project advanced the field of passive sampling on two major fronts: 1) Developed an engineering approach to extend in-situ passive sampling to high molecular weight compounds in sediment porewater, and 2) Explored an equilibrium passive sampling approach for MeHg in sediment porewater. Both proof-of-concept developments are novel and were successful in paving the way for further research to operationalize the extension of passive sampling to these heretofore difficult to measure analytes in sediment porewater.

15. SUBJECT TERMS
passive sampling, sediment, porewater, vibration, PCB, PAH, methylmercury

16. SECURITY CLASSIFICATION OF:			17. LIMITATION OF ABSTRACT	18. NUMBER OF PAGES	19a. NAME OF RESPONSIBLE PERSON
a. REPORT	b. ABSTRACT	c. THIS PAGE			Upal Ghosh
U	U	U	UU	123	**19b. TELEPHONE NUMBER (include area code)** 4104558665

Page Intentionally Left Blank

Page Intentionally Left Blank

TABLE OF CONTENTS

1.0 ABSTRACT

This 1-year SEED project advanced the field of passive sampling on two major fronts: 1) Developed an engineering approach to extend *in-situ* passive sampling to high molecular weight compounds in sediment porewater, and 2) Explored an equilibrium passive sampling approach for MeHg in sediment porewater. Both proof-of-concept developments are novel and were successful in paving the way for further research to operationalize the extension of passive sampling to these heretofore difficult to measure analytes in sediment porewater.

Passive sampling for the measurement of freely dissolved concentrations of organic pollutants in sediment pore water has emerged as a very promising approach, but *in situ* measurements are complicated by slow mass transfer of strongly hydrophobic compounds. The primary resistance to mass transfer arises in the sediment side where a static boundary layer develops in the vicinity of the polymeric passive sampling material. The slow mass transfer results in under-equilibrated passive sampler measurements that need to be corrected for equilibrium, typically by extrapolation of the loss kinetics of performance reference compounds. Such corrections are prone to large errors, especially when deviation from equilibrium is large. In this research we address the challenge of slow mass transfer by disrupting the external aqueous boundary layer around an *in-situ* passive sampler using periodic mechanical vibration. We report an engineering innovation of adapting low-cost motors used for producing haptic feedback in cell phones for the use in disrupting aqueous boundary layer in a passive sampler deployed in sediments. We demonstrate through laboratory experiments and numerical modeling that short periodic shaking of a passive sampler deployed in static sediment greatly enhances the rate of mass transfer and reduces the difference in the extent of equilibrium achieved compared to a well stirred laboratory equilibrium. The improvement over static sediment deployment is especially evident for the high molecular weight compounds such as benzo(a)pyrene. We also demonstrate this method for strongly hydrophobic chlorinated organics using PCB congeners in the log K_{ow} range of 6-8. Deployment of the vibrated passive sampler in laboratory mesocosms of field-collected sediments shows that the porewater concentrations of up to octachlorobiphenyls can be measured accurately even with a 7-day deployment of the sampler *in situ*. In contrast, a static deployment of passive samplers for 28 days results in a measurement that is 4-fold higher than the true equilibrium value. Further work is needed to operationalize the vibrating passive sampler concept and include:

1) Further optimization of vibration frequency through laboratory experiments.

2) Testing on strongly hydrophobic compounds such as dioxins and furans in sediments.

3) Confirmation through laboratory experiments that the concept of using freely dissolved concentrations in sediment porewater to predict biouptake can be extended to high molecular weight PCBs and dioxins and furans.

4) Field testing of the sampler platform along with traditional deployment of passive samplers.

This research also laid the groundwork for the development of a passive equilibrium sampler for MeHg in sediment. Several polymer composites were developed and tested based on the concept of equilibrium partitioning of MeHg between bioavailable species in porewater and a well characterized sorbent held within a polymer film. Among the materials tested, several combinations showed the greatest promise based on sorption capacity and linearity of sorption behavior: activated carbon embedded in agarose or polyvinylidinefluoride polymer, cystine in polyethylene terephthalate, and thiols embedded in agarose or polyvinylidinefluoride. While, the presence of dissolved organic matter reduced uptake in the polymers, this is expected based on speciation of MeHg. Going forward we should be able to design the polymers to respond to the bioavailable fraction of MeHg. We believe that initial results presented in this report show great promise for pursuing the concept of equilibrium passive sampling for Hg and MeHg.

Further work is needed to advance the technology development for passive sampling of Hg and MeHg and are listed below:

1) Complete testing of a suite of selected polymers in a range of MeHg complexes prior to testing against benthic organicsms.

2) Empirically determine which passive sampler sorbents and pore size predict MeHg uptake by benthic organisms.

3) Develop enriched stable isotope spikes as performance reference compounds in these samplers

1.1 List of acronyms

C_{free}: freely dissolved concentration

PRCs: performance reference compounds

PCBs: polychlorinated biphenyls

PAHs: polyaromatic hydrocarbons

PE: polyethylene

DGT: diffusive gradient in a thin film

FCVs: final chronic values

K_{PEw}: polyethylene-water partitioning coefficient

L_p: half thickness of polyethylene strip

L_w: thickness of sediment/porewater

S: sediment concentration

T: time

K_d : sediment−water partition coefficient

k: first -order desorption rate constant

C_w: chemical concentration in water

C_{PE}: chemical concentration in PE

D_{PE}: chemical diffusivity in PE

ρ: sediment bulk density

ε: porosity

D_w: diffusivity in water

S_0: initial chemical concentration in sediment

C_w0: initial chemical concentration in water

$K_{sed\text{-} PE}$: sediment-polyethylene partitioning coefficient

k_0: overall mass transfer rate constant

δ: diffusion distance

PCDD/Fs: polychorinate dibenzo-p-dioxins/dibenzofurans

k_f: fast desorption rate constant

k_s: slow desorption rate constant

$C_{PE,eq}$: chemical equilibrium concentration in polyethylene

1.2 List of Figures

1.3 List of Tables

2.0 OBJECTIVES

Accurate bioavailability measurements are needed for improved site risk assessments, proper selection of remedy, and post-remediation monitoring. While freely dissolved porewater concentrations of organic contaminants and aqueous concentrations of bioavailable forms of trace metals in sediments have been demonstrated to be the ideal metrics for assessing bioavailability, accurate measurements of the low environmentally relevant concentrations has been a challenge. For hydrophobic organics, the primary resistance to mass transfer is in the sediment side where a static boundary layer develops in the vicinity of the polymeric passive sampling material. The slow mass transfer results in under-equilibrated passive sampler measurements that need to be corrected for equilibrium, typically by extrapolation of the loss kinetics of performance reference compounds. Such corrections are prone to large errors, especially when deviation from equilibrium is large. In addition, there has been little development of equilibrium passive sampling for metals. Key objectives of this research therefore are to:

1) Explore a novel approach of <u>enhancing mass transfer by introducing mechanical vibration</u> to disrupt the aqueous boundary layer around passive samplers deployed *in situ*,

2) Test this approach for <u>strongly hydrophobic compounds</u>, and

3) Evaluate a range of polymer types for use as <u>passive equilibrium samplers for methylmercury</u>.

The ultimate goal is to develop an *in situ*, actively shaken deployment platform that can accommodate multiple types of passive samplers (for strongly hydrophobic organics and metals). This research directly addresses the SEED SON through new innovation in passive sampling measurements for pollutant bioavailability in sediments. Specifically, the research addresses two key needs described in the SEED SON:

i) <u>Development of a multi-purpose passive sampling device capable of collecting data on several contaminants of interest</u>. We developed an actively shaken platform for the deployment of equilibrium passive samplers in the field. The active shaking innovation will allow achievement of a state of pollutant uptake in the passive samplers that is closer to thermodynamic equilibrium and will reduce the high uncertainties associated with corrections using performance reference compounds when the sampler is far from equilibrium.

ii) <u>Development of passive sampling strategies for very hydrophobic chemicals such as dioxins/furans and metals such as Hg</u>. Our strategy for dioxins/furans is to deal with the issue of slow mass transfer expected of these compounds by actively enhancing *in situ* mass transfer rates using mechanical disruption of the aqueous boundary layer around the passive sampler. This has never been tried before and is a promising innovation in the field of passive sampling that addresses the high uncertainty associated with performance reference compounds when the extent of equilibrium achieved is low. For mercury, we focused on the species most relevant

from a risk standpoint, methylmercury (MeHg), and to identify a polymer partitioning approach by developing and testing a range of polymeric material types. We also anticipate that future work can expand this approach to include other metals of interest such as As, Zn, Pb, Cd, and inorganic Hg through the right choice of ligands embedded in the polymer.

3.0 BACKGROUND

3.1 Relevance of porewater measurements for predicting bioaccumulation of dioxins/furans and MeHg.

Several studies have shown that freely dissolved concentrations (C_{free}) of organics in sediment porewater can be related to toxicity and bioaccumulation (Mayer et al. 2014; Peijnenburg et al. 2014). Our recent work with soil contaminated with dioxins and furans demonstrated that uptake by earthworms is correlated to freely dissolved concentrations measured using passive equilibrium sampling (Figure 3.1a; Fagervold et al. 2010 Supporting Information). Similarly, we showed that uptake of MeHg by sediment-dwelling worms is correlated to filterable MeHg concentrations in sediment porewater (Figure 3.1b; Gilmour et al. 2013). In both of these cases, the measurements of porewater concentrations were made in *ex situ* laboratory studies. There is a great need to be able to perform concentration measurements in sediment porewater and surface waters in the field to capture actual exposure concentrations for native biota.

a. dioxins/furans   b. methylmercury
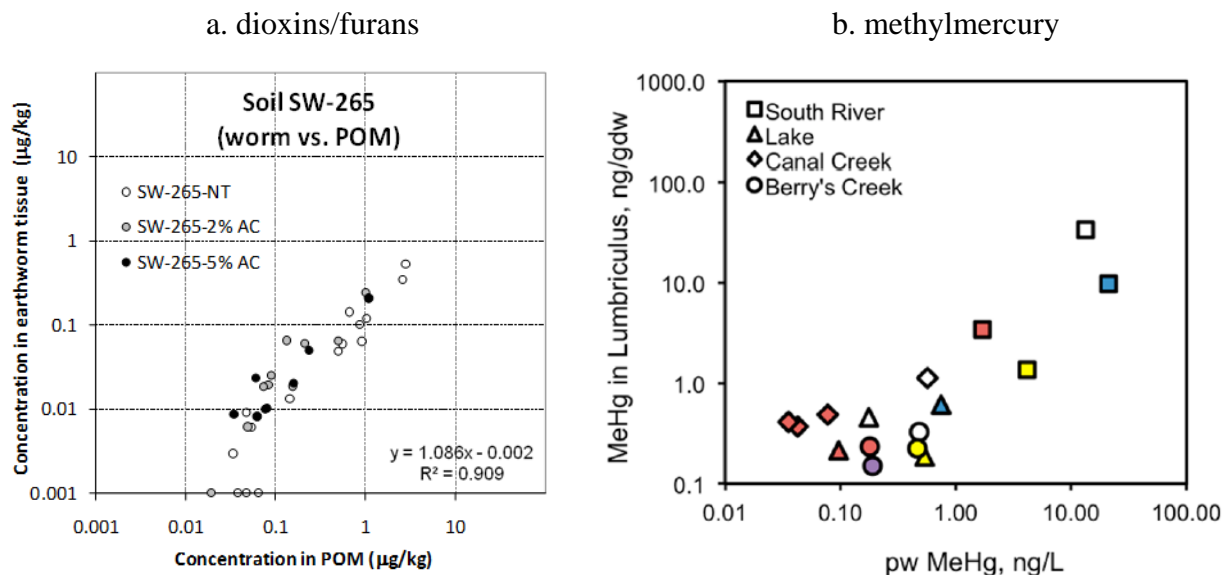
Figure 3.1. Correlation of dioxin/furan uptake in earthworms with uptake in passive samplers (a; Fagervold et al. 2010) and correlation of MeHg uptake in aquatic worms to porewater MeHg measured directly (b; Gilmour et al. 2013).

3.2 Challenges for *in situ* passive sampling.

The *in situ* approach is used when it is critical to capture conditions in the field. In this approach, the polymer is inserted directly into sediments or suspended in the water column above the sediment in the field and left in place for sufficient duration to allow the derivation of C_{free} (Oen et al., 2011; Fernandez et al. 2009a,b; Beckingham and Ghosh 2013; Lampert et al. 2013). However, the ability to attain equilibrium and demonstrate that equilibrium has been achieved is often more difficult for the *in situ* approach as compared to the ex situ approach. To overcome these challenges, Huckins et al. (1993, 2002) suggested the use of performance reference compounds (PRCs) to calculate C_{free} from non-equilibrium PSM measurements (C_P). PRCs are analytically noninterfering chemicals that are embedded in the passive sampler prior to environmental exposure (Huckins et al. 2002). Examples of surrogate chemicals include stable isotope-labeled or deuterated forms of the analytes of interest, substances with a log K_{ow} that is similar to that of the target analytes (Huckins et al. 2002; Fernandez et al. 2009a), or rare PCB congeners (Tomaszewski and Luthy 2008). The depletion rate of a PRC during sampler deployment reflects the uptake rates of a target analyte, assuming isotropic exchange kinetics occur (Figure 3.2). Because of the differences in the compound properties for the PRC and the target analyte, correction is needed to calculate the fractional approach to equilibrium for the target analyte ($C_{(t)}/C_{(ss)}$) from the fractional PRC dissipation ($1\text{-}C_{PRC(t)}/C_{PRC(0)}$) at time *t*. In addition, PRC correction becomes difficult if sorption in the surrounding media is concentration-dependent or compound-dependent. Several approaches to calibration using PRC data have been suggested (Fernandez et al. 2009b; Huckins et al. 2006; Tomaszewski and Luthy 2008; Reible and Lotufo 2012). In all of these approaches, the uncertainties introduced by the PRC correction are larger when the extent of equilibrium is low, which is the case for strongly hydrophobic compounds such as dioxins and furans.
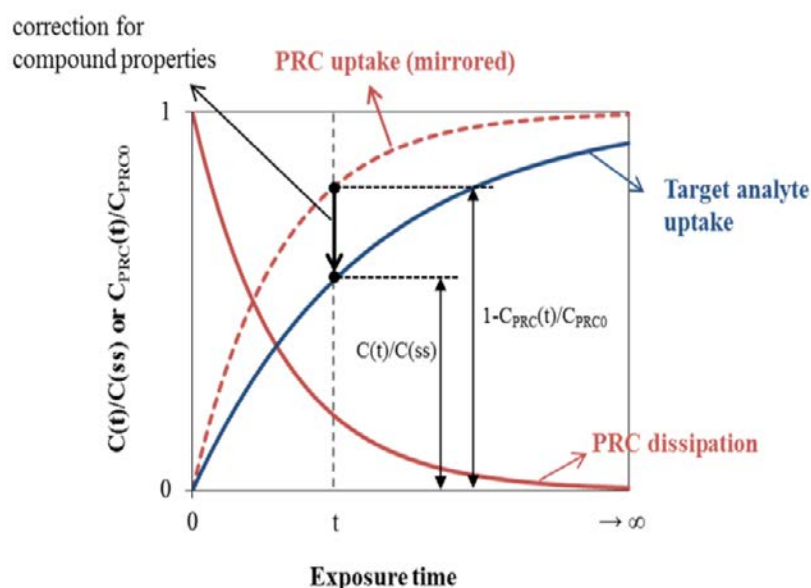
Figure 3.2. PRC dissipation and compound uptake kinetics generally assumed for the performance reference compound (PRC) approach. C(t) and C(ss) refer to target analyte concentrations in the passive sampler at time t and steady state, respectively; CPRC(t) and CPRC(0) refer to PRC concentrations in the passive sampler at time t and 0, respectively. (Ghosh et al. 2014)

3.3 Measurement of porewater dioxins/furans.

The field of passive sampling has been sufficiently advanced for organic compounds in the low- to mid-range of hydrophobicity, including PCBs up to pentachlorobiphenyls and PAHs at least up to chrysene. The USEPA has published a guidance document for the monitoring of organic contaminants at Superfund sediment sites which discusses the use of passive sampling (USEPA 2012). A recently published practical guidance (Ghosh et al. 2014) developed as part of a SETAC Pellston workshop on passive sampling provides the current consensus for the use of passive sampling for PAHs and PCBs. By contrast, <u>very little information exists on the use of passive sampling for dioxins and furans</u>. Our previous work with dioxin-contaminated soils demonstrated that freely dissolved equilibrium concentrations in soil correlated well with uptake in earthworms (Figure 3.1a; Fagervold et al. 2010). In these studies, we used a well-mixed batch system to achieve close to an equilibrium state. We anticipate that the <u>major obstacle</u> to performing *in situ* passive sampling measurements of dioxins and furans in porewater will be <u>the slow external mass transfer</u> for these strongly hydrophobic compounds (log K_{ow} range from 6.4-8.8).

3.4 Measurement of porewater methylmercury.

Accurate information regarding the amounts and distribution of the various species of mercury in sediment and other aquatic environmental matrices is critical to a realistic assessment of risk. Methylmercury, the mercury species of greatest toxicological concern, is formed primarily by anaerobic microorganisms, which take up and methylate inorganic mercury species. In sediment environments, MeHg is taken up by benthic and epibenthic organisms and undergoes substantial biomagnification, ultimately leading to toxic risk for humans (Mason and Lawrence 1999). Porewater concentration measurements are most useful to risk assessors when they can be used to predict MeHg uptake and bioaccumulation potential in these lower trophic level organisms residing at the base of the aquatic food chain, but to date no passive sampling scheme has achieved wide acceptance for this purpose.

Neither the free MeHg cation nor simple MeHg salts (e.g. MeHgCl) are dominant forms of MeHg in sediment porewaters. Rather, MeHg is mainly complexed with colloidal natural organic matter (Bergamaschi et al. 2012); which can enhance partitioning from sediments into the total porewater phase (Hammerschmidt et al. 2004; Hollweg et al. 2009) but can limit uptake by benthic infauna (Luengen et al. 2012; Lawrence and Mason 2001). Methylmercury thiols may be particularly bioavailable (Leaner and Mason 2001), but overall bioavailability of MeHg in sediment porewaters remains poorly understood. The bioavailability of MeHg to organisms is highly dependent on phase and complexation. Like PCBs, the sediment:water partition coefficient for MeHg can be a strong predictor of bioavailability to benthic fauna (Wang et al. 1998; Williams et al. 2010). Further, we found that the concentration of filter-passing MeHg is well correlated with uptake by benthic organisms in laboratory tests (Gilmour et al. 2013).

Currently, the most widely used passive sampler for MeHg is the diffusive gradient in a thin film (DGT) device. Briefly, analytes diffuse through a gel of known thickness and the molecules which traverse the entire gel within the sampling time are tightly bound to a high-affinity stationary phase which is collected and extracted for mercury analysis (Diviš et al. 2005a). DGT has been developed and refined for roughly twenty years, but doubts remain as to its ability to generate reliable estimates of bioavailability, particularly in sediment. For one, the question of which species are measured (that is, which ones are sufficiently "labile" to penetrate the gel and reach the stationary phase during the deployment time) is not well characterized (Hsu-Kim et al. 2013). In addition, the fact that DGT operates in a kinetic (as opposed to equilibrium) uptake regime presents an important challenge unique to sediment environments. Concerns persist regarding porewater depletion and resupply of MeHg in the vicinity of the DGT device (Clarisse et al. 2011). Passive polymer sampler surfaces may offer an empirical approach to monitoring bioavailability by mimicking the partitioning of MeHg complexes in porewaters to cell surfaces.

3.5 Literature cited

Beckingham B, Ghosh U. Polyoxymethylene passive samplers to monitor changes in bioavailability and diffusive flux of PCBs after activated carbon amendment to sediment in the field. *Chemosphere*. **2013**; *91*:1401-1407.

Clarisse O, Dimock B, Hintelmann H, Best EPH. Predicting net mercury methylation in sediments using diffusive gradient in thin films measurements. *Environ Sci Technol*. **2011**; *45*(4):1506-1512.

Diviš P, Leermakers M, Dočekalová H, Gao Y. Application of diffusive gradient in thin films technique (DGT) to measurement of mercury in aquatic systems. *Talanta*. **2005a**; *65*:1174-1178.

Fagervold SK, Chai Y, Davis JW, Wilken M, Cornelissen G, Ghosh U. Bioaccumulation of polychlorinated dibenzo-*p*-dioxins /dibenzofurans in *E. fetida* from floodplain soils and the effect of activated carbon amendment. *Environ Sci Technol*. **2010**; *44*:5546-5552.

Fernandez LA, MacFarlane JK, Tcaciuc AP, Gschwend PM. Using performance reference compounds in polyethylene passive samplers to deduce sediment porewater concentrations for numerous target chemicals. *Environ Sci Technol*. **2009a**; *43*:8888-8894.

Fernandez LA, MacFarlane JK, Tcaciuc AP, Gschwend PM. Measurement of freely dissolved PAH concentrations in sediment beds using passive sampling with low-density polyethylene

strips. *Environ Sci Technol*. **2009b**; *43*:1430-1436.

Ghosh U, Driscoll SK, Burgess RM, Jonker MTO, Reible D, Gobas F, Choi Y, Apitz SE, Maruya KA, Gala WR, Mortimer M, Beegan C. Passive sampling methods for contaminated sediments: practical guidance for selection, calibration, and implementation. *Integr Environ Assess Manag*. **2014**; DOI: 10.1002/ieam.1507.

Gilmour CC, Riedel GS, Riedel G, Kwon S, Landis R, Brown SS, Menzie CA, Ghosh U. Activated carbon mitigates mercury and methylmercury bioavailability in contaminated sediments. *Environ Sci Technol*. **2013**; *47*:13001-13010.

Hammerschmidt CR, Fitzgerald WF. Geochemical controls on the production and distribution of methylmercury in near-shore marine sediments. *Environ Sci Technol*. **2004**; *38*:1487-1495.

Hollweg TA, Gilmour CC, Mason RP. Methylmercury production in sediments of Chesapeake Bay and the mid-Atlantic continental margin. *Mar Chem*. **2009**; *114*:86-101.

Hsu-Kim H, Kucharzyk KH, Zhang T, Deshusses MA. Mechanisms regulating mercury bioavailability for methylating microorganisms in the aquatic environment: A critical review. *Environ Sci Technol*. **2013**; *47*(6):2441-2456.

Huckins JN, Manuweera GK, Petty JD, Mackay D, Lebo JA. Lipid-containing semipermeable membrane devices for monitoring organic contaminants in water. *Environ Sci Technol*. **1993**; *27*:2489-2496.

Huckins JN, Petty JD, Lebo JA, Almeida FV, Booij K, Alvarez DA, Cranor WL, Clark RC, Mogensen BB. Development of the permeability/performance reference compound approach for *in situ* calibration of semipermeable membrane devices. *Environ Sci Technol*. **2002**; *36*:85-91.

Lampert DJ, Lu X, Reible DD. Long-term PAH monitoring results from the Anacostia River active capping demonstration using polydimethylsiloxane (PDMS) fibers. *Environ Sci Process Impacts*. **2013**; *15*:554-562.

Lawrence AL, Mason RP. Factors controlling the bioaccumulation of mercury and methylmercury by the estuarine amphipod *Leptocheirus plumulosus*. *Environ Pollut* **2001**; *111*:217-231.

Leaner JJ, Mason RP. The effect of thiolate organic compounds on methylmercury accumulation and redistribution in sheepshead minnows, Cyprinodon variegatus. *Environ Toxicol Chem*. **2001**; *20*:1557-1563.

Luengen AC, Fisher NS, Bergamaschi BA. Dissolved organic matter reduces algal accumulation of methylmercury. *Environ Toxicol Chem*. **2012**; *31*:1712-1719.

Mason RP, Lawrence AL. Concentration, distribution, and bioavailability of mercury and methylmercury in sediments of Baltimore Harbor and Chesapeake Bay, Maryland, USA. *Environ Toxicol Chem*. **1999**; *18*(11):2438-2447.

Mayer P, Parkerton TF, Adams RG, Cargill JG, Gan J, Gouin T, Gschwend PM, Hawthorne SB, Helm P, Witt G, You J, Escher BI. Passive sampling methods for contaminated sediments: scientific rationale supporting use of freely dissolved concentrations. *Integr Environ Assess Manag*. **2014**; DOI: 10.1002/ieam.1508.

Oen AMP, Janssen EML, Cornelissen G, Breedveld GD, Eek E, Luthy RG. *In situ* measurement of PCB pore water concentration profiles in activated carbon-amended sediment using passive samplers. *Environ Sci Technol*. **2011**; *45*:4053-4059.

Peijnenburg WJGM, Teasdale PR, Reible D, Mondon J, Bennett WW, Campbell PGC. Passive sampling methods for contaminated sediments: state of the science for metals. *Integr Environ Assess Manag*. **2014**; DOI: 10.1002/ieam.1502.

Reible DD, Lotufo G. Final Technical Report: Demonstration and Evaluation of Solid Phase Microextraction for the Assessment of Bioavailability and Contaminant Mobility. SERDP Environmental Restoration Project ER-0624 May 2012.

Tomaszewski JE, Luthy RG. Field deployment of polyethylene devices to measure PCB concentrations in pore water of contaminated sediment. *Environ Sci Technol*. **2008**; *42*:6086-6091.

USEPA *Guidelines for Using Passive Samplers to Monitor Organic Contaminants at Superfund Sediment Sites*; United States Environmental Protection Agency: Washington, DC, **2012**; http://www.epa.gov/superfund/health/conmedia/sediment/pdfs/Passive_Sampler_SAMS_Final_Camera_Ready_-_Jan_2013.pdf.

Wang WX, Stupakoff I, Gagnon C, Fisher NS. Bioavailability of inorganic and methylmercury to a marine deposit feeding polychaete. *Environ Sci Technol.* **1998**; *32*:2564-2571.

Williams JJ, Dutton J, Chen CY, Fisher NS. Metal (As, Cd, Hg, and CH_3Hg) bioaccumulation from water and food by the benthic amphipod *Leptocheirus plumulosus*. *Environ Toxicol Chem.* **2010**; *29*(8).

4.0 ORGANISATION OF THE REPORT

This research project entailed three key research objectives as described below. Results and discussion associated with each of the objectives have been written separately, with the ultimate goal of being able to submit each for separate peer-reviewed publications. Also, keeping them separate allows more fussed discussion of each objective separately. The first document associated with objective 1 has been published in the journal Environmental Science and Technology (Jalalizadeh and Ghosh, *Environ. Sci. Technol*. 2016, 50, 8741−8749). The other two are still being worked into final manuscripts.

1) Explore a novel approach of enhancing mass transfer by introducing mechanical vibration to disrupt the aqueous boundary layer around passive samplers deployed *in situ*. (Chapter 5)

2) Test this approach for strongly hydrophobic compounds like dioxins and furans. (Chapter 6)

3) Evaluate a range of polymer types for use as passive equilibrium samplers for methylmercury. (Chapter 7)

5.0 RESEARCH OBJECTIVE #1: Explore a novel approach of enhancing mass transfer by introducing mechanical vibration to disrupt the aqueous boundary layer around passive samplers deployed *in situ*.

5.1 Introduction

The freely dissolved concentration of hydrophobic pollutants in sediment porewater is a critical measurement that is useful in assessing fate, transport, and bioavailability of these compounds.[1] Accurate measurement of low aqueous concentrations of hydrophobic compounds is challenging due to the association with colloidal and dissolved organic matter in porewater. This has led to the development of passive sampling approaches using well characterized polymeric materials. When the polymeric material is able to reach equilibrium with the sediment porewater, such as in a well-stirred laboratory measurement, the estimation of freely dissolved porewater concentration (C_{free}) becomes a trivial exercise based on the measured partition constant of the polymer.[2] [3] However, in several situations, an *in situ* measurement in sediment is desired. Such measurements have been challenged by the difficulty in reaching equilibrium between porewater and the passive sampler as mass transfer through the depletion layer outside the commonly used polymers (with commonly used thicknesses) becomes limiting in the absence of active mixing.[4] It has been shown that for strongly hydrophobic compounds equilibrium may not be achieved in the field even after one year in 51 µm polyethylene (PE).[5] Several researchers have adopted the use of performance reference compounds (PRCs) dosed in the polymer to assess the kinetics of mass transfer and correct for non-equilibrium.[6-14] While corrections based on PRC loss work reasonably well for compounds with low to mid-range hydrophobicity, the corrections become increasingly erroneous for strongly hydrophobic compounds when the departure from equilibrium increases.[14] Several approaches for calibration using PRC data have been suggested.[6-10] In all of these approaches, the uncertainties introduced by the PRC correction are larger when the extent of equilibrium is low, which is the case for strongly hydrophobic compounds in the field.

A primary uncertainty in the PRC correction arises from the fact that nearly always it is the sediment side mass transfer in the immediate vicinity of the passive sampler that controls overall kinetics.[4] The retarded diffusion in the sediment side is impacted by the site-specific sorption characteristics of the sediment, which can vary across orders of magnitude. For example Hawthorne et al.[15] reported a 3-4 orders of magnitude range for site-specific K_{oc} values for polycyclic aromatic hydrocarbons (PAHs). Thus, to be able to correct for non-equilibrium and estimate *in situ* porewater concentrations we need to first have an estimate of site-specific partitioning of the analytes of interest. The loss kinetics of a few PRC compounds into sediment is used to infer the desorption behavior of a large range of analyte compounds from sediment.[8]

Thinner polymeric materials can be used to increase the surface area to volume ratio and reduce the depletion per unit area[6] and reduce deployment time. However, even with some of the thinnest polymers practically deployable in the field (e.g. 25 µm thick PE), sediment-side mass transfer limitation can be significant.[4] Making the polymers too thin makes them prone to damage during deployment in sediment, reduces the total mass of polymer sampling material

(impacting detection limits), and also poses a physical challenge of insertion in sediments if the polymer surface area is very large.

To address these challenges, we take a very different approach of manipulating the external depletion layer in the sediment side of a passive sampler. We demonstrate for the first time a novel approach of *in situ* passive sampling that overcomes the slow approach to equilibrium for hydrophobic organic compounds in static sediments. Our approach involves mechanical disruption of the depletion layer outside the polymer surface using periodic vibration performed *in situ*. We adapted small vibration motors used for haptic feedback in cell phones and other electronic devices to create vibrations in *in situ* passive sampling frames programmed to trigger at pre-determined time intervals. The concept of passive sampling still applies to the vibrated deployment because the disruptions introduced by the periodic vibration is not unlike natural sediment processes induced by burying and sediment ingesting worms that also achieve chemical equilibrium through small-scale physical disruptions in sediments. Laboratory experiments were performed using PAH-impacted field sediments to compare the approach to equilibrium under static, well-mixed, and differently shaken passive sampling modes. We also performed numerical modeling of the mass transfer process to mechanistically explain our observations and optimize the duration and periodicity of the vibrations in order to minimize the energy requirement to drive the vibration motors.

5.2 Materials and methods

Materials. Low density PE sheets (25μm thickness), manufactured by Poly-America (Grand Prairie, TX, USA) were purchased from the Home Depot. PAH and deuterated PAH stock solutions were purchased from Fisher Scientific (Pittsburg, PA, USA). Cylindrical vibrating motors with a diameter of 9 mm and length of 25 mm were purchased from Precision Microdrives (London, UK). The motors operated at a rated voltage of 3V, operating current of 130mA, and vibrating speed of 13,500 rpm. Pulse-pause timers (model 60H) were purchased from Velleman Inc. (Fort Worth, TX, USA). Prior to use, PE sheets were soaked twice in hexane/ acetone (50/50) and left on a shaker for 24 h each time to remove oligomers and any target and non-target contaminants. Clean PE sheets were then cut into 6mm × 2cm strips (2.8 mg) and were soaked in a PRC solution (80:20 methanol:water with pyrene-d10 and phenanthrene-d10) and allowed to equilibrate for 15 days on an orbital shaker.

After impregnation, all strips were removed from the PRC solution and rinsed with DI water to remove residual methanol on the surface. Two strips were extracted immediately in a 1:1 hexane and acetone mixture (3 × 24 h) to determine the initial PRC concentration in the PE strips.

In situ shaken passive sampler design. Two motors were connected in parallel to a timer and a power supply (2 rechargeable batteries 1.2 V, 700 mAh each) (Figure 5.1). The timers were powered by a 12 V power supply and were programmed to control motor vibration duration and frequency: 5 seconds pulse and 2 minutes pause (high frequency), 2 seconds pulse and 5 minutes pause (low frequency). The small PE sheets described above were enclosed in stainless steel mesh (14 mesh from TWP Inc, Berkeley, CA) and were attached like radial fins on cylindrical motors (four fins on each motor) as shown in Figure 5.1 and SI Figures S5.1-5.3.
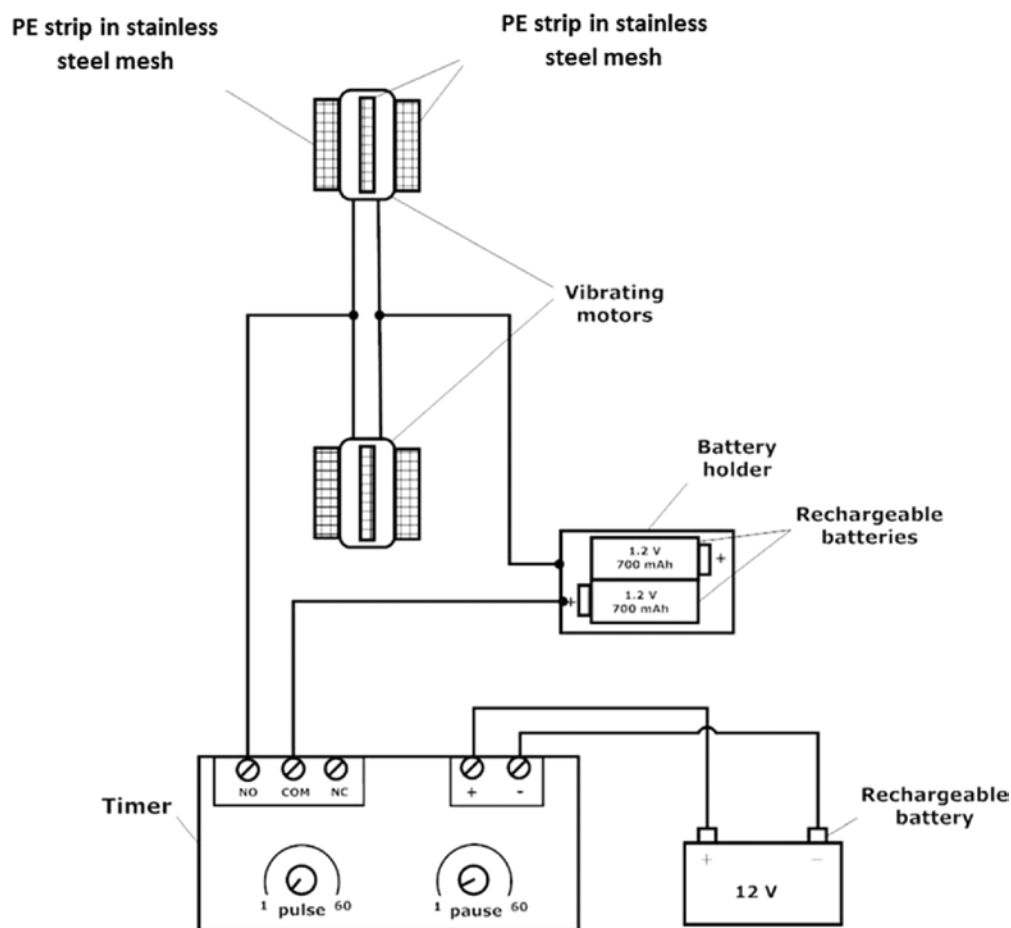
Figure 5.1- Wire diagram of a vibrating passive sampler. PE samplers, enclosed in stainless steel mesh, were attached to the motors. Two motors were connected in parallel to a timer and a power supply (2 rechargeable batteries 1.2 V each). The timers were powered by a 12 V battery.

PAH contaminated river sediment samples from the vicinity of former manufactured gas plants studied previously (identified as HD-3 and HD-5 in Khalil et al.[16]) were used in the present work. The two sediments were combined to obtain a sufficient quantity for the present experiments. The sediment was mixed with DI water containing 200 mg/L sodium azide to make a slurry with weight ratio of 1:2 (dry sediment/water). Water addition was performed to make the sediment more fluid and allow good mixing in the jars.[3] For the well-mixed exposure, 250 mL of the sediment-water slurry and eight of the prepared PE samplers were transferred to a wide mouth jar with a Teflon-lined cap. The jar was placed on a rotary agitator and tumbled at 28 rpm. The rest of the sediment slurry was placed in a large glass tray (25cm×35cm×6cm). Four motors were placed inside the sediment in the tray with 10 cm separation to prevent influencing each other. Two motors vibrated at the high frequency mode and two at the low frequency mode. Eight additional PE samplers, enclosed in stainless steel mesh without motors, were placed inside the same tray in a static mode at least 10 cm away from any vibrating motor to simulate a static deployment. The tray was then covered with aluminum foil. Two PE strips were removed from the well mixed, static, and vibrating systems and analyzed for native PAHs and PRC compounds after 7, 14, 28 and 56 days.

PAH extraction and analysis. Upon removal from the sediment, PE strips were rinsed with water and wiped with laboratory tissue to remove water and adhering particles. Prior to extraction anthracene-d10 surrogate was added to assess the effectiveness of sample processing, and extracts with lower than 80% surrogate recoveries were discarded. Samplers were extracted with a 1:1 hexane and acetone mixture (3×24 h, with sequential extracts pooled). The final extraction volumes were blown down to 1mL using a stream of nitrogen gas. PAHs from sediment were extracted by sonication (EPA method 3550B) and cleaned using activated silica gel (EPA method 3630C). Four internal standards were added to the final extracts before analysis (1-fluoronapthalene, p-terphenyl-d14, benzo(a)pyrene-d12, and dibenz(a,h)anthracene-d14). The 16 USEPA priority pollutant PAHs were analyzed in an Agilent 6890 gas chromatograph coupled to an Agilent 5973N MS detector as described in Khalil et al.[16]

Modeling uptake of analytes from sediment porewater

A numerical modeling approach was used to describe the mass transfer process involved in the static, vibrating, and well-mixed deployments of passive samplers. The modeling structure for static and vibrating deployments are similar and are described first with respective boundary conditions. Finally the well-mixed model is described where mass transfer limitation is only in the polymer side.

Static system. Two modeling approaches were implemented to simulate mass transfer of PAHs from sediment particles into porewater, and from porewater into polymer during static deployment. The first approach is based on the one-dimensional diffusion model presented by Fernandez et al.,[8] but solved numerically. In this model mass transfer within the sediment particle is assumed to be fast and instantaneous equilibrium between sediment particles and porewater is assumed (local equilibrium model). Mass transfer within the polymer and in porewater is described by Fick's 2nd Law of diffusion. Instantaneous equilibrium is assumed at the polymer surface boundary with porewater as done in previous work.[4,8] This model is explained in more detail in the SI.

The second approach is based on the assumption that mass transfer from sediment particles into porewater is described by first order kinetics.[4,18] The model was solved using two different hypothesis: 1) All PAHs are associated with the slow desorbing pool in sediment and desorption is characterized by the slow desorption rate constant. 2) All PAHs are associated with the fast desorbing pool in sediment and desorption is characterized by the fast desorption rate constant. First order desorption rate constants were obtained from a study by Ghosh et al.[17], where sediment from a similar manufactured gas plant impacted site was used (see SI).

In a system containing a PE strip with the thickness of $2l_p$ and sediment/porewater with thickness of l_w on both sides, sediment concentration (S) changes following first order kinetics.[4,18]

$$\frac{\partial S}{\partial t} = k(K_d C_w - S) \qquad\qquad l_p < x < l_p + l_w \quad and \quad -l_p < x < -l_p - l_w \qquad (1)$$

Where t is time (s), S is chemical concentration in sediment (ng/g), K_d is sediment-water partition coefficient (cm³/g), k is first order desorption rate constant (s^{-1}) and C_w is chemical concentration in water (ng/cm³)

For a PE strip with concentration C_{PE} and at point x and time t:

$$\frac{\partial C_{PE}}{\partial t} = D_{PE} \frac{\partial^2 C_{PE}}{\partial x^2} \qquad\qquad -l_p < x < l_p \qquad\qquad (2)$$

Where C_{PE} is chemical concentration in PE (ng/cm³) and D_{PE} is chemical diffusivity in PE (cm²/s)

The transport equation in porewater with concentration of C_w at point x and time t will be as follows:

$$\frac{\partial C_w}{\partial t} = D \frac{\partial^2 C_w}{\partial x^2} - \left(\frac{\rho}{\varepsilon}\right)\frac{\partial S}{\partial t} \qquad\qquad l_p < x < l_p + l_w \quad and \quad -l_p < x < -l_p - l_w \quad (3)$$

Where ρ is sediment bulk density (g/cm³) and ε is porosity (cm³/ cm³)

D is the diffusivity in water (D_w) after correction for tortuosity:

$$D = \frac{D_w}{1 - \ln\varepsilon^2} \qquad\qquad (4)$$

Substituting Equation (1) in Equation (3), the transport equation in porewater can be re-written as:

$$\frac{\partial C_w}{\partial t} = D \frac{\partial^2 C_w}{\partial x^2} - \left(\frac{\rho}{\varepsilon}\right)k(K_d C_w - S) \qquad\qquad (5)$$

Initial conditions

The polymer was initially clean and porewater was assumed to be in equilibrium with sediment.

$$C_{PE} = 0 \qquad\qquad -l_p \leq x \leq l_p \qquad\qquad (6)$$

$$C_{w0} = S_0/K_d \qquad\qquad l_p < x < l_p + l_w \quad and \quad -l_p < x < -l_p - l_w \qquad (7)$$

Where S_0 is initial chemical concentration in sediment (ng/g) and C_{w0} is initial chemical concentration in water (ng/cm³)

Boundary conditions

Continuity of flux and equilibrium condition was assumed at the PE-water boundary as done in previous work.[8]

$$D_{PE} \frac{\partial C_{PE}}{\partial x_{PE}} = D \frac{\partial C_w}{\partial x_w} \qquad\qquad x = l_p \; and \; x = -l_p, \; t > 0 \quad (8)$$

$$C_{PE} = K_{PEw} C_w \qquad\qquad x = l_p \; and \; x = -l_p \qquad (9)$$

Where K_{PEw} is the PE-water partition coefficient (cm^3/cm^3)

Due to symmetry the flux will be zero at the center of the PE sheet. Porewater concentration is equal to the initial concentration far away from the polymer at $x=l_p+l_w$ and does not change over time:

$$\frac{\partial C_{PE}}{\partial x} = 0 \qquad\qquad x = 0 \qquad\qquad (10)$$

$$\frac{\partial C_w}{\partial t} = \frac{\partial S}{\partial t} = 0 \qquad\qquad x = l_p+l_w \quad and \quad x = -l_p-l_w \quad (11)$$

<u>Vibrating system.</u> In the vibrating system, when the motor is in pause mode, the mass transfer is similar to the static mode and sediment and porewater concentration in the vicinity of the polymer depletes with time. Every time the motor vibrates, the sediment and porewater in the vicinity of the polymer is mixed up. Our visual observation of the vibration system indicated that the extent of fluidized mixing was at least 1 cm from the surface of the device with pressure waves from the vibration extending to 2-3 cm from the device (SI Figure S5.3). We assumed that this mixing is enough to increase sediment concentration to the initial concentration in sediment (S_0). Porewater concentration right after each vibration pulse will also increase to the initial concentration:

$$C_w = C_{w0} ; \quad S = S_0 \qquad\qquad l_p < x < l_p+l_w \quad and \quad -l_p < x < -l_p-l_w, \quad (12)$$

<u>Well-mixed system.</u> Diffusion in a polymer with thickness of $2l_p$ follows Fick's second law:

$$\frac{\partial C_{PE}}{\partial t} = D_{PE}\frac{\partial^2 C_{PE}}{\partial x^2} \qquad\qquad -l_p < x < l_p \qquad\qquad (13)$$

The passive sampler was assumed to be initially clean. Since the system is perfectly mixed, the porewater concentration remains constant and equal to the initial value (S_0/K_d) during the deployment time. The boundary condition is defined as:

$$C_{PE} = K_{PEw}C_{w0} \qquad\qquad x = l_p \; and \; x = -l_p \qquad\qquad (14)$$

The model equations were solved in Matlab using an explicit, finite-difference numerical modeling technique.[19] To check the numerical model, the fractional uptake of chrysene into PE was simulated and the solution was found to be identical to the analytical solution based on Fernandez et al.[8] Details of parameter estimation, numerical solutions and Matlab codes are provided in the SI.

5.3 Results and discussion

<u>Equilibrium PAH concentration in sediment and porewater.</u> The concentrations of the 16 EPA priority pollutant PAHs in sediment are shown in Figure 5.2. The four most abundant PAHs were phenanthrene, fluoranthene, pyrene, and benzo(a)pyrene. The total concentration of PAHs in the sediment was 128 µg/g. The 2-4 ring PAHs comprised 60% of the total in sediment. The equilibrium concentrations in PE ($C_{PE,eq}$) were determined by extracting the PE samplers after 56 days of deployment in the well-mixed PE-sediment system. Another time point measurement of PE concentration after 77 days of deployment confirmed that equilibrium had reached in PE for

all PAHs in 56 days (SI Table S5.3). Both PRCs (pyrene-d10 and phenanthrene-d10) were depleted completely in the well-mixed exposure in 30 days (SI Figure S5.5). The freely dissolved porewater concentrations were calculated from equilibrium concentration of PAHs in PE and reported values for K_{PEw}[5] (Equation 9).

As shown in Figure 5.2, acenaphthene and phenanthrene are the dominant PAHs in porewater. PAHs up to chrysene contributed to 99% of the total porewater concentration at equilibrium. Toxic units were estimated for each PAH by dividing porewater concentrations by final chronic values (FCVs).[20] The total toxic units of 16 PAHs measured in the sediment porewater was approximately 9.33 indicating that PAHs in this sediment likely pose narcosis toxicity to benthic invertebrates.[20]
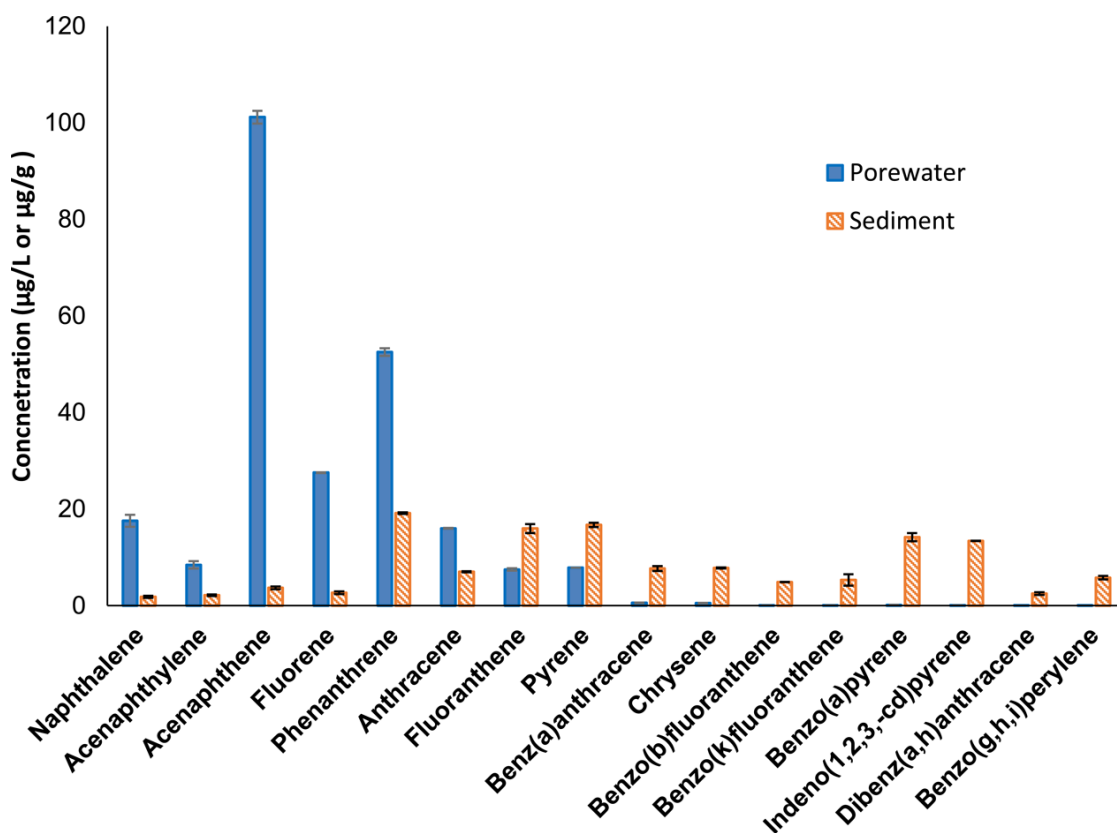
Figure 5.2- PAH concentration in porewater (μg/L) and sediment (μg/g). Sediment concentrations are mean values from triplicate measurements. Porewater concentrations were obtained using eq 9 and $C_{PE,eq}$, which are mean values from duplicate measurements of PE concentration after 56 days of exposure in the well-mixed system.

PAH uptake in static deployment. As expected, the uptake of all PAHs was slowest in the static exposure. In fact, none of the PAHs from fluoranthene to indeno(1,2,3,-cd)pyrene reached equilibrium in 56 days of contact. The fractional uptake of benz(a)anthracene, benzo(k)fluoranthene and indeno(1,2,3,-cd)pyrene were only 35%, 11%, and 8%, respectively after 28 days. Previous studies have reported similar slow uptake in a static exposure,[11-13] especially for larger molecular weight compounds. For example, Fernandez et al.[11] calculated the fractional equilibration of PCBs into 25μm PE by measuring the fractional loss of ^{13}C-labeled

PCBs after 44 days of field deployment. The average fractional equilibration of penta- and hexachlorobiphenyls from different locations in the field were only 37% and 33%, respectively.

Effect of vibration on polymer uptake rate. Periodic vibration of the PE sampler resulted in faster uptake compared to static deployment for all PAHs measured. As shown in Figure 5.3, the uptake of chrysene after 56 days was only 40% of equilibrium in static exposure compared to 100% for the vibrating system. Even after 7 days of exposure, the vibrating system reaches 63% of equilibrium for chrysene compared to 20% in the static system. Comparison between the static and vibrating system for several other PAH compounds is shown in Figure 5.4 and SI Figure S5.4. Both PRCs were lost more than 90% at the first time point of measurement for the vibrating systems and well-mixed systems (SI Figure S5.5), which generally agreed with the uptake of the analogous PAHs. As PRC performance was not the focus of this study, using a full range of high molecular weight PRCs and performing shorter duration measurements of PRC loss are recommended in future work in order to provide a more robust analysis of PRC performance in the vibrating system.

For PAH compounds less hydrophobic than chrysene (e.g. fluoranthene and pyrene), the static system showed reasonable uptake of close to 70% in 56 days while the vibrating system reached equilibrium during that exposure. When the passive sampler is close to equilibrium, the correction for non-equilibrium is relatively accurate. However, as the kinetics slow down and only a small fraction of equilibrium is achieved in the sampler, the correction for non-equilibrium becomes error-prone.[9] This is the case for the PAH compounds that are more hydrophobic than chrysene. The improvement over static system was more evident for larger molecular weight PAHs. For example, the measured fractional uptake of benzo(a)pyrene was improved from 6% to 55% in 7 days and from 23% to 90% after 56 days. The fact that vibration was more effective on uptake rate of heavier PAHs can be explained based on the nature of the overall mass transfer resistance in a passive sampler[6]

$$\frac{1}{k_0} = \frac{\delta}{D_w} + \frac{1}{K_{PEw}D_{PE}} \tag{15}$$

Where k_0 is the overall mass transfer rate constant and δ is the diffusion distance.

The first term on the right hand side of Equation 15, describes the sediment-side mass transfer resistance. The large K_{PEw} values of the more hydrophobic compounds makes the second term smaller than the first, thereby making the first term or the water side mass transfer more dominant. The ratio of diffusivities in water and polymer (D_w/D_{PE}) also increases as the compound becomes more hydrophobic. However, K_{PEw} tends to be the dominant factor influencing which side controls mass transfer since K_{PEw} changes over a wider range of values compared to the range where the diffusivity ratios vary for different compounds.[21] As a result, disrupting the depletion layer (decreasing apparent δ) by means of vibration will be more effective on the overall mass transfer rate of larger molecular weight PAHs. Our experimental data indicated that concentration of larger molecular weight PAHs (log K_{ow}>5.5) reached more than 50% of their equilibrium concentration in PE within 14 days of deployment in the vibrating system (SI Figure S5.4). Thus, field deployment of passive samplers with periodic vibration will encounter less challenges of non-equilibrium correction for larger molecular weight compounds.

Results from the vibration work demonstrated a great improvement of PE uptake after short exposure times (1-2 weeks). The faster exchange will also allow the use of high molecular weight PRCs to accurately correct for the remaining non-equilibrium in a vibrating system without the need for long exposure times.

Comparison of three modeling approaches in static, vibration and well-mixed deployments. Figure 5.3-a and 5.3-b demonstrate modeling results for chrysene in static and vibrating systems based on local equilibrium, slow desorption, and fast desorption models. As shown in Figure 5.3-a, in static deployment, overall mass transfer into the polymer is slow and the predictions based on local equilibrium assumption and the fast desorption rate model are indistinguishable. Also, both predictions are close to the observed uptake of chrysene in the static deployment. However, the slow rate of desorption model predicts uptake that is slower than the observed values. Thus, it appears that for modeling static deployments, due to the rate limiting mass transfer through the depletion layer, it is adequate to assume local equilibrium between sediment and water.

For the vibrating system, assuming that the sediment is effectively mixed after vibration, the model predictions based on local equilibrium and fast rate of desorption deviated as shown in Figure 5.3-b. While the fast rate of desorption model prediction is close to the measured uptake of chrysene, the prediction based on local equilibrium greatly over-predicts uptake. The same results were observed for pyrene as indicated in SI Figure S5.6. Thus, it appears that as the depletion layer is disrupted by vibration and mass transfer is enhanced, desorption from sediment becomes limiting and local equilibrium between sediment and water can no longer be assumed. The fast desorption rate adequately predicts uptake while the slow desorption rate still under-predicts uptake in the polymer. Past work has demonstrated that PAH desorption from MGP-impacted sediments is characterized by slow and fast desorbing PAH fractions.[17] However, the overall kinetics for the vibration system appear to be driven by the fast desorption kinetics and not the slow desorption likely because the sediments are not being depleted enough to reach the slow desorption regime.

For the well-mixed system, a local-equilibrium model was implemented. As shown in Figure 5.3-c, the model agrees reasonably with the observed fast uptake of chrysene and the attainment of equilibrium in the matter of a few days. The well-mixed system brings a large volume of sediment to contribute to the required uptake by the passive sampler and hence the kinetics are fast enough to appear close to instantaneous equilibrium.
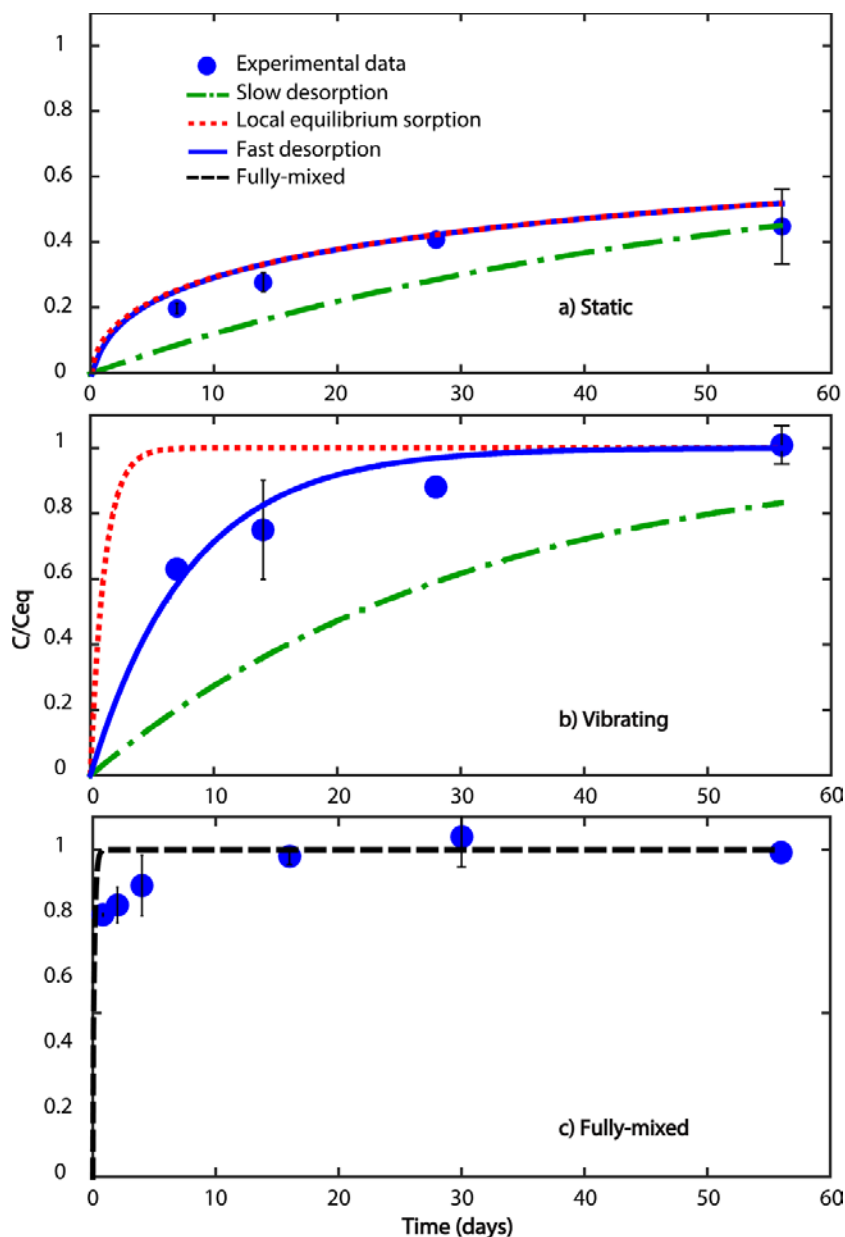
Figure 5.3- Fractional uptake of chrysene in PE passive sampler in static (a), vibrating (b), and well-mixed (c) systems. Experimental data have been shown by circles, and model simulations have been shown by lines. Note that for the static system the local equilibrium and fast desorption models overlap.

Modeling uptake of pyrene, chrysene, and benzo(a)pyrene. Experimental and modeling results for pyrene (log K_{ow} = 4.9), chrysene (log K_{ow} = 5.7) and benzo(a)pyrene (log K_{ow} = 6.1) in static, vibrating, and well-mixed systems are shown in Figure 5.4. Based on the discussion above, only the fast desorption model was used for predicting uptake in static and vibrating systems, and a local equilibrium model was used for predicting the well-mixed system. As shown in Figure 5.4, the model predictions reasonably agreed with the uptake profiles of the 3 PAHs in all three

modes of exposure. For all three PAHs, although there were small differences between the experimental results from 2 min and 5 min pause times (not statistically significant except for pyrene at day 14), the model predicted that there should not be a significant difference between the two (see SI Tables S5.4, S5.5, and S5.6). In the model we assumed that both pulse durations are long enough to mix up the sediment to initial bulk concentration. However, in reality short pulse time (2 seconds) in the low frequency system may not be long enough to satisfy the model assumption.
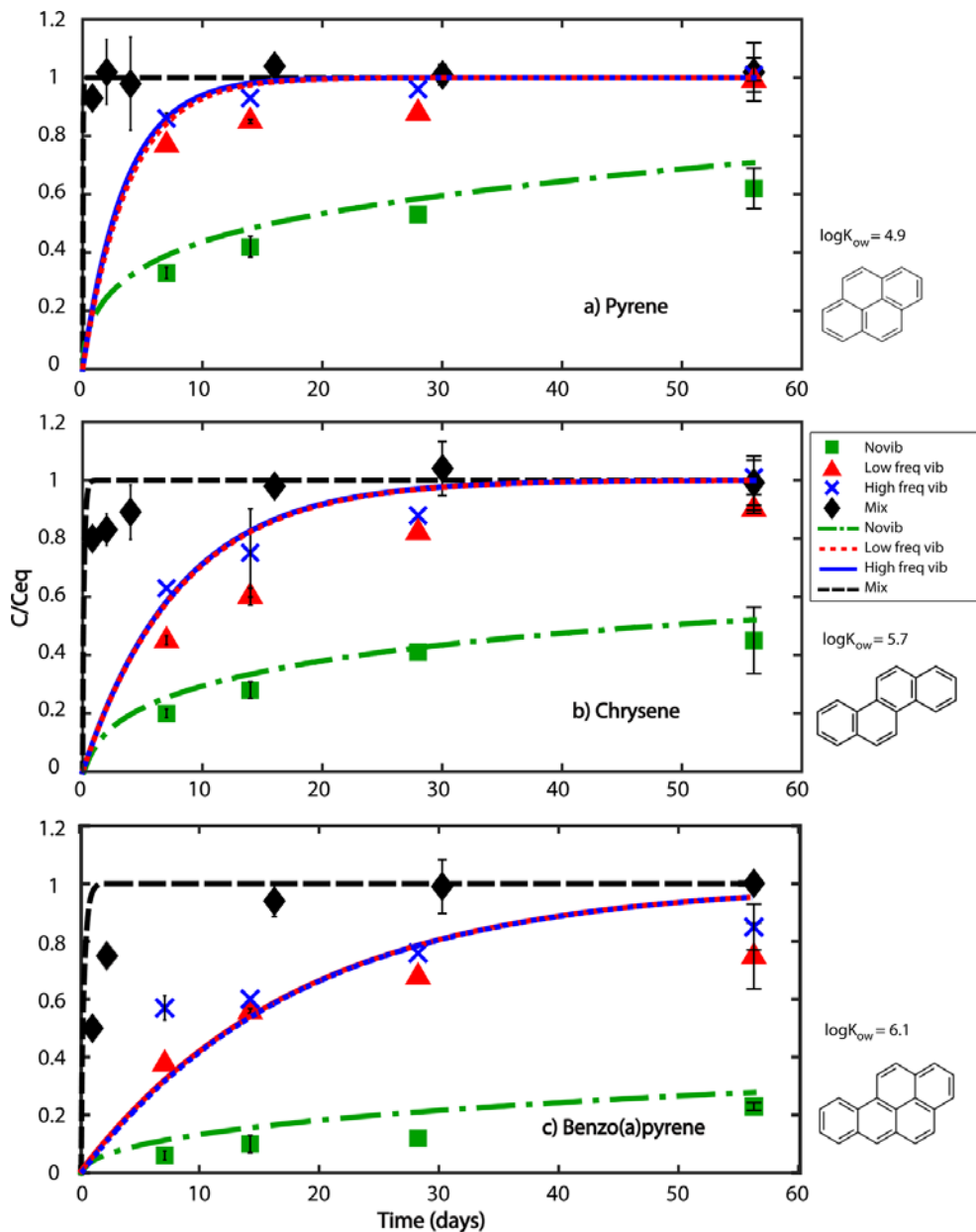
Figure 5.4- Fractional uptake of pyrene (a), chrysene (b), and benzo(a)pyrene (c) in PE passive sampler in four differently exposed systems. Experimental data have been shown by symbols, and fast desorption model simulations have been shown by lines.

To better illustrate how the periodic vibration impacts development of the sediment-side depletion layer, the concentration profiles in the sediment and half width of the PE sampler was plotted for chrysene as a function of exposure time. As shown in Figure 5.5 left panel for the static deployment, chrysene in the sediment side is depleted well into 300 μm distance from the PE surface after 20 days. The concentration values for PE plotted in Figure 5.5 have been multiplied with K_{sed-PE} to make the values directly comparable to the sediment concentration. As indicated in Figure 5.5, left panel, the concentration in PE reaches equilibrium with the depleted concentration in the sediment adjacent to the surface in 2 days or less and the mass transfer limitation is moved to the sediment-side depleted layer. Also, after the first few hours of exposure, there is no concentration gradient within the polymer indicating all mass transfer resistance is in the sediment side. In stark comparison, for the periodic vibration deployment, since the sediment side is mixed up at frequent intervals, the deep depletion layer in the sediment side is not able to develop and the mass transfer resistance is limited to a few microns near the polymer surface. In fact, as seen in the 2-day simulation for the concentration gradient within PE in the vibrating system, the model suggests that there is still some polymer-side resistance. As a result, the concentration in PE rises much more rapidly than in the static case.
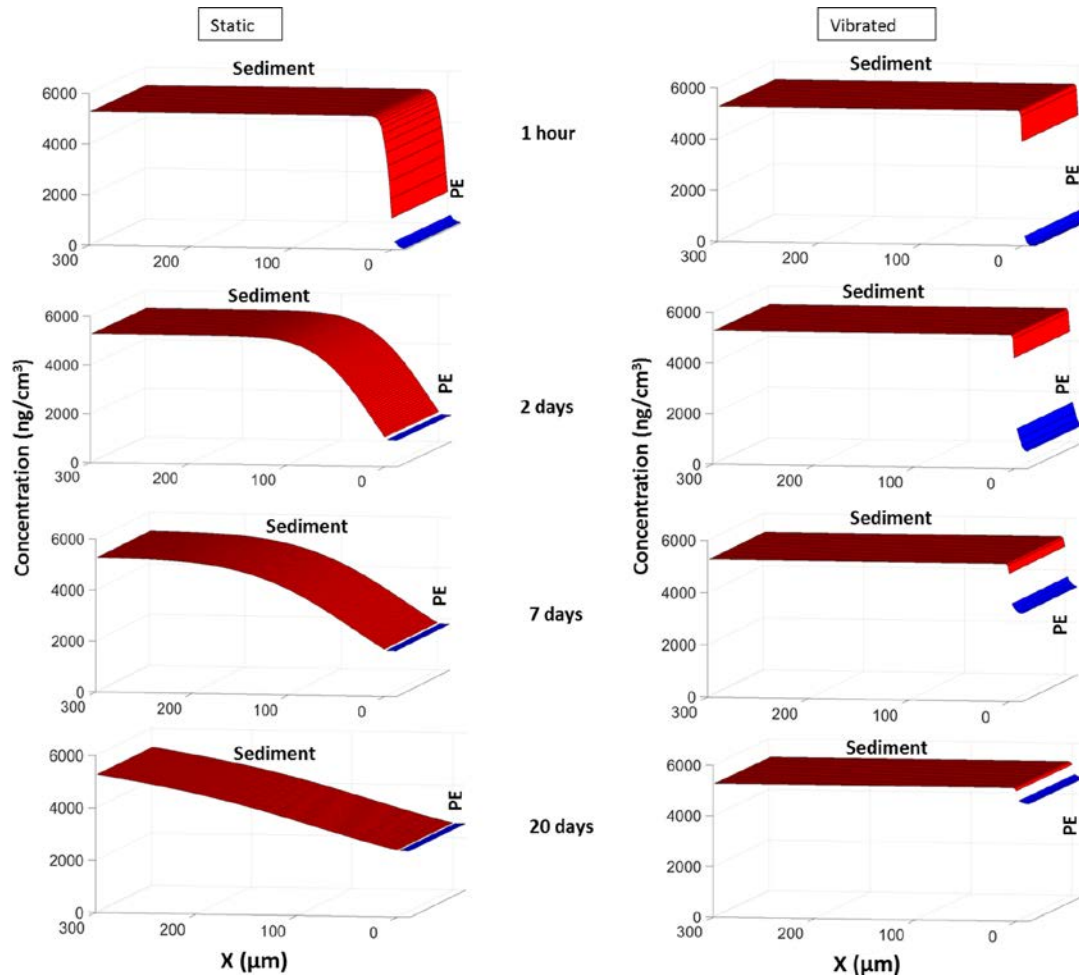
Figure 5.5- Model simulations of chrysene concentration profile within sediment and PE for static and periodic vibration deployments. The values shown on the Y-axis are chrysene concentration in sediment and concentration in PE multiplied by sediment−PE partition constant ($C_{PE} \times K_{sed-PE}$).

For the well-mixed system, pyrene uptake is fast and modeled reasonably well by the well-mixed local-equilibrium model (Figure 5.4-a). However, the model is not accurate for early times for the more hydrophobic compounds, especially benzo(a)pyrene (Figure 5.4-c). This could be due to inaccuracy of reported diffusivity in PE, slow desorption from sediment, or inefficient mixing of the system. Inefficient mixing slows the uptake of more hydrophobic compounds since sediment-side mass transfer is dominant for high molecular weight PAHs (as described earlier) and disruption of depletion layer by efficient mixing is more important. Previous studies[22] have observed slower uptake of larger PCBs in well mixed sediment-slurry systems and attributed the slow kinetics to inefficient mixing and slow desorption.

Optimization of vibration frequency. Results of the vibration model for PE uptake of chrysene were used to test the effect of different vibration frequencies and to optimize power requirement. All vibration frequencies had pulse duration of 5 seconds and varied in pause time. The modeling results were based on the fast desorption model and pause times were set at: 2 min, 5 min, 6 hour, 1 day, and 5 days (Figure 5.6). Small differences (6% or less) were observed between the 2-min and 6-hour pause models (see SI Table S5.7). Even the 1-day pause model predicted an uptake profile which was not greatly different from the 2 min-pause model. The 5-day pause profile tracked the unmixed profile for the first 5 days, then jumped up to a higher uptake profile as the mixing altered the boundary condition. Although the 5 day-pause model does not show significant improvement over the static system in short deployment times (<7 days), the model still predicts 75% fractional uptake after 28 days. In comparison the fractional uptake of chrysene is only 40% in static system for the same exposure duration. These results indicate that significant improvement over the static system is possible with lower frequencies of vibration (large pause times). Increasing pause time is desirable as there is no energy consumption during the pause time when the motor is not vibrating. In order to optimize pause time, energy consumption was estimated for deploying a vibration system for 15 days and a range of pause times. The fractional uptake of three PAHs (pyrene, chrysene and benzo(a)pyrene) in PE after 15 days was also determined with the model for each pause time and plotted versus energy consumption (SI Figure S5.7). Only 30mWh is required to enhance the fractional uptake of chrysene to 80% in 15 days of deployment. In comparison, a typical AA size NiMH rechargeable battery can provide about 1000 mWh of energy. However, further enhancement of fractional uptake in PE from 80% to 82% increases the energy requirement to 2340mWh. This is also evident from Figure 5.6 where we see little enhancement of uptake when the pause time is reduced below 6 hours.
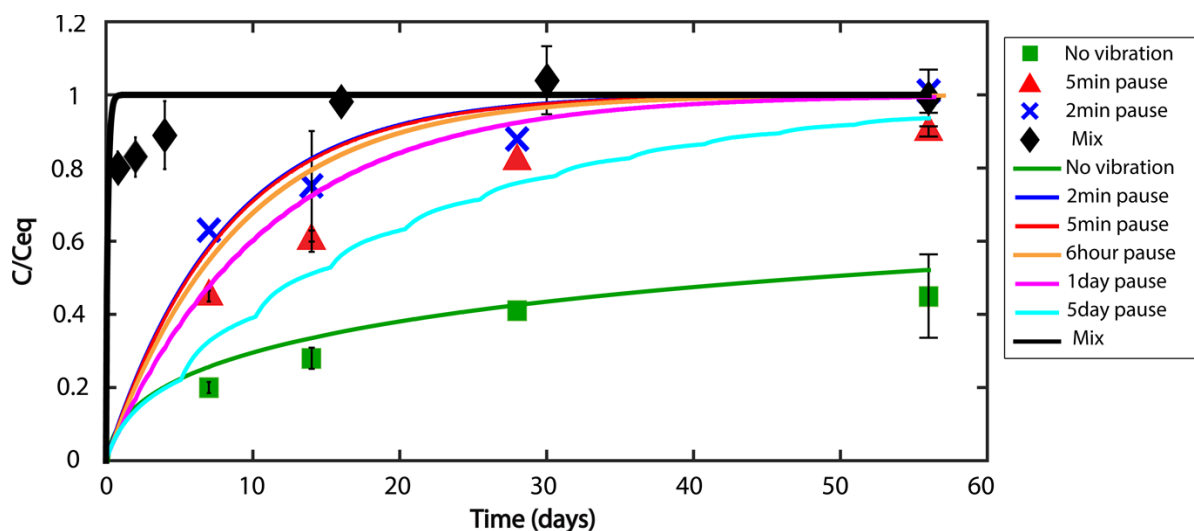
Figure 5.6- Model simulation of chrysene uptake in vibrating system with different pause times of vibration. Experimental data have been shown by symbols, and fast desorption model simulations have been shown by lines.

5.4 Implications

A recent review article on passive sampling by Booij et al.[23] concluded that options to reduce time for equilibrium are limited to manipulation of area/volume ratio of sampler, choice of sampler material, and flow rate. Past work has led to significant optimization of the physical aspects of the passive samplers, yet attainment of equilibrium remains difficult for strongly hydrophobic compounds especially for *in situ* sediment porewater measurements. Also, there is little that can be done in the sediment environment to enhance porewater velocity. This study advances the practice of passive sampling by addressing a key bottleneck through the novel introduction of periodic vibration in the sampling platform to disrupt the depletion layer that develops in the sediment side and slows mass transfer. Through mass transfer modeling, we also provide a mechanistic interpretation of how periodic vibration enhances the approach to equilibrium. While PRC corrections have allowed extension of passive sampling to compounds that do not achieve equilibrium during a reasonable period of deployment, the introduction of vibration greatly enhances approach to equilibrium, reduces deployment times, and extends the use of passive sampling in conjunction with PRCs to strongly hydrophobic compounds as shown for benzo(a)pyrene in this study. Further development is necessary to build robust prototypes and perform tests in the field. The size of the devices and motors may also need to be increased to enable deployment of larger passive samplers to target low concentrations in sediment.

5.5 Literature Cited

(1)   Mayer, P.; Parkerton, T. F.; Adams, R. G.; Cargill, J. C.; Gan, J.; Gouin, T.; Gschwend, P. M.; Hawthorne, S. B.; Helm, P.; Witt, G.; You, J.; Escher, B. I. Passive sampling methods for contaminated sediments: Scientific rationale supporting use of freely dissolved concentrations. *Integr. Environ. Assess. Manage.* 2014, 10, 197−209.

(2)   Mayer, P.; Tolls, J.; Tolls, J. L. M.; Mackay, D. Equilibrium sampling devices. *Environ. Sci. Technol.* 2003, 37 (9), 184A- 191A.

(3)   Ghosh, U.; Kane Driscoll, S.; Burgess, R. M.; Jonker, M. T. O.; Reible, D.; Gobas, F.; Choi, Y.; Apitz, S. E.; Maruya, K. A.; Gala, W. R.; Mortimer, M.; Beegan, C. Passive Sampling Methods for Contaminated Sediments: Practical Guidance for Selection, Calibration, and Implementation. *Integr. Environ. Assess. Manage*. 2014, 10, 210−223.

(4)   Lampert, D. An assessment of the design of *in situ* management approaches for contaminated sediments. Ph.D. Thesis, The University of Texas at Austin, May 2010.

(5)   Lohmann, R. Critical Review of Low-Density Polyethylene's Partitioning and Diffusion Coefficients for Trace Organic Contaminants and Implications for Its Use As a Passive Sampler. *Environ. Sci. Technol*. 2011, 46, 606-618.

(6)   Huckins, J. N.; Petty, J. D.; Booij, K. Monitors of Organic Chemicals in the Environment,   Springer: New York, NY, 2006.

(7)   Huckins, J. N.; Petty, J. D.; Lebo, J. A.; Almeida, F. V.; Booij, K.;Alvarez, D. A.; Clark, R. C.; Mogensen, B. B. Development of the permeability/performance reference compound approach for *in situ* calibration of semipermeable membrane devices. *Environ. Sci. Technol*. 2002, 36 (1), 85–91.

(8)   Fernandez, L. A.; Harvey, C. F.; Gschwend, P. M. Using performance reference compounds in polyethylene passive samplers to deduce sediment porewater concentrations for numerous target chemicals. *Environ. Sci. Technol.* 2009, 43, 8888–8894.

(9)   Booij, K.; Smedes, F. An improved method for estimatig *in situ* sampling rates of nonpolar passive samplers. *Environ. Sci. Technol*. 2010, 44, 6789-6794.

(10)   Booij, K.; Hoedemaker, J. R.; Bakker, J. F. Dissolved PCBs, PAHs, and HCB in Pore Waters and Overlying Waters of Contaminated Harbor Sediments. *Environ. Sci. Technol*. 2003, 37 (18), 4213-4220.

(11)   Fernandez, L. A.; Lao, W.; Maruya, K. A.; Burgess, R. M. Calculating the Diffusive Flux of Persistent Organic Pollutants between Sediments and the Water Column on the Palos Verdes Shelf Superfund Site Using Polymeric Passive Samplers. . *Environ. Sci. Technol*. 2014, 48 (7), 3925-3934.

(12)   Oen, A. M. P.; Janssen, E. M. L.; Cornelissen, G.; Breedveld, G. D.; Eek, E.; Luthy, R. G. In-situ measurement of PCB pore water concentration profiles in activated carbon-amended sediment using passive samplers. *Environ. Sci. Technol*. 2011, 44, 4053–4059

(13)   Tomaszewski, J.; Luthy, R. G. Field deployment of polyethylene devices to measure PCB concentrations in pore water of contaminated sediment. *Environ. Sci. Technol.* 2008, 42 (16), 6086–6091.

(14)   Apell, J. N.; Gschwend, P. M. Validating the use of performance reference compounds in passive samplers to assess porewater concentrations in sediment beds. *Environ. Sci. Technol.* 2014, 48, 10301 − 10307.

(15)   Hawthorne, S. B.; Grabanski, C. B.; Miller, D. J. Measured partitioning coefficients for parent and alkyl polycyclic aromatic hydrocarbons in 114 historically contaminated sediments: Part 1. Koc values. *Environ. Toxicol. Chem*. 2006, 25, 2901-2911.

(16)   Khalil, M. F.; Ghosh, U.; Kreitinger, J. P. Role of Weathered Coal Tar Pitch in the Partitioning of Polycyclic Aromatic Hydrocarbons in Manufactured Gas Plant Site Sediments. *Environ. Sci. Technol*. 2006, 40, 5681-5687.

(17)   Ghosh, U.; Zimmerman, J. R.; Luthy, R. G. PCB and PAH Speciation among Particle Types in Contaminated Harbor Sediments and Effects on PAH Bioavailability. *Environ. Sci. Technol*. 2003, 37, 2209-2217.

(18)   Werner, D.; Ghosh, U.; Luthy, R. G. Modeling polychlorinated biphenyl mass transfer after amendment of contaminated sediment with activated carbon. *Environ. Sci. Technol.* 2006, 40, 4211–4218.

(19)   Crank, J. *The Mathematics of Diffusion*, 2nd ed.; Oxford University Press: Oxford, 1975; p 414.

(20)   United States Environmental Protection Agency. Equilibrium Partitioning Sediment Benchmarks (ESBs) for the Protection of Benthic Organisms: Procedures for the Determination of the Freely Dissolved Interstitial Water Concentrations of Nonionic Organics. EPA-600-R-02-012. Office of Research and Development, Washington, DC, USA, 2012.

(21)   Thompson, J.; Hsieh, C.; Luthy, R. G. Modeling Uptake of Hydrophobic Organic Contaminants into Polyethylene Passive Samplers. *Environ. Sci. Technol*. 2015, 49 (4), 2270–2277.

(22)   Arp, H. P. H.; Hale, S. E.; Elmquist Kruså, M.; Cornelissen, G.; Grabanski, C. B.; Miller, D. J.; Hawthorne, S. B. Review of polyoxymethylene passive sampling methods for quantifying freely dissolved porewater concentrations of hydrophobic organic contaminants. *Environ. Toxicol. Chem*. 2015, 9999, 1-11.

(23)   Booij, K., Robinson, C.D., Burgess, R.M., Mayer, P., Roberts, C.A., Ahrens, L., Allan, I.J., Brant, J., Jones, L., Kraus, U.R., Larsen, M.M., Lepom, P., Petersen, J., Pröfrock, D., Roose, P., Schäfer, S., Smedes, F., Tixier, C., Vorkamp, K., Whitehouse, P. Passive Sampling in Regulatory Chemical Monitoring of Nonpolar Organic Compounds in the Aquatic Environment. *Environ. Sci. Technol*. 2015, 50, 3-17.

6.0 RESEARCH OBJECTIVE #2: Test the *in-situ* vibration approach for strongly hydrophobic compounds like dioxins and furans.

6.1 Introduction

In the previous chapter, we proposed using a vibrating platform for the deployment of passive sampling devices in sediments. We demonstrated through laboratory measurements and numerical modeling that the proposed platform greatly enhanced the rate of mass transfer of PAHs into PE passive samplers. In this chapter we present an extension of the work demonstrating effectiveness for strongly hydrophobic chlorinated organics in sediments. As shown in Figure 6.1, most polychlorinated dibenzofurans (PCDFs) and polychlorinated dibenzodioxins (PCDDs) have the same range of $K_{ow}s$ (6.5≤ Log K_{ow}≤8) as hexa-, hepta-, and octachloro- PCBs. Thus, for this SEED project, the most abundant hydrophobic PCB congeners were used as analogs for dioxins and furans. A sediment sample from a DoD site containing highly chlorinated PCBs was used in laboratory mesocosms to test the effectiveness of the vibrating platform on uptake rate of hydrophobic PCB congeners into PE passive samplers. In this section, the experimental procedure and results of PCB uptake in PE under static, vibrating, and well mixed conditions are presented.
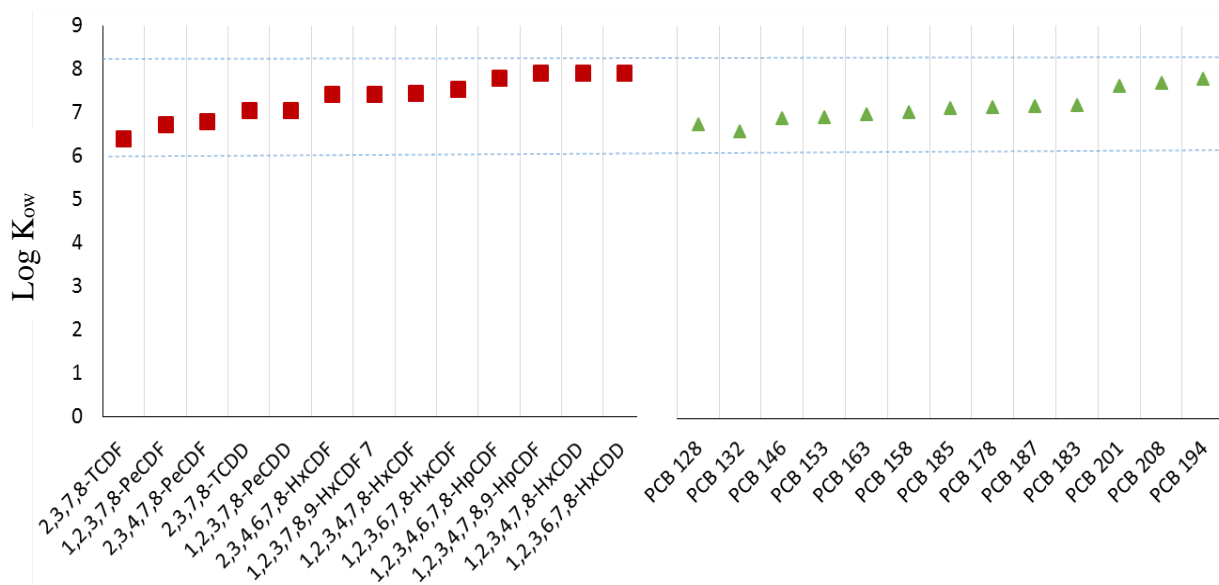
Figure 6.1. Comparison of Log $K_{ow}s$ of PCBs (obtained from Hawker and Connell, 1988) and PCDD/Fs (obtained from Sacan et al., 2005)

6.2 Materials and methods

<u>Materials.</u> Low density polyethylene (LDPE) sheets (25μm thickness), manufactured by Poly-America (Grand Prairie, TX, USA) were purchased from the Home Depot (local store in Baltimore, MD). PCB stock solutions were purchased from Fisher Scientific (Pittsburg, PA, USA). Cylindrical vibrating motors with a diameter of 24 mm and length of 31 mm were purchased from Precision Microdrives (London, United Kingdom). The motors operated at the rated voltage of 3V and operation current of 190 mA. Their rated vibrating speed and typical normalized amplitude of vibration were 5000 rpm and 10 G, respectively. Pulse-pause timers (model 60H) used to control the vibration motors were purchased from Velleman Inc. (Fort Worth, TX). Prior to use, PE sheets were soaked twice in hexane/ acetone (50/50) and left on a shaker for 24 h each time to remove oligomers and any target and non-target contaminants. Clean PE sheets were cut into 20 mg (2cm×5cm) and 40 mg (4cm×5cm) strips. PE strips were then soaked in a 80:20 methanol/water solution containing four PRCs (2,4,5-trichlorobiphenyl (PCB 29), 2,3',4,6-tetrachlorobiphenyl (PCB 69), 2,2',4,4',6,6'-hexachlorobiphenyl (PCB 155), and 2,3,3',4,5,5',6-heptachlorobiphenyl (PCB 192)). The PRC solution was allowed to equilibrate for 15 days on an orbital shaker. After impregnation with PRCs, the strips were transferred into a DI water jar and left on an orbital shaker overnight to remove the methanol from PE strips. Upon removal from water, three strips were extracted immediately in hexane (3×24 h) to determine the initial PRC concentration on PE strips.

<u>Source of Sediments.</u> PCB contaminated sediment samples from Site 102 Abraham's Creek were used in this study. The site is located in the Marine Corps Combat Development Command (MCCDC) military training facility in Quantico, Virginia, 35 miles south of Washington, D.C.

<u>*In Situ* Shaken Passive Sampler Design.</u> A platform made of copper was fabricated with assistance from the UMBC machine shop (Figure S6.4). The platform consisted of a copper pipe section, inside which the motor was located. Four fins made of copper plates and meshes were attached radially to the copper pipe. The copper wire mesh fins were designed as pockets that could hold PE sheets sandwiched within. A 20 mg PE strip (prepared as discussed above) was located inside each pocket and the open edge was sewn with copper wire.

Two platforms were connected in parallel to a timer and a power supply (2 rechargeable batteries 1.2 V, 700 mAh each). The timers were powered by a 12 V power supply and were programmed to control motor vibration duration and frequency. Two experiments were conducted in order to measure the uptake rate of PCBs into PE under different deployment modes. In the first experiment (experiment 1), PE sheets were deployed in sediment under static, well-mixed, and high frequency vibrating modes. In the second experiment (experiment 2), PE sheets were deployed under static and low frequency vibrating modes. The pulse duration of vibrating motors was 5 s and the pause period was 2 min and 5 d in the high and low frequency vibrating systems, respectively. Details of experimental set up are as follows:

Experiment 1- The sediment was mixed with DI water containing 200 mg/L sodium azide to make a slurry with weight ratio of 1:2 (dry sediment/water). For the well-mixed exposure, three wide mouth jars with Teflon-lined lids were prepared. The sediment-water slurry (400 mL) and four of the 20 mg PE samplers were transferred into each jar. The jars were placed on a rotary agitator and tumbled with the speed of 28 rpm. The rest of the sediment slurry was placed in two large glass trays (60 cm×10 cm× 10 cm). Three motors were placed inside the sediment in the

33

trays (two of the motors were placed in one tray with 10 cm separation to prevent influencing each other). The timer was programmed to vibrate the motors with the frequency of 2 min pause and 5 s pulse. Twelve additional PE samplers with a mass of 40 mg each were enclosed in stainless steel mesh without motors and were placed inside the same trays in a static mode at least 10 cm away from the vibrating motors and 5 cm apart from each other to simulate a static system. The trays were then covered with aluminum foil. PE strips were removed from the well-mixed, static, and vibrating systems and analyzed for PCBs and PRC compounds after 7, 14, 28 and 56 days. At each time point, three strips were collected from each system for extraction and analysis.

Experiment 2- PE deployment under static and vibrating modes was repeated in a slurry made with fresh portion from the same sediment as discussed. This time the motors vibrated with the frequency of 5 s pulse and 5 d pause by manual connection to the power supply. PE strips were collected in triplicates from static and vibrating systems and analyzed for PCBs after 7, 14, 28 and 56 days.

PCB Extraction and Analysis. Upon removal from the sediment, PE strips were rinsed with water and wiped with laboratory tissue to remove water and adhering particles. Prior to extraction PCB congeners BZ#14 and 65 were added as surrogate standards to assess the effectiveness of sample processing, and results with lower than 80% surrogate recoveries were discarded. Samplers were extracted with hexane (3×24 h, with sequential extracts pooled). The final extraction volumes were blown down to 1mL using a stream of nitrogen gas. Sediment PCBs were extracted by sonication (EPA method 3550B). Final extracts from passive samplers and sediment were cleaned using deactivated silica gel (EPA method 3630C). Two internal standards were added to the final extracts before analysis (PCB congeners BZ#30 and 204). PCBs were analyzed in an Agilent 6890N Gas Chromatograph with an electron capture detector (ECD) based on analytical method described in Beckingham and Ghosh.[12]

PCB Desorption Study. The desorption rates of PCBs from sediment particles into water were measured based on procedures in Ghosh et al.[13] Briefly, Tenax beads (0.5 g) and sediment sample (5 g) were added to 12-mL glass vials. DI water (10 mL) containing sodium azide (1 g/l) was added to each vial. The vials were palced on a rotary agitator and tumbled with the speed of 28 rpm. At sampling times of 2 h, 4 h, 8 h, 12h, and 48 h the sediment was allowed to settle and Tenax beads to float up. Tenax beads were scooped out from each vial and a fresh portion was added. The Tanax beads were dried with anhydrous sodium sulfate and extracted by adding three volumes of 15 mL 50/50 (v/v) hexane-acetone in a 20-mL vial and shaking horizontally on a rotary shaker for 24 h. Prior to extraction PCB congeners BZ#14 and 65 were added as surrogate standards to assess the effectiveness of sample processing, and extracts with lower than 80% surrogate recoveries were discarded. The final extraction volumes were blown down to 1mL using a stream of nitrogen gas and were cleaned using deactivated silica gel (EPA method 3630C). The extracts were then analyzed for PCBs.

A two-compartment model (Ghosh et al.[13]) was used to describe the desorption kinetics of PCBs from sediment particles into porewater (see Supporting Information for more details). The model was fitted to the normalized desorption data for PCB 128, 183, and 194 in order to find the desorption rate constants (Supporting Information Figure S6.5).

PRC Correction for Non-equilibrium. We used a graphical user interface (GUI, Tcaciuc et al.[14]) to calculate the extent of equilibrium of target PCBs from PRC losses. This GUI is developed based on the mass transfer model presented in Fernandez et al.[6] PRC losses in static and vibrating systems were used to determine the extent of equilibrium of target PCBs in the corresponding systems. PCB and PRC concentration measurements were conducted in triplicates and PRC losses from each PE strip were used to calculate the extent of equilibrium of PCBs in the same strip.

Modeling Uptake of Analytes from Sediment Porewter. Mass transfer models described in Jalalizadeh and Ghosh[1] were employed to describe PCB diffusion from sediment particles into porewater, and from porewater into the polymer under static, vibrating, and well-mixed modes. Briefly, for static deployment mass transfer within the polymer and in porewater was described by Fick's 2nd law of diffusion. Instantaneous equilibrium was assumed at the polymer surface boundary with porewater. PCB desorption from sediment particles into porewater followed a first order kinetics, assuming all PCBs are associated with the fast desorbing pool in sediment. The diffusion model with the assumption of instantaneous equilibrium between sediment particles and porewater (local equilibrium model) adequately predicted the PE uptake in a static system in some previous work (Fernandez et al., 2009). However, local equilibrium cannot be assumed in a vibrating system (Jalalizadeh and Ghosh[1]) because mass transfer from sediment becomes limiting due to disruption of the depletion layer by vibration. In our previous work (Jalalizadeh and Ghosh[1]) we showed that model predictions based on local equilibrium and fast rate of desorption were identical in a static system. However, the simulations deviated for the vibrating system. We also showed that the overall kinetics of PAHs for the vibrating system were driven by the fast desorption kinetics and not the slow desorption, likely because the sediments are not depleted enough to reach the slow regime. The fast desorption rate constants determined from PCB desorption study were used for model simulation.

The same modeling structure for the static deployment was employed for the vibrating system when motors are in the pause mode. We assumed that vibration mixes up and increases the sediment concentration at the vicinity of the polymer to the initial concentration in sediment. This assumption was validated by visual observation of the vibrating system in our previous work (Jalalizadeh and Ghosh[1]), which indicated that the extent of fluidized mixing by vibration is at least 1 cm from the surface of the device. Vibrating motors in the previous work had smaller amplitude of vibration (6 G) and the sediment slurry had similar porosity and density compared to the current study.

For the well-mixed system mass transfer was assumed to be limited by the polymer side. Since sediment is perfectly mixed, porewater concentration remains constant and equal to the initial value during deployment time. In addition, local equilibrium was assumed between sediment particles and porewater as mixing brings large volume of sediment to the vicinity of the polymer and kinetics are fast enough to appear close to instantaneous equilibrium.

Model equations were solved in Matlab using an explicit, finite-difference numerical modeling technique (Crank[15]). The equations and the details of parameter estimation, numerical solution, and Matlab codes are indicated in the Supporting Information.

6.3- Results and discussion

PCB Concentration in Sediment. As shown in Figure 6.2, hexa-, hepta-, and octachloro- PCBs were the most abundant homologs in the sediment. Mono- and dichloro- PCBs were not detected, and the total PCB concentration was 88 ng/g in the sediment. This sediment sample was found to be suitable for the present study because it had a relatively low level of PCBs (pushing our analytical effort) and our target homologs were dominant in sediment (mimicking PCDD/Fs).
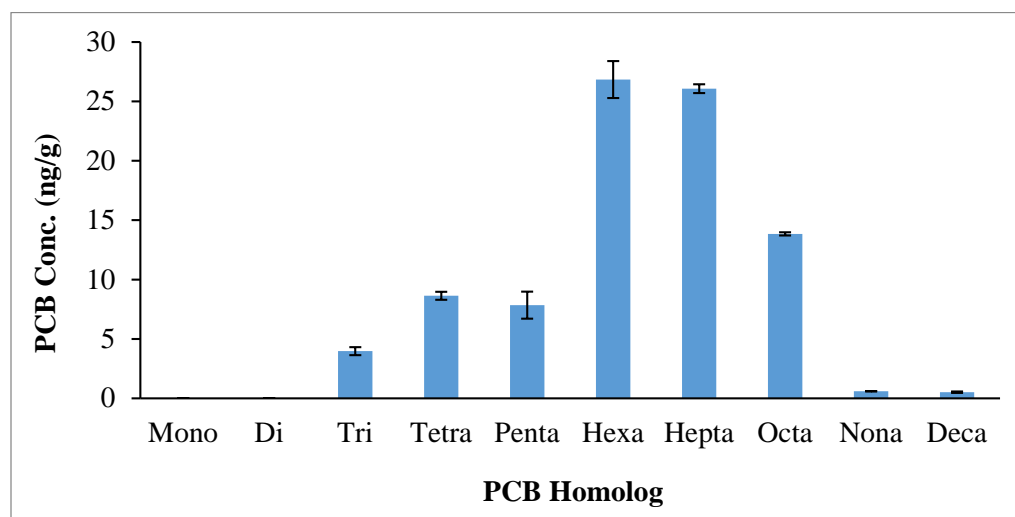
Figure 6.2. PCB Homolog distribution in sediment based on the mean of three measurements

Effect of Vibration with High Frequency on PCB Uptake into PE. The uptake profiles of six PCB congeners (each representing a homolog group) are compared in static, vibrating and well-mixed systems in Figure 6.3. Since measurements of PE uptake in static system from experiment 1 and 2 were not significantly different for all PCBs (Supporting Information Table S6.4), only the results from experiment 1 are shown for the static deployment. The concentrations reported are in ng/g PE. PCBs had very slow uptake rates into PE in the static exposure system. Periodic vibration of the PE sampler with high frequency resulted in much faster uptake compared to static deployment for all congeners. For example, after 28 days of deployment, the fractional uptake of PCB 99, PCB 132, and PCB (87+182) were 37%, 26%, and 22%, respectively in the static system compared to 100%, 85%, and 72% in the vibrating system. All PCBs reached to 95 – 100% of equilibrium after 56 days of deployment in the high frequency vibrating system. This is while, none of the congeners reached to more than 50% of equilibrium in static deployment for the same period. For example, the uptake of PCB 201 after 56 days was only 30% of equilibrium in static exposure compared to 100% in the vibrating system. Even after 7 days of exposure, the vibrating system reaches 35% of equilibrium for PCB 201 compared to 16% in the static system. Thus, with vibration it is apparent that *in situ* measurements of the full range of PCB congeners in sediments would approach very high fraction equilibrium allowing more accurate estimation of the existing porewater concentration in sediment.

In the well-mixed system, no change in the PE concentration was observed for any of the congeners after 28 days (PE concentrations after 28 and 56 days of exposure were not significantly different as shown in Supporting Information Table S6.2). Thus, PE concentrations from fully mixed system after 56 days of exposure were chosen as equilibrium concentrations for all PCB congeners.
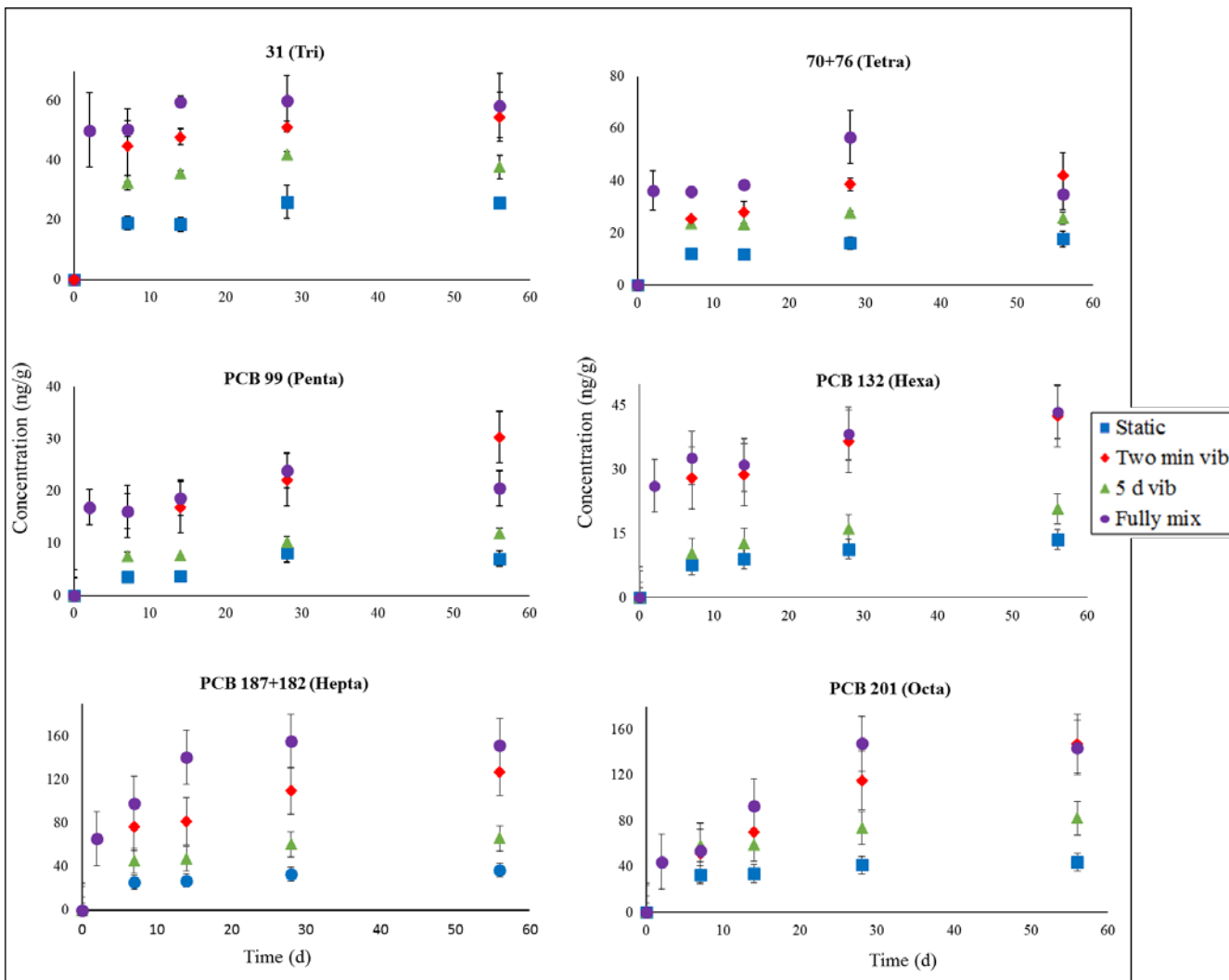
Figure 6.3. Comparison of PCBs uptake into PE in static, vibrating, and fully mixed systems

<u>Effect of Vibration with Low Frequency on PCB Uptake into PE.</u> The fractional uptake of all PCBs in the low frequency vibrating system improved within a factor of 1.5 and 2 over the static system after 28 days (Figure 6.2, and Supporting Information Figures S6.1-S6.3). However, all PCBs reached to only 30% to 60% of equilibrium in the vibrating system, except for PCB 31, PCB 70+76, and PCB 185 that reached to approximately 70%. Even after 56 days the fractional uptake of all PCBs were between 40% and 72% (77% for PCB 185). These results indicated that the motors need to vibrate with pause durations less than 5 days in order to improve the uptake of

37

larger molecular weight PCBs (hexa-, hepta-, and octachloro-congeners) to more than 60% in 28 days.

Estimation of PCB desorption rate constants. Modeling of uptake rates into PE were conducted for PCB 128 (2,2′,3,3′,4,4′-hexachlorobiphenyl; log K_{ow} = 6.74), PCB 183 (2,2′,3,4,4′,5′,6-heptachlorobiphenyl; log K_{ow} = 7.2), and PCB 194 (2,2′,3,3′,4,4′,5,5′-octachlorobiphenyl; log K_{ow} = 7.8). Thus, the fast (k_f) and slow (k_s) desorption rate constants are only reported for the three mentioned PCBs (Supporting Information Table S6.8) and only K_f values were used for model simulation.

The measured K_fs for three PCBs were approximately one order of magnitude larger compared to the reported rates by Zimmerman et al.[16] The authors measured the desorption rate of PCBs from an untreated sediment collected from the intertidal region of South Basin at Hunters Point. K_f values from this study were also two orders of magnitude larger compared to the rates measured by Ghosh et al.[17] in field-contaminated sediment obtained from Aluminum Corporation of America (at 25˚C).

Modeling the Uptake of PCBs. Experimental and modeling results for PCB 128, PCB 183, and PCB 194 in static, vibrating and well-mixed systems are indicated in Figure 6.4. As shown in the Figure, modeling results had good agreement with the uptake rate of three PCBs in static and vibrating systems with low and high frequency of vibration.

The well-mixed model over predicted the earlier time point measurements (Figure 6.3), likely due to slow desorption of PCBs from sediment particles or inefficient mixing of the sediment. Slower kinetics of larger hydrophobic chemicals in well-mixed system has been also observed in previous studies (Jalalizadeh and Ghosh[1]; Arp et al.[18]). Deviations between the model simulation and experimental data were more obvious for more hydrophobic PCBs (PCB 183 and PCB 194), as mass transfer of these compounds is mostly controlled by the sediment-side (Jalalizadeh and Ghosh[1]).
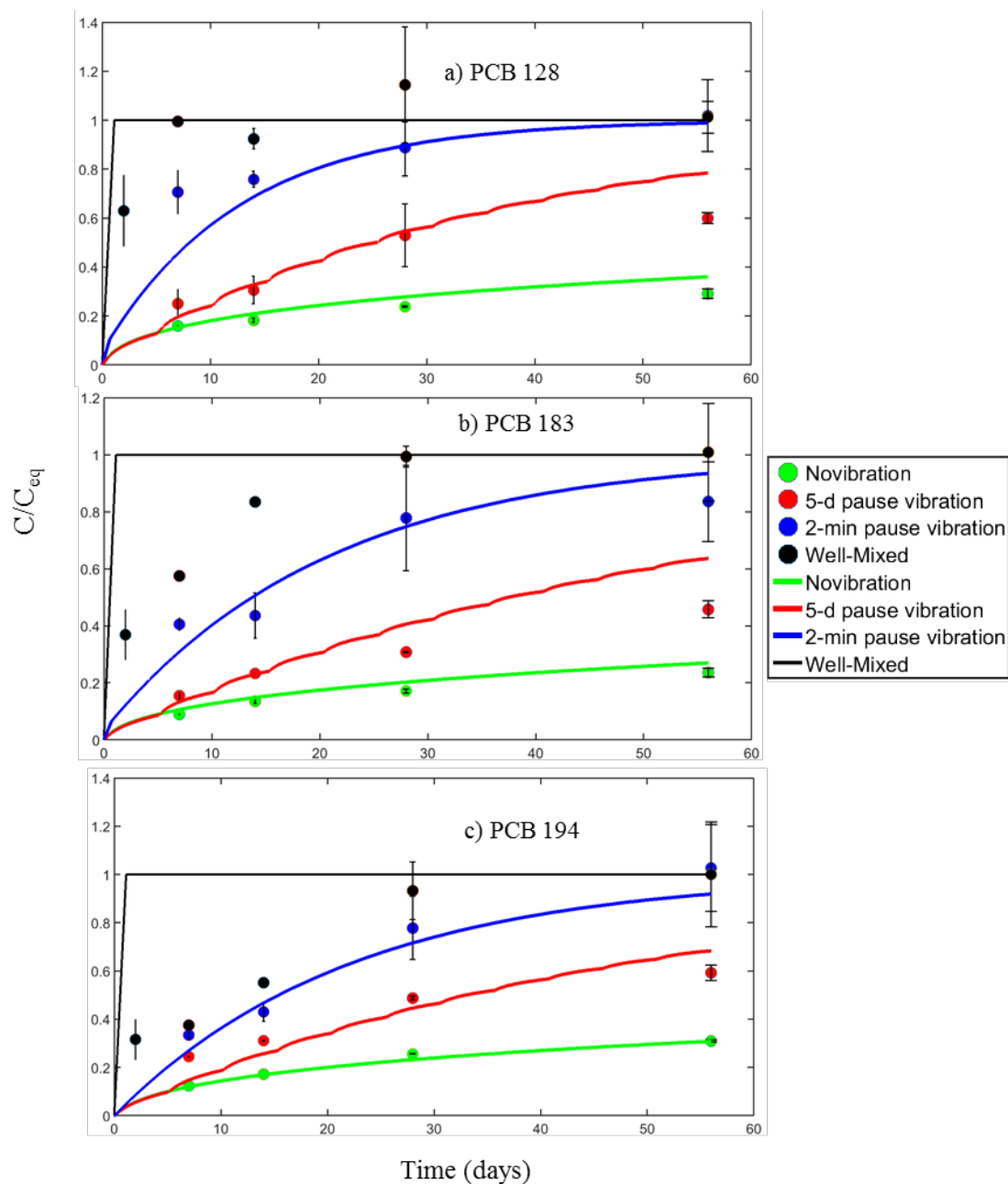
Figure 6.4. Fractional uptake of PCB 128 (a), PCB 183 (b), and PCB 194 (c) in PE passive sampler in four differently exposed systems. Experimental data have been shown by symbols, and fast desorption model simulations have been shown by lines.

Effect of Vibration on PRC Loss from PE. The fraction of PRC remaining in PE (f_{PRC}) was measured for the four PRCs in static, vibrating, and well mixed systems (Figure 6.5). The fractional loss of lower molecular weight PRCs such as PCB 29 and PCB 69, were 55% and 46% after 28 days of deployment in the static system, respectively. However, both PCBs were 100% dissipated from PE after the same exposure time in the high frequency (2 min-pause) vibrating system. The effect of vibration on PRC loss was more evident for larger molecular weight PRCs.

For example, the fractional loss was increased from 22% to 87% for PCB 155 (hexachloro-congener) and from 12% to 63% for PCB 192 (heptachloro-congener) after 28 days. As shown in Figure 6.5, f_{PRC} for PCB 29 and 69 were nearly identical in high frequency vibrating and well-mixed exposures. In fact, more than 95% of both PRCs were lost in the vibrating system only after 7 days of exposure. The differences between f_{PRCs} in high frequency vibrating and well mixed systems were larger for more hydrophobic PRCs (PCB 155 and PCB 192). However, the fractional losses of these PRCs were still reasonably large in the high frequency vibrating system (63% after 28 days and 80% after 56 days for PCB 192).

The measured f_{PRC} values in static system from experiment 1 and 2 were identical for all PRCs as compared in the Supporting Information Tables S6.5 and S6.6. Thus, only the results from experiment 1 are shown for the static deployment in Figure 6.4. As indicated in the figure, vibration with low frequency (5 d-pause) was not as effective in improving the dissipation rate of high molecular weight PRCs. For example, the fractional losses of PCB 29 and PCB 69 were increased to approximately 70% after 28 days in the low frequency vibrating system. However, the fractional loss was less than 60% for 155, and only 25% for PCB 192. We anticipate that higher fractional loss of PRCs and closer approach to equilibrium for the analytes would result in greatly improved accuracy of porewater measurement. This hypothesis has been tested using PRC data in high and low frequency vibrating systems in the following section.
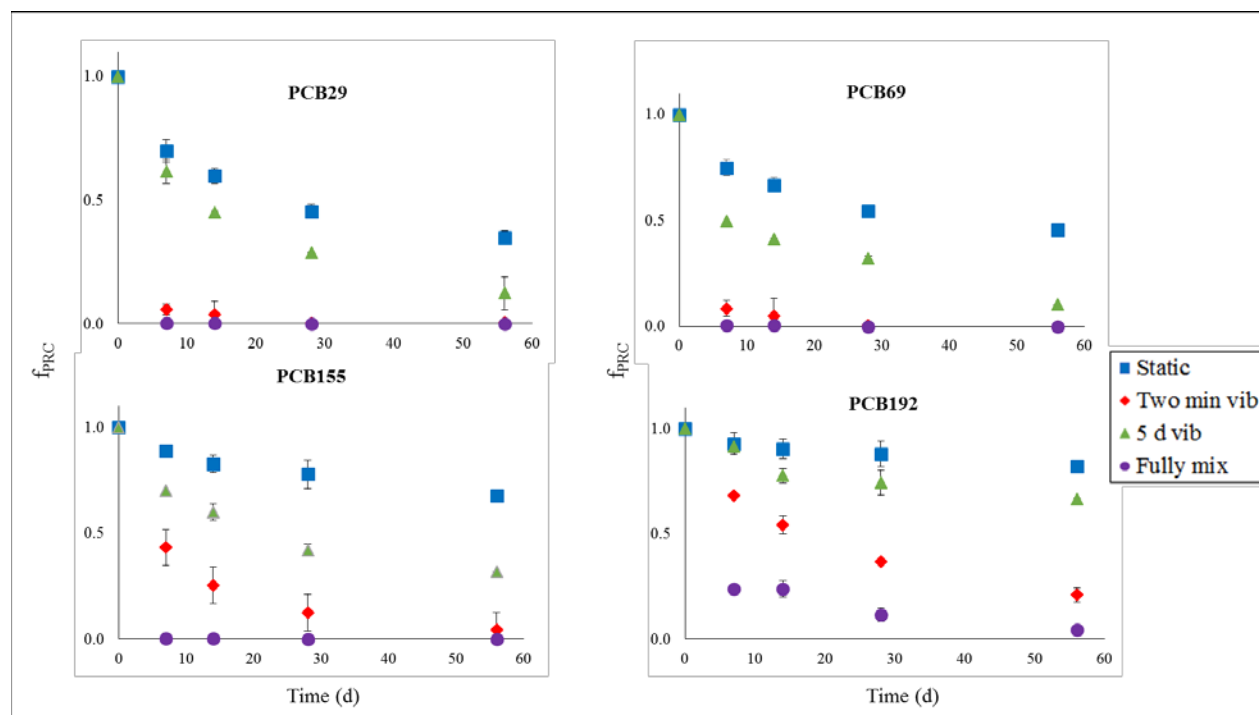
Figure 6.5. Comparison of PRC fraction remaining in PE (f_{PRC}) in static, vibrating, and fully mixed systems

Prediction of Porewater Concentration Based on Static vs. Shaken Deployment. PCB concentrations in PE measured using the static and vibration deployment were corrected for non-equilibrium based on the fractional loss of PRCs. Since four PRCs were available for use in correction, the method by Fernandez et al. [6] was used as described in the methods section. PE equilibrium concentrations were also determined from the 56-day well-mixed deployment. PCB concentrations in PE were converted to C_{free} using the individual congener PE-water partition constants (K_{PEw}). K_{PEw} values for PCB congeners were estimated from the correlation provided in Ghosh et al.[19] (Supporting Information Table S6.7). To compare the accuracy of the porewater estimations, the estimated C_{free}s based on PRC-corrected concentrations in PE were compared to the actual measurements of C_{free} from the well-mixed system. The PRC-corrected C_{free}s measured with 28- and 7-day static and vibrating passive samplers are plotted in Figure 6.6 and Figure 6.7, respectively and compared against the true C_{free}s. In both figures, the PRC-corrected C_{free}s that are statistically different from the true values (with alpha level of 5%) are indicated with a star. Since the *in situ* exposures were performed in lab mesocosms with static overlying water, we expect that the porewater concentrations in sediment would approach thermodynamic equilibrium with the sediment, especially for the strongly hydrophobic and recalcitrant compounds. Thus, porewater concentrations measured in the well-mixed equilibrium exposures should closely represent the true porewater concentration to be expected in the static and vibrating passive sampler deployments.
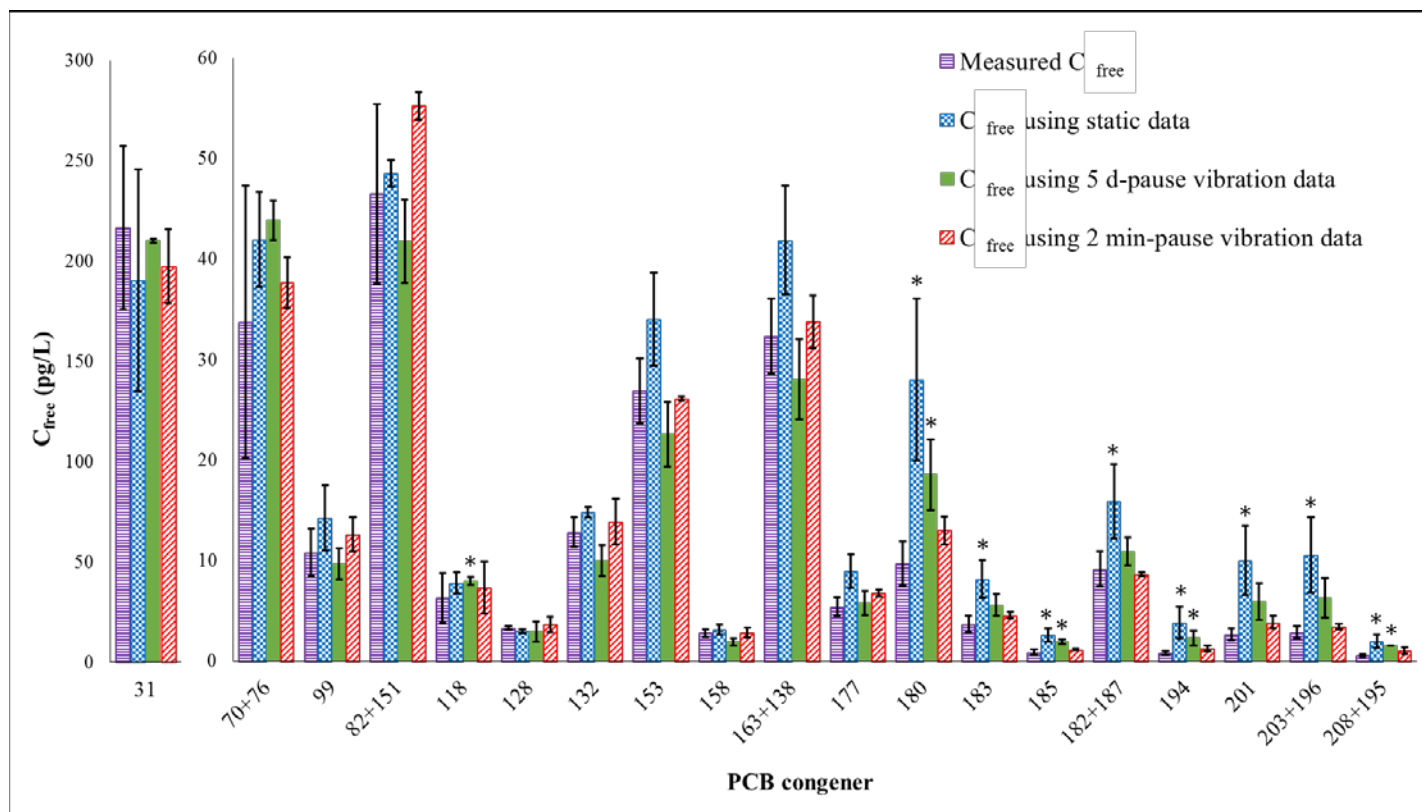
Figure 6.6. Comparison of PRC-corrected C_{free} using 28-day static and vibrating passive samplers with measured C_{free}. The corrected C_{free} was calculated based on the PRC-corrected PE equilibrium concentration in static and vibrating systems. The measured C_{free} was estimated based on the measured equilibrium

concentration in PE after 56 days of deployment in the fully mixed system. The corrected concentrations that are statistically different from the measured C_{free} values (with alpha level of 5%) are indicated with a star
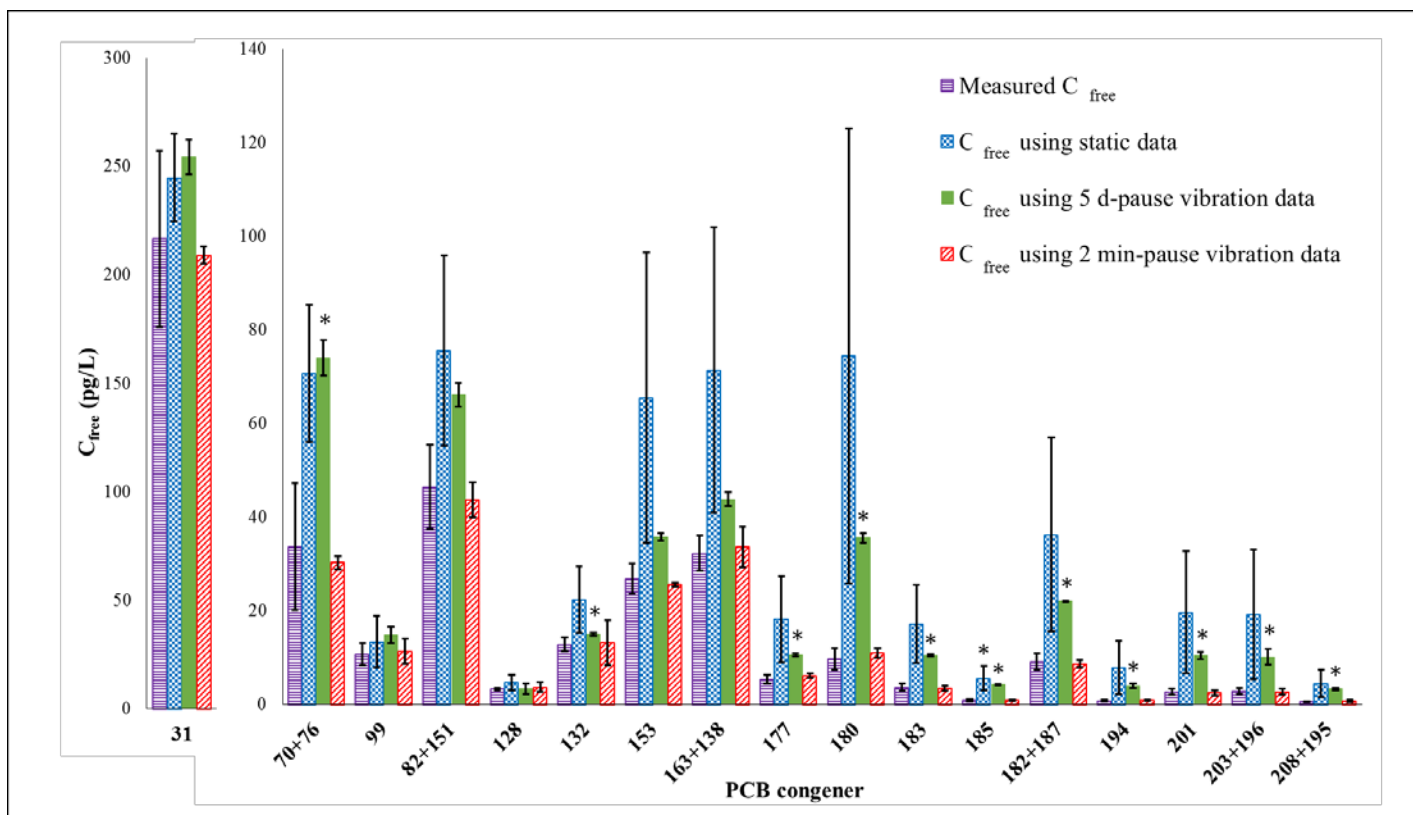
Figure 6.7. Comparison of PRC-corrected C_{free} using 7-day static and vibrating passive samplers with measured C_{free}. The corrected C_{free} was calculated based on the PRC-corrected PE equilibrium concentration in static and vibrating systems. The measured C_{free} was estimated based on the measured equilibrium concentration in PE after 56 days of deployment in the fully mixed system. The corrected concentrations that are statistically different from the measured C_{free} values (with alpha level of 5%) are indicated with a star

As shown in Figure 6.6, the tri-, tetra, and pentachloro-congeners are generally well predicted by both static and vibration passive samplers (within a factor of 2). For these moderate K_{ow} congeners the PRC losses are high in either system and correction for non-equilibrium is relatively accurate. The measurements using static deployment start deviating strongly for the dominant higher chlorinated PCBs. There appears to be a consistent positive bias for the estimation from static deployment. The error bars are also large, indicating poor precision. The PRC-corrected C_{free}s from the low frequency vibration deployment are more accurate and have smaller error bars compared to measurements from the static deployment. However, these estimations are statistically different from the true values for highly chlorinated congeners, as shown in Figure 6.6. For example, for the dominant heptachloro-congener, PCB 180, C_{free} estimation based on static and low frequency vibration deployment is nearly 4-fold and 3-fold higher compared to the true C_{free}, respectively. In the case of the dominant octachloro-congener, PCB (203 + 193), the PRC-corrected C_{free} based on static and low frequency vibration

deployment is nearly 5-fold and 4-fold higher than the true measurement, respectively. In comparison, the PRC-corrected C_{free}s from the high frequency vibration deployment are indistinguishable from the true values for all PCBs.

As expected, C_{free} estimations using the 7-day deployment data in static system were less accurate compared to the estimations using 28-day deployment data, especially for higher molecular weight PCBs (Figure 6.7). For example, for hexa-, hepta-, and octachloro-congeners deviations of C_{free} from true values were within a factor of 1.4 to 10 using 7-day, and within a factor of 1.1 to 5 when using 28-day data. As indicated in Figure 6.6, PRC-corrected C_{free} values estimated with static deployment are not statistically different from the measurements, as the estimated concentrations have very poor precisions. Higher precisions in estimation of C_{free} using the low frequency vibrating deployment results in concnetrations that are statistically different from the true values. This is while, predicted C_{free}s in the latter system has less deviations from the measured values. Similar to the 28-day deployment results, the predicted C_{free}s for all PCBs were statistically indistinguishable from the true values when using the high frequency vibrating passive sampler.

6.4- Implications

Strongly hydrophobic compounds such as large molecular weight PCBs (hexa- to octachloro biphenyls) in sediment porewater are known to be difficult to measure *in situ* due to slow mass transfer. The slow mass transfer also introduces errors when correcting for non-equilibrium using the loss kinetics of PRC compounds. In chapter 5 we demonstrated the development of a periodically vibrating platform for the *in situ* deployment of passive samplers and demonstrated that the technology enhances the mass transfer of PAHs into passive samplers. In this chapter, we extend the work by presenting the applicability of the vibrating platform in sediment contaminated with strongly hydrophobic PCBs. The current platform is more robust compared to the one in chapter 5 and enables deployment of larger passive samplers to target low concentrations in sediment. The proposed platform allowed accurate measurement of porewater concentrations of large molecular weight PCBs in short deployment times and reduced the errors with the PRC correction method. Results from this study indicate that for the strongly hydrophobic congeners, the static deployment is prone to a strong positive bias in estimation of porewater concentrations. The estimations were improved even with a very low frequency of vibration (with 5 d-pause). However, the predicted concentrations were still statistically different from the measured values. High frequency vibration deployment (with 2 min-pause) in the other hand, provided accurate measurement of porewater concentrations only after 7 days of deployment. Shorter deployment times lower the risk of loss, destruction, and vandalism of deployed passive sampler platforms in the field. In general, the findings from this study, pave the way for extension of the *in situ* passive sampling approach to full range of PCBs, and possibly PCDD/Fs as well.

6.5- Literature Cited

Jalalizadeh, M.; Ghosh, U. *In Situ* Passive Sampling of Sediment Porewater Enhanced by Periodic Vibration. *Environ. Sci. Technol.* **2016**, 50, 8741−8749.

(2) Mayer, P.; Parkerton, T. F.; Adams, R. G.; Cargill, J. G.; Gan, J.; Gouin, T.; Gschwend, P. M.; Hawthorne, S. B.; Helm, P.; Witt, G.; You, J.; Escher, B. I. Passive sampling methods for contaminated sediments: scientific rationale supporting use of freely dissolved concentrations. *Integr. Environ. Assess. Manag*. 2014, DOI: 10.1002/ieam.1508.

(3) Peijnenburg, W. J. G. M.; Teasdale, P. R.; Reible, D.; Mondon, J.; Bennett, W. W.; Campbell, P. G. C. Passive sampling methods for contaminated sediments: state of the science for metals. *Integr. Environ. Assess. Manag*. 2014, DOI: 10.1002/ieam.1502.

(4) Lampert, D. An assessment of the design of *in situ* management approaches for contaminated sediments. Ph.D. Thesis, The University of Texas at Austin, May 2010.

(5) Hawthorne, S. B.; Grabanski, C. B.; Miller, D. J. Measured partitioning coefficients for parent and alkyl polycyclic aromatic hydrocarbons in 114 historically contaminated sediments: Part 1. Koc values. *Environ. Toxicol. Chem*. **2006**, 25, 2901–2911.

(6) Fernandez, L. A.; Harvey, C. F.; Gschwend, P. M. Using performance reference compounds in polyethylene passive samplers to deduce sediment porewater concentrations for numerous target chemicals. *Environ. Sci. Technol.* **2009**, 43, 8888–8894.

(7) Cornelissen, G.; Wiberg, K.; Broman, D.; Arp, H. P. H; Persson, Y.; Sundqvist, K.; Jonsson, P. Freely dissolved concentrations and sediment-water activity ratios of PCDD/Fs and PCBs in the open Baltic Sea. *Environ. Sci. Technol.* **2008**, 42 (23), 8733−8739.

(8) Cornelissen, G.; Pfttersen, A.; Broman, D.; Mayer, P.; Breedveld, G. D. Field testing of equilibrium passive samplers to determine freely dissolved native polycyclic aromatic hydrocarbon concentrations. *Environ. Toxicol. Chem.* **2008**, 27 (3), 499−508.

(9) Fagervold, S. K.; Chai, Y.; Davis, J. W,; Wilken, M.; Cornelissen, G., Ghosh, U. Bioaccumulation of polychlorinated dibenzo-p-dioxins /dibenzofurans in E. fetida from floodplain soils and the effect of activated carbon amendment. *Environ Sci Technol*. **2010**, 44,5546-5552.

(10) Chai, Y.; Currie, R. J.; Davis, J. W.; Wilken, M.; Martin, G. D.; Fishman, V. N.; Ghosh, U. Effectiveness of activated carbon and biochar in reducing the availability of polychlorinated dibenzo-pdioxins/dibenzofurans in soils. *Environ. Sci. Technol*. **2011**, 46 (2), 1035−1043.

(11) Gschwend, P. M.; Macfarlane, J. K.; Reible, D. D.; Lu, X.; Hawthorne, S. B.; Nakles, D. V.; Thompson, T. Comparison of polymeric samplers for accurately assessing PCBs in pore waters. *Environ. Toxicol. Chem.* **2011**, 30 (6), 1288−1296.

(12) Beckingham, B.; Ghosh, U. Field-scale reduction of PCB bioavailability with activated carbon amendment to river sediments. *Environ. Sci. Technol*. **2011**, 45 (24), 10567−10574.

(13) Ghosh, U.; Talley, J. W.; Luthy, R. G. Particle-scale investigation of PAH desorption kinetics and thermodynamics from sediment. *Environ. Sci. Technol*. 2001, 35, 3468−3475.

(14) Tcaciuc, A. P.; Apell, J. N.; Gschwend, P. M. Performance Reference Compound Calculator for Use in Support of PE Passive Samplers. http://www.serdp.org/Program-Areas/Environmental-Restoration/Contaminated-Sediments/ER-200915.

(15) Crank, J. *The Mathematics of Diffusion*, 2nd ed.; Oxford University Press: Oxford, 1975; p 414.

(16) Zimmerman, J. R.; Ghosh, U.; Millward, R. N.; Bridges, T. S.; Luthy, R. G. Addition of carbon sorbents to reduce PCB and PAH bioavailability in marine sediments: Physicochemical tests. *Environ. Sci. Technol*. **2004**, 38 (20), 5458–5464.

(17) Ghosh, U.; Weber, A. S.; Jensen, J. N.; Smith, J. R. J. Congener level PCB desorption kinetics of field-contaminated sediments. *Soil Contamination.* 1999, 8, 593-613.

(18) Arp, H. P. H.; Hale, S. E.; Elmquist Kruså, M.; Cornelissen, G.; Grabanski, C. B.; Miller, D. J.; Hawthorne, S. B. Review of polyoxymethylene passive sampling methods for quantifying freely dissolved porewater concentrations of hydrophobic organic contaminants. *Environ. Toxicol. Chem.* **2015**, 34, 710−720.

(19) Ghosh, U.; Kane Driscoll, S.; Burgess, R. M.; Jonker, M. T. O.; Reible, D.; Gobas, F.; Choi, Y.; Apitz, S. E.; Maruya, K. A.; Gala, W. R.; Mortimer, M.; Beegan, C. Passive sampling methods for contaminated sediments: Practical guidance for selection, calibration, and implementation. *Integr. Environ. Assess. Manage*. **2014**, 10, 210−223.

7.0 RESEARCH OBJECTIVE #3: Evaluate a range of polymer types for use as passive equilibrium samplers for methylmercury.

7.1 Introduction

The most relevant form of mercury from the standpoint of human health risk assessment is monomethylmercury, *i.e.*, CH_3Hg^+ and CH_3Hg-R, hereafter collectively abbreviated MeHg (Sunderland et al. 2007). It is a potent neurotoxin that is capable of crossing biological membranes and the blood-brain barrier. MeHg is not typically introduced to the environment due to direct contamination, but rather as a result of the methylation of inorganic mercury(II) (Hg_i) by anaerobic microorganisms in sediments and saturated soils (Gilmour et al. 2013). Methylmercury bioaccumulates in aquatic food webs through direct uptake by single cell organisms, by benthic organisms and by efflux to the water column (e.g. Williams et al. 2010; Taylor et al. 2014). For risk assessors and decision makers, it is critical to be able to predict both net MeHg production and its bioavailability to food webs.

MeHg complexation in sediments and soils. In natural waters, both Hg_i and MeHg form a wide variety of complexes with ligands such as Cl^-, OH^-, and SH^-. Due to the extremely high affinity of the soft acid-soft base associations involved, reduced sulfur of all kinds tends to dominate mercury speciation in sediments, sediment pore waters and many surface waters (Hsu-Kim et al. 2013). This includes inorganic sulfides, simple organic thiols such as the amino acids cysteine and glutathione, and the reduced sulfur functional groups associated with dissolved organic matter (DOM) (Skyllberg et al. 2006; Haitzer et al. 2002). Generally, DOM is defined operationally as the organic fraction that passes a 0.45 μm filter (Aiken et al. 2011). A large part of this fraction comprises humic substances, which occur as complex mixtures of aliphatic and aromatic compounds with varying levels of solubility, and molecular weights ranging from a few hundred Daltons to many thousands (Liao et al. 1982). The sulfur content of humic substances is typically around one percent and comprises a variety of chemical functionalities, including sulfides, thiols, and thiophenes under reducing conditions and sulfonates and sulfates under oxidizing conditions (Xia et al. 1998). Conditional stability constants for DOM complexes with Hg_i and MeHg are very high (approaching those reported for simple thiols), suggesting that thiol functionalities are the primary sites of interaction with DOM molecules (Schwarzenbach and Schellenberg 1965; Amirbahman et al. 2002; Haitzer et. al 2002). Because of the considerable heterogeneity of reduced sulfur and DOM ligands in natural waters, Hg_i and MeHg species can occupy a broad range of molecular weights, ionic charges, and hydrophibicities. Hg_i speciation is further complicated by the formation of non-equilibrium, mercury-sulfide polynuclear clusters and nanoparticles, whose dynamic interactions are an area of ongoing research (Deonarine et al 2009; Hsu-Kim et al. 2013).

In most natural waters, even high chloride marine systems, high molecular weight DOC complexes are the dominant form of both Hg and MeHg (e.g. Han et al. 2005; Skyllberg et al. 2010). In anoxic sediments and soils, where sulfide is commonly present, nanoparticulate HgS may dominate, but it is generally associated with DOC colloids (Aiken et al. 2011). The role of sulfides and nanoparticles in MeHg complexation in sulfidic systems has received little attention.

MeHg bioavailability to aquatic food webs. For toxic trace metals, bioavailability has often been modeled based on an estimate of concentration of the free ion (e.g. AVS/SEM model; Allen et al. 1993; or the Sediment BLM; Di Toro et al., 2005). However, free $Hg2+$ and $MeHg+$ ions are present in natural waters at vanishingly small concentrations (commonly $< 10^{-25}$ M). Therefore, it is ineffective and probably inappropriate to model Hg and MeHg bioavailability based on their free ions.

Unfortunately, the MeHg uptake mechanism(s) by single cell organisms at the bottom of aquatic food webs remain effectively unknown, and so bioavailable species have been evaluated based on empirical observations with selected complexes. An early paradigm was bioavailability of neutrally charged species (like MeHgCl and $HgCl_2$) via passive diffusion (Mason et al. 1996; Benoit et al. 1999), and early models for bioavailability were based on the modeled equilibrium concentrations of these species. Several studies in the last decade support active, or at least facilitated, uptake of MeHg by algae (Pickhardt and Fisher 2007; Le Faucheur et al. 2011, 2014) and Hg(II) uptake by bacteria (Golding et al. 2002; Schaefer et al. 2009). One well-known MeHg active uptake system is the broad Hg transporter (*merE*) in the mercury detoxification system of Hg-resistant bacteria (Boyd and Barkay 2012). No other Hg or MeHg transporters have been identified.

Empirical measurements show that MeHg salts (MeHgOH, MeHgCl, $MeHgNO_3$) are highly available for uptake by microbes (Benoit et al. 1999; Hsu-Kim et al. 2013). It is possible that algae can readily access MeHg bound to small thiols, as bacteria can do for Hg-cysteine (Schaefer et al. 2009; Gilmour et al. 2011; Graham et al. 2012). In oxic natural waters, the presence of dissolved organic matter (DOM) inhibits but does not block MeHg uptake by algae (Luengen et al. 2012) and bacteria (Ndu et al. 2012) suggesting that these large complexes are not directly taken up. However, DOC can dramatically enhance the bioavailability of Hg(II) to microbes in sulfidic sediments and soils, by slowing the precipitation of particulate HgS, keeping Hg(II) in the aqueous phase (Graham et al. 2012; Zhang et al. 2012). We don't know how microbes access Hg from these high mw and/or nanoparticulate forms. Most likely they are in rapid equilibrium with smaller bioavailable forms; alternatively some exchange may be occurring on cell surfaces.

Benthic invertebrates have many uptake routes for MeHg, including ingestion of MeHg associated with sediment organic and inorganic matter (e.g. Gagnon et al. 1997), grazing from the water column, and probably uptake from dissolved and particulate MeHg-DOC complexes

(Williams et al. 2010; Taylor et al. 2014), although DOC can reduce MeHg bioavailability (Lawrence et al. 2001). Laboratory toxicity and exposure tests rarely take all of these routes into account (Wang and Fisher et al. 1999). Development of PS that mimics bioavailable MeHg would allow at least partial replacement of expensive exposure studies, and a wider spatial and temporal coverage for lower cost.

To summarize, MeHg may be available to aquatic food webs from colloids and nanoparticles in addition to salts and low molecular weight thiols, but bioavailability from these classes varies, and the mechanism(s) of their bioavailability are not understood. All of this implies a high degree of uncertainty in modeling and quantifying MeHg bioavailability, and in developing passive sampling devices that assess or mimic the bioavailable pool.

Measuring MeHg bioavailability. Pore water MeHg concentrations and/or sediment/water MeHg partition coefficients (K_D) have proved the most accurate indicators of MeHg bioavailability to benthic organisms to date, but remain uncertain predictors (Gilmour et al. 2013). "Bioreporters" – microbes genetically engineered with a Hg or MeHg transporter (Scott et al. 2001; Golding et al. 2002; Dahl et al. 2011; Ndu et al. 2012)– can provide information of the concentration of available forms, but only forms available to those specific transporters. Active sampling methods such as pore water withdrawal via syringe ("sippers") or sediment core removal and centrifugation can be labor intensive and may obscure important temporal, spatial, and speciation information. They also do not provide a measure of the bioavailable fraction of Hg or MeHg in pore water. Equilibrium dialysis chambers ("peepers") exclude (or limit) higher molecular weight MeHg complexes that may have some bioavailability.

Development of passive samplers for Hg/MeHg. The two major strategies for passive sampling of contaminants are equilibrium samplers and diffusion based samplers, such as DGT or Chemcatchers®. Equilibrium samplers are mainly used for HOCs, for which the freely dissolved concentration in sediment pore waters is widely used as a proxy measure of bioavailability. Equilibrium samplers make use of thin polymers sheets with partition coefficients for HOCs similar to their binding constants to sediment organic matter. They effectively concentrate dissolved-phase HOCs onto the polymers sheets, which can then be extracted for analysis. Because of the relatively small mass to surface area ratio of the polymer exposed to sediment, the samplers don't deplete pore water pools, or create concentration gradients that could lead to significant HOC depletion from the adjacent sediments. If diffusive boundary layer (DBL) issues are overcome, and the samplers come to equilibrium, the equation for predicting aqueous HOC concentrations is simple:

Cpw = Csorbent/K(sorbent-water)

Here, C is the concentration of the HOC of interest, and K is the partition coefficient between water and the polymer sorbent. However, the bioavailable fraction is MeHg in natural waters is

poorly defined, and is probably not fully reflected by the "freely dissolved" fraction. Performance reference materials are used to check for equilibrium and to correct for non-equilibrium when needed.

Non-equilibrium diffusion samplers have been the more common approach for metals. These methods are based on the movement of metal ions through an ion-permeable diffusive layer and accumulation in the binding resin behind. The diffusion layer limits the size of the molecules that penetrate the samplers, generally limiting the sampling to low molecular weight compounds. Diffusion-based samplers for metals are designed to estimate the "labile" fraction of metals of interest. This fraction is empirically defined, and depends on the sampler design and chemistry. It includes free metal cations, metal salts and may include some low molecular weight compounds depending on the diffusion gel. The accumulation rate and selectivity of the device for different metal complexes are regulated by the choice of materials for the diffusion and binding layers. Diffusions layers can be made with materials or different effective pore sizes, and materials can be selected to limit sorption of the target compound. The sorptive ligands in the binding layer can also be adjusted for specific chemicals.

Diffusion-based samplers are designed for use as non-equilibrium, samplers. The binding layer, containing a strong metal-binding ligand, and often 100's of μm thick, acts effectively as an infinite sink. The "labile" concentration of contaminant in the aqueous phase (C_{DGT}) is calculated based on a lab-calibrated diffusion rate (in cm sec-1) through the diffusion gel, which generally has long path length (100's of μm) in comparison to the DBL.

The estimated concentration of "labile" metal (C_{DGT}) depends on both the size and the binding strength of metal complexes in solution. If metal-ligand complexes that don't penetrate the diffusion gel dissociate rapidly and completely in solution, the mass of metal accumulated in the DGT binding layer is the sum of the fluxes from each species present. Effective fluxes from species with higher binding strengths will be lower (fill eqts from Holger paper). Work with several metals other than Hg suggests that DGT assesses most of the <1kDa fraction in natural, oxic surface waters (Davison and Zhang 2012).

By testing DGT metal accumulation against a range of DOC concentrations, the fraction of metal complexed to DOC can be estimated. Further, a comparison of C_{DGT} with the molar ratio of metal to DOC can provide information on DOC binding site affinities (Town et al. 2009).

Additionally, adjustment of the pore size in the diffusion gel may allow some fraction of metal-DOC or metal nanoparticles to penetrate the gel (Fernández-Gómez et al 2014). Agarose pore sizes may be as large as 74 nm, while standard DGT polyacrylamide gels may be <2 nm. Particles with a diameter of 5–6 nm should have a diffusion coefficient in water approximately 8 times less than that of free metal ions (Davison and Zhang 2012). Thus readily exchangeable metals on DOC, and metal-DOC complexes may be accessible by DGT. However, the samplers would need to be calibrated for each site and against a range of DOC concentrations in order to

estimate what complexes comprise C_{DGT}, and in what ratio.

Chemcatchers (Vrana et al. 2005) also have diffusion and binding layers, made from commercially-available thin membranes. The diffusive boundary layer in the aqueous phase becomes particularly important for these thin diffusion layers. For Chemcatcher-type samplers, Cw is estimated from an empirical "sampling rate," Rs, with units of volume sampled over time. Rs is also derived from laboratory calibration:

m = C Rst

Where m equals the mass of analyte accumulated in the receiving phase after an exposure time (t) and C is the analyte concentration in solution and Rs is sampling rate in ml/h

Of these approaches, DGT has been the most fully developed for inorganic HgII (hereafter HgII) and MeHg (Docekalova et al. 2005; Divis et al. 2005; Clarisse et al. 2009, 2011; Divis et al. 2010; Gao et al. 2011; Fernández-Gómez et al. 2011, 2014, 2015; Pelcova et al. 2015; Noh et al. 2015). Several adjustments to standard metals DGT have been made. Ideally a diffusion gel should have diffusion coefficient the same as water, and ions should move freely through the gel to the binding layer. However, Docekalov et al. (2005) measured a concentration factor of 700 for Hg(II) in the polyacrylamine gel commonly used in DGT, relative to water (Hg binds amide groups in the polyacrylamide). They switched to agarose diffusion gel, which showed only a factor of 4 concentrations from water. Membrane properties have also been adjusted to also limit sorption (e.g. Clarisse et al. 2006; Fernández-Gómez et al. 2014). Several binding materials have been tested to improve sorption and specificity (Docekalov_et al. 2005; Clarisse et al. 2006; Divis et al. 2010; Gao et al. 2011; Fernández-Gómez et al. 2014). All of the most successful are some form of thiol, most effectively 3-mercaptopropyl-functionalized silica gel (Gao et al. 2011; Clarisse et al. 2009, 2011).

Some deployments of MeHg DGT samplers have predicted aqueous total MeHg concentrations reasonably well, especially in saline surface waters where MeHgCl may be an important complex (Clarisse et al. 2006; 2011; Noh et al. 2015). However, the effective diffusion rate for MeHg must be tested ahead of time in the lab for water evaluated (Noh et al. 2015). In high DOC waters, DGT samplers under predicts Cw, unless one assumes different diffusivities for MeHgDOC, as calibrates the samplers to the sample water. In one of only tests of DGT samplers for prediction of MeHg uptake by animals (Clarisse et al. 2009), DGT samplers predicted MeHg uptake by *Macoma balthica* under controlled conditions in the lab, across a wide range of salinities; but under predicted uptake at very low MeHg concentrations, or when DOC was added to the tests. DGT samplers specific for MeHg also predicted MeHg uptake by rice after the samplers were calibrated for the rice paddy soil pore waters (Liu et al. 2012). In sulfidic systems, DGT models do particularly poorly in predicting Cw (Clarisse et. al 2009). Laboratory studies show the presence of HgS nanoparticles in sulfidic samples deposit on the surface of samplers, slowing the migration of dissolved species into the samplers (Pham et al. 2015).

To summarize, the most developed passive sampling approach for MeHg, DGT, remains complex to use, but can provide estimates of bioavailable MeHg if the samplers are calibrated based on a specific measured diffusion rates for the study water. They provide uncertain results in with regard to the precise species of mercury sampled, although a range of deployment times and gel thicknesses can be used to help assess MeHg size, speciation and its relationship to bioavailability. DGT samplers require site-specific calibration (Pelcova et al. 2014; Noh et al. 2015). DGT does not directly access higher molecular weight complexes like MeHg-DOC colloids HgS nanoparticles that are potentially bioavailable forms of MeHg.

MeHg passive sampler development strategy. There remains a need for a simple, passive sampling system designed specifically to quantify the time-weighted average bioavailable MeHg concentration in a reproducible fashion. However, we still must define, at least empirically, the MeHg complexes and phases that are available to organisms, <u>We believe that one of the most important aspects of MeHg passive sampler development will be the use of a range of sampler types and chemistries to begin to understand and define the bioavailable pool of MeHg in sediments and soils.</u>

While our main goal is to develop a passive sampler that provides an estimate of the bioavailable fraction of MeHg, our near-term objective is to use a range of passive sampler chemistries and designs to assess the chemical and physical forms of MeHg available to organisms. This would be an improvement on current methods for MeHg, which assume the "freely dissolved" fraction is equivalent to the bioavailable pool.

Our general approach is to develop an equilibrium method in which the binding material mimics the chemistry and partition coefficient of natural MeHg ligands on cell surfaces. We chose an equilibrium method to try and avoid the limitations of methods that rely on kinetic calibrations for each potential MeHg complex. We are testing both diffusion-based and single-layer polymers gels in order to evaluate the bioavailability MeHg in colloids or nano-particles.

In this study, we began development of MeHg samplers by evaluating potential materials. Our goal in this research was to identify and prepare materials with affinity for MeHg and capable of accumulating detectable and reproducible amounts in proportion to aqueous concentrations. More specifically, we are working toward a small set of materials for testing against animal bioavailability. These materials should have a range of properties including:

- Partition coefficients close to the measured K for MeHg in natural sediments (10^3 to 10^5).
- Linear uptake isotherms across the concentration range of interest, i.e. from the pg/L range commonly found in natural uncontaminated sediment pore waters to the high ng/L concentrations found in the most contaminated pore waters.

- Capable of accumulating detectable and reproducible masses of MeHg in thin layer deployments (ultimately 10's of microns) at natural MeHg concentrations.
  - The absolute MeHg DLs in our lab are about 1-5 pg per sample. A good target for easy detection for labs with less sophisticated analytical methods (i.e. CVAf) would be ~0.1 ng per sample.
- Reasonably rapid equilibrium from complex aquatic matrices, including dissolved organic matter.
- Ability to manufacture in consistent thin films, to limit depletion of MeHg complexes in pore waters

A range of polymer and polymer composites were prepared to test sorption capacity and linearity. Target sorbents included activated carbon and a suite of thiol ligands and thiol-functionalized sorbents in the solid and aqueous phase. Polymers were chosen for pore sizes, sorbent capacity of MeHg, and ability to potentially include sorbents. A wide variety of polymers with and without sorbent inclusions were synthesized and tested. The binding capacity of polymers and polymer/sorbents mixtures were measured. MeHg partitioning coefficients were measured in 14-d isotherms in 3 ppt saline solutions using simple MeHg salts. Several sets of isotherms were done as we learned about the properties of our materials and began to build mixtures that best approximated MeHg equilibrium with sediments. Finally, materials showing promise in isotherms were tested under more environmentally realistic experimental conditions with the inclusion of DOM.

7.2 Materials and methods

Development of passive sampling polymers for methylmercury. Many polymers with and without sorbent inclusions were tested in this study (Table 7.1). The first materials tested were simple hydrophobic polymers. Some, including polyethylene (PE), polyoxymethylene (POM), and polydimethylsiloxane (PDMS), are widely used for passive sampling of organic contaminants. However, these standard polymers were not sufficiently sorptive for MeHg, which is much less lipophilic (see Results and Discussion). To address this, attempts were made to achieve greater chemical affinity by modifying existing polymer types. To this end, two separate strategies were investigated in parallel. The first was incorporation of activated carbon in the sampling material. Selection of ACs for trial was based on Gomez-Eyles et al. (2013), in study of Hg_i and MeHg isotherms for a variety of commercially available and lab-synthesized ACs and biochars. All exhibited linear partitioning across a range of environmentally relevant water concentrations, with log K_d values from 3.8 to 5.5. It may be possible to exploit this behavior for a passive sampling application by immobilizing AC in a polymeric matrix. Choi (2010) reported a method for embedding powdered activated carbon in a poly(vinylidene fluoride) (PVDF)

polymer. This procedure was followed in the present work and also adapted to produce an assortment of PVDF-ACs with varying carbon contents and physical attributes (Figure 7.1). For example, it is possible to adjust the cross-sectional pore structure, porosity, and permeability of PVDF by manipulating variables such as solvent proportions during synthesis (Sukitpaneenit and Chung 2009; Wang et al. 2008; Wang et al. 2013). Agarose was chosen as another possible support material for AC because it has proven effective as the diffusive gel in DGT sampling for MeHg (Gao et al. 2014). It is also possible to manipulate the structure of agarose gels by incorporating dopants during gel preparation to promote either micro- or macroporosity (Charlionet et al. 1996). For this project, agarose gels containing suspended AC were prepared and found to be stable in water for at least 28 d, the typical deployment time for our lab's passive sampler deployments in the field.
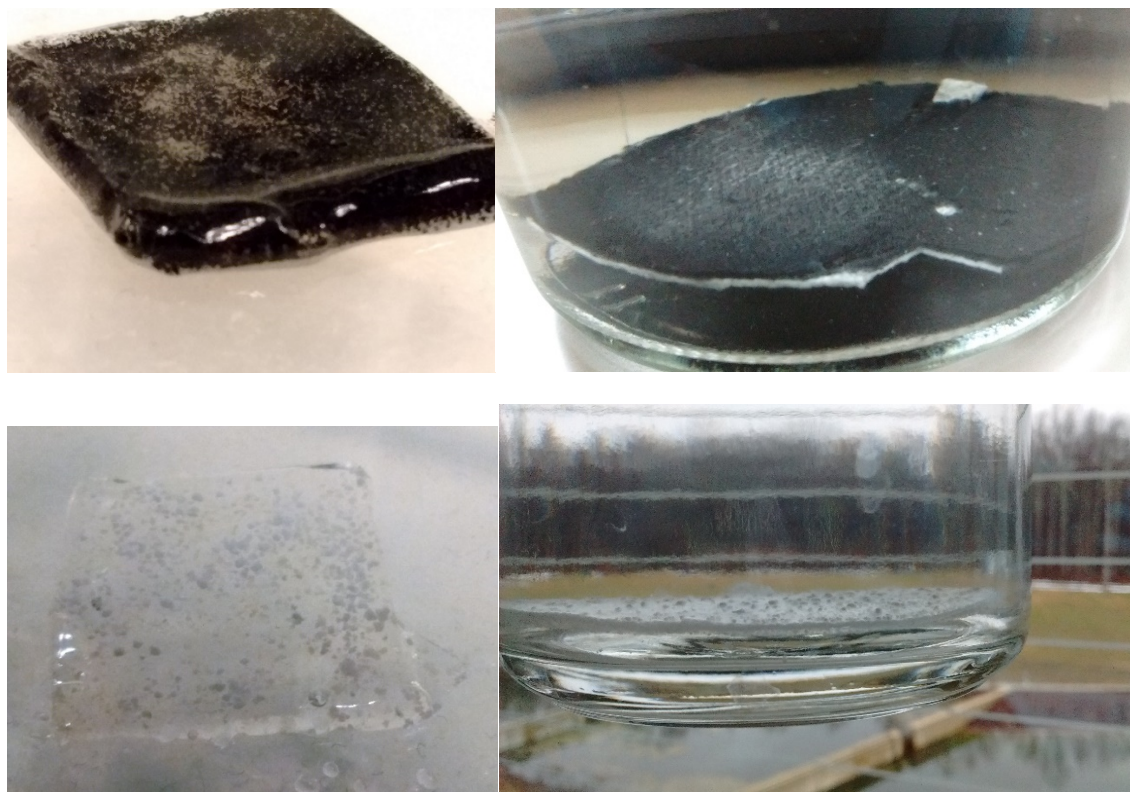
Figure 7.1. Assortment of agarose polymers. Clockwise from upper left: with embedded GAC; with embedded GAC and coated on a glass fiber filter; with embedded thiol-SAMMS and coated on a glass fiber filter; with embedded thiol-SAMMS.

The second type of polymer modification investigated was the incorporation of reduced sulfur chemical functionality in the sampling material. This approach not only promises to enhance affinity for MeHg, but may also represent a step toward the goal of biomimesis by drawing upon

the chemistry underlying many of mercury's biological interactions. Biomedical researchers have developed an assortment of thiolated polymers for use in pharmaceuticals, where their ability to form sulfide bonds confers mucoadhesive properties that facilitate controlled drug delivery (Bernkop-Schnürch 2005). Several of these were synthesized for the present work, including a chitosan-thioglycolic acid conjugate (Kast and Bernkop-Schnürch 2001), and alginate and xyloglucans functionalized with L-cysteine (Bernkop-Schnürch et al. 2001; Bhalekar et al. 2013). Generally, the physical and mechanical properties of these materials as prepared were unsuitable for deployment in sediment, so suspensions of the materials in agarose were prepared to obtain greater stability. Also included in preliminary isotherms were diatomaceous earth particles that were covalently thiolated according to Yu et al. (2012) and suspended in agarose. Other tested materials included polyethylene terephthalate sheets with covalently immobilized L-cysteine, PVDF doped with L-cysteine, and PVDF and agarose suspensions of thiol-SAMMS (Self-Assembled Monolayers on Mesoporous Supports, an engineered sorbent for aqueous metal cations (Feng et al. 1997)). Photographs of some of the PVDF-based polymer composites are shown in Figure 7.2.
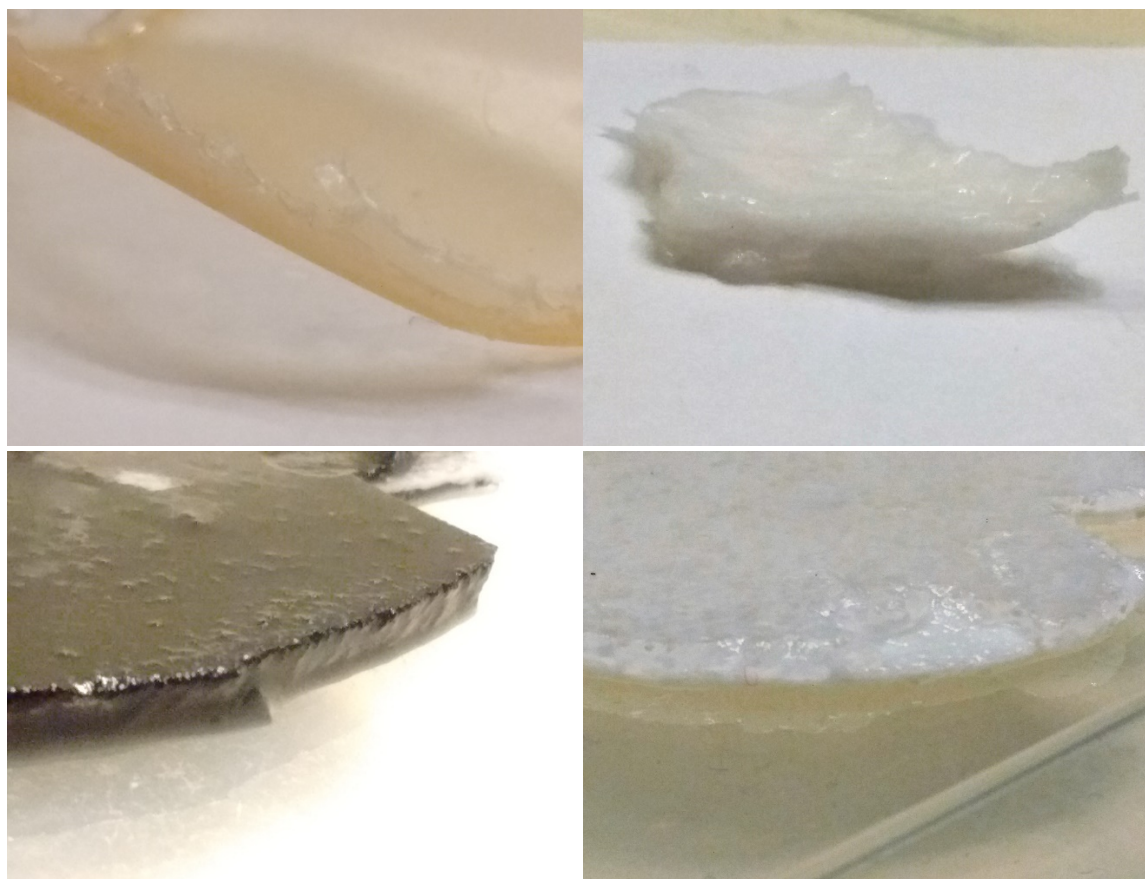
Figure 7.2. Assortment of magnified photos of lab-synthesized PVDF polymers. Clockwise from upper left: unmodified; with embedded cysteine; with embedded thiol-SAMMS and coated on a glass fiber filter; with embedded GAC and coated on a glass fiber filter.

MeHg isotherm studies with polymers. In initial isotherm experiments, a piece of test polymer was added to 50 mL deionized water adjusted to 3 ppt salinity with Instant Ocean (Spectrum Brands, Blacksburg, VA) and spiked with MeHg at one of a series of concentrations typically spanning two orders of magnitude. Samples were contained in 60-mL polyethylene terephthalate glycol copolymer (PETG) bottles. Incubations were carried out at 4 °C with orbital shaking at 120 rpm. Following incubation, samples were passed through 0.45 μm glass microfiber filters using disposable plastic syringes. Polymers were saved and frozen, and filtered water samples were distilled and analyzed according to methods described by Mitchell and Gilmour (2008). Briefly, an isotopic dilution spike was added, the samples were buffered with citrate, derivatized with sodium tetraethylborate to facilitate volatilization, purged and concentrated on a Tenax trap, thermally desorbed, separated on an OV-3/Chromasorb column, and introduced into an ICP-MS for detection. $K_{polymer}$ for each sample was calculated as follows:

$$K_{polymer} = \frac{C_s}{C_w} \qquad\qquad (1)$$

where C_w is the measured final concentration in water, and C_s is the sorbent concentration. The mass of MeHg on each sorbent was inferred from the difference between spiked and "recovered" MeHg (the final measured concentration multiplied by the sample volume). A significant amount of sorption to PETG bottle walls occurred in blank spikes, and this could have introduced substantial error in the K_d measurements of very weak sorbents. However, this phenomenon is a much smaller source of relative error for sorbents stronger than PETG by one or more orders of magnitude (i.e., any polymers worthy of further consideration). For this reason, no blank correction was applied to calculations.

For this preliminary screening phase, a target range of sampler partitioning was set at between $10^{3.0}$ and $10^{4.5}$ L kg^{-1}. This range was chosen as a first attempt to approximate benthic bioaccumulation and so that the sampler can compete with sediment for MeHg. For comparison, MeHg log K_d values in the Chesapeake Bay have been measured in the range of about 2.5 to 4 (Hollweg et al. 2009). It is also important to avoid oversampling. Materials with excessively high affinity can act as sinks for MeHg in pore water, inducing desorption and resupply from sediment stores and resulting in overestimation of equilibrium water concentrations (Clarisse et al. 2009).

Mercury and Methylmercury Analyses. Total Hg and MeHg analyses were carried out by isotope dilution ICP-MS, after sample preparation by digestion, distillation, extraction or other methods as described in detail in our cited publications (Gilmour et al. 2013; Graham et al. 2012; Mitchell et al. 2012; Hollweg et al. 2010). These methods are adaptations of EPA Methods 1630 and 1631. Isotope dilution ICP-MS significantly improves the accuracy and precision of these multistep methods. QA/QC will include blanks, replicates, spikes and suitable certified reference materials.

Modeling sorption in polymers. To assess diffusion of MeHg into the test polymers, measured K values were compared with those that would be predicted strictly on a mass basis. For example, given the composition of an AC-containing polymer and the K_d values of the AC measured by Gomez-Eyles et al. (2013; $10^{5.4}$ L kg^{-1}) and the unmodified polymers (this work), one could make the following approximation:

$$K_{d,predicted} = f_{polymer}K_{polymer} + f_{AC}K_{AC} \qquad (2)$$

where f is the fractional contribution of each constituent to the total mass of the material.

Most of the modified polymers performed well (log K in the target range). To narrow the selection, a subset of the materials with the most desirable partitioning behavior and physical properties was chosen to proceed to a second phase of testing. This phase was designed to investigate sampler partitioning of MeHg in the presence of dissolved organic matter (DOM), a crucial environmental ligand. Here, MeHg isotherms were set up similarly, but with the addition of Suwannee River Humic Acid II (hereafter SRHA; International Humic Substances Society), a well-characterized, organic-rich isolate with a high degree of aromaticity that tends to make it reactive toward mercury (Graham et al. 2013). SRHA was added to achieve a DOM:MeHg ratio of 10^6 in each sample. This was done because, according to Haitzer et al. (2002), affinity experiments at DOM:Hg mass ratios at or below 10^5 are misleading because they give the impression that mercury associates primarily with the relatively plentiful hydroxyl groups on DOM. In fact, speciation is controlled by a small fraction of reactive thiol functional groups under typical environmental conditions. MeHg spikes were chosen in consideration of the detection range of the analytical method and the anticipated partitioning coefficients of the materials in the presence of DOM, which as a first guess were anticipated to be one order of magnitude lower than those measured in the DOM-free solutions. DOM and MeHg were allowed to equilibrate overnight before the addition of sorbents (Figure 7.3). The samples incubated for 14 d and were processed and analyzed for MeHg as before.

Figure 7.3. Sample bottles for MeHg-DOM/polymer isotherm experiment.

7.3 Results and discussion

The first polymers tested, including PE, POM, and PDMS, have sufficiently high affinity for PCBs and polyaromatic hydrocarbons (PAHs) to serve as passive sampling materials due to the hydrophobicity of the compounds (log K_{ow} between 3 and 8 (Hawker and Connell 1988; de Maagd et al. 1998)). MeHg salts, by contrast, are only weakly hydrophobic, if at all (log K_{ow} between -1 and 2 (Mason 2002)). It is therefore not surprising that the measured partitioning coefficients in this first experiment were one to two orders of magnitude below our target range (see Figure 7.4 below). This experiment also included early attempts at AC-enhanced PVDF and agarose. The initial agarose+AC performed poorly, leading to adjustments in the preparation procedure for subsequent experiments. However, the measured K_d of the PVDF+AC was roughly an order of magnitude higher than those of the unmodified polymers, providing the first evidence that the modification strategy could be effective. Overall, the key findings of the first set of isotherm studies were that the pure polymers had weak sorption for MeHg and inclusion of AC particles greatly enhanced sorption and maintained the observed linear sorption behavior of MeHg in AC.
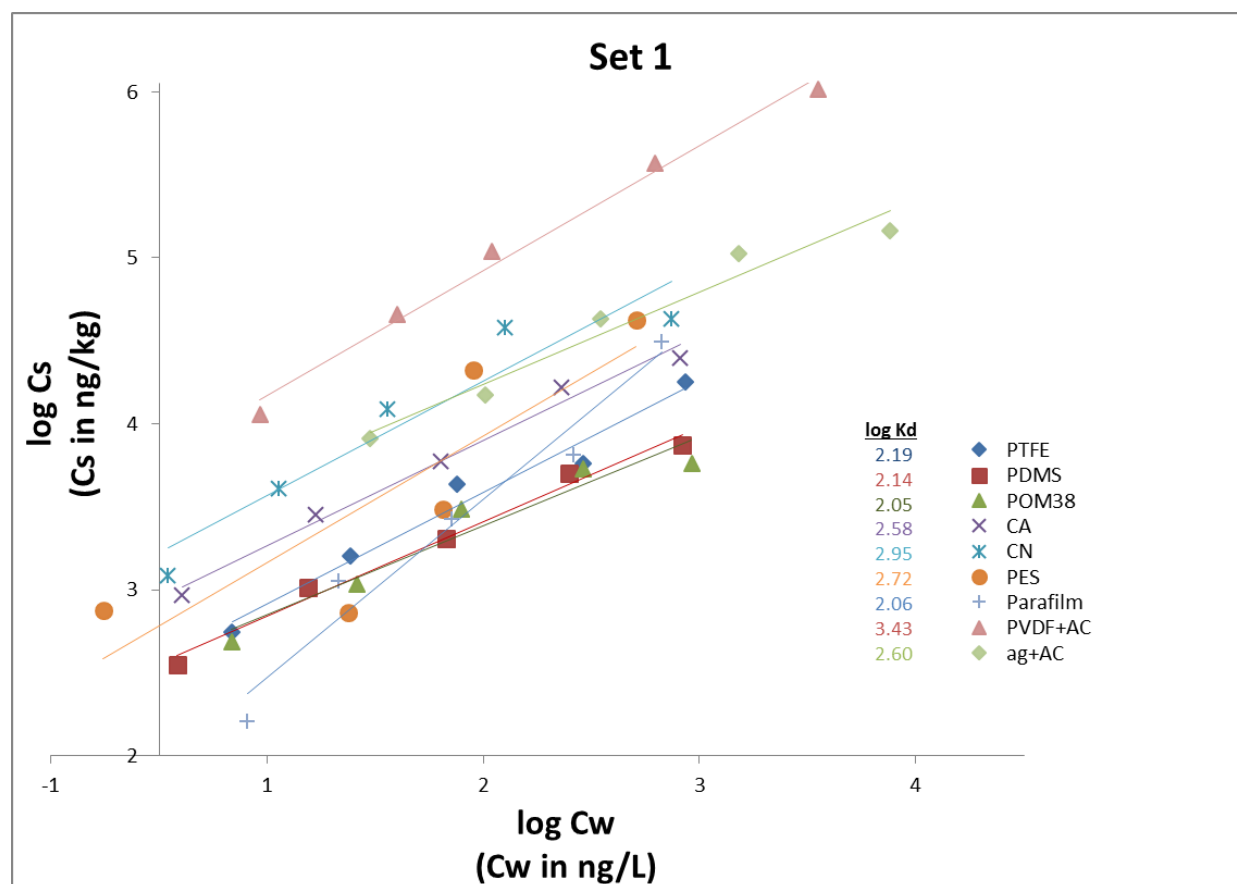
Figure 7.4. Results of first MeHg isotherm study focusing on unmodified hydrophobic polymers. See Table 7.1 for descriptions of all materials tested.

A second set of isotherms provided further support for the polymer-AC approach (see Figure 7.5 below). An assortment of PVDF+ACs prepared using different ACs and polymerizing nonsolvents performed similarly, and all were an order of magnitude more sorptive than unmodified PVDF. A second iteration of agarose+AC partitioned much more strongly than the first, and more than unmodified agarose. The thiolated polymers tested in this set leached sulfur into solution, causing analytical interferences and confounding the results. For subsequent preparations, greater care was taken to pre-clean these materials, leading to fewer analytical difficulties.
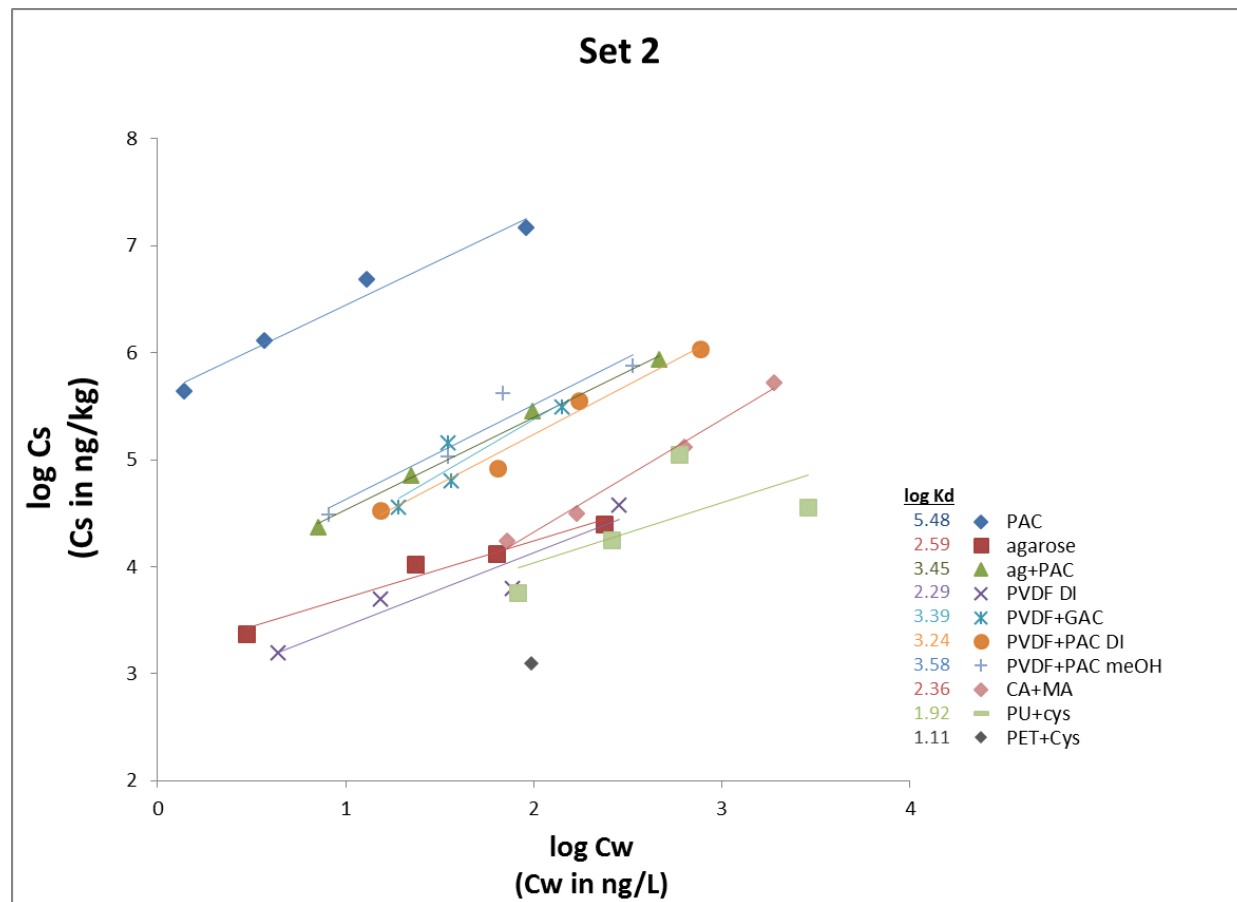
Figure 7.5. Results of second isotherm study, including AC- and thiol-based polymers. See Table 7.1 for descriptions of all materials tested.

The third set of isotherms focused on a selection of thiolated materials (Figure 7.6). PVDF with suspended cysteine performed very well, while an agarose suspension of cysteine did not. This may have been because the cysteine was not stable in the more hydrophilic and porous agarose matrix and may have partially leached into solution. By contrast, the agarose suspension of thiol-SAMMS was the strongest sorbent yet tested, and the only one to date with a measured log K_d greater than 5. The biomedical thiomers performed reasonably well, but given the complexities

involved in their preparation and the fact that they were no more sorptive than polymers containing SAMMS or AC, they were excluded from further consideration. All polymers tested with inclusions of thiolated ligands demonstrated strong and linear sorption behavior as demonstrated in Figure 7.6.
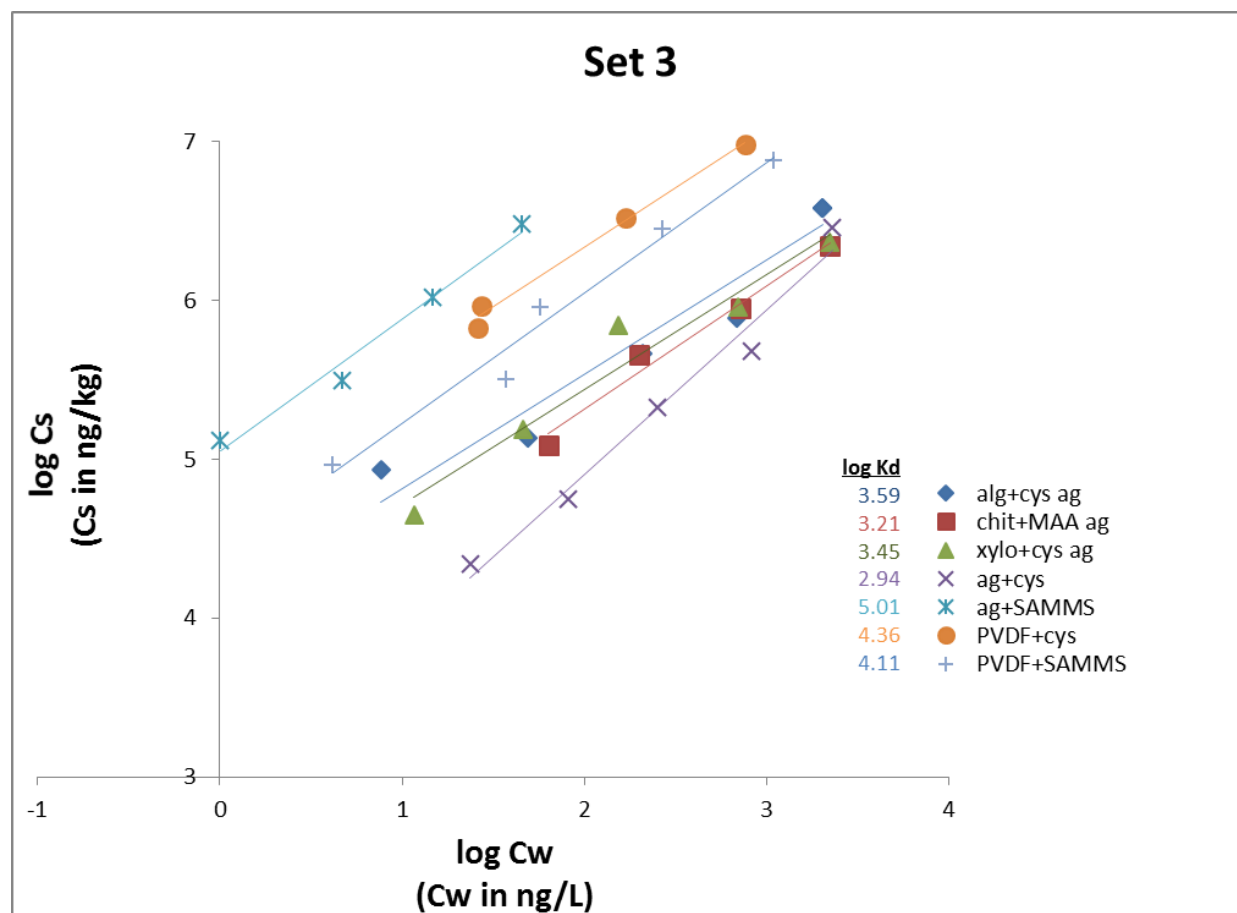
Figure 7.6. Results of third isotherm study, including thiomers and other sulfur-based polymers. See Table 7.1 for descriptions of all materials tested.

In the fourth set of screening isotherms (Figure 7.8), the mercapto-functionalized diatomaceous earth proved to be an exceedingly strong sorbent and, importantly, was as effective as predicted when suspended in agarose ($K_{measured}$:$K_{predicted} = 1$). A second preparation of cysteine-functionalized polyethylene terephthalate (Figure 7.7) also performed well. Suspensions of AC and SAMMS in an agarose doped with polyethylene glycol (which promotes macroporosity) performed similarly to their undoped analogs. This result is not surprising in the simple, moderately saline test solutions, but also leaves open the possibility that PEG doping could confer different sorption behavior in more realistic matrices with bulkier ligands.
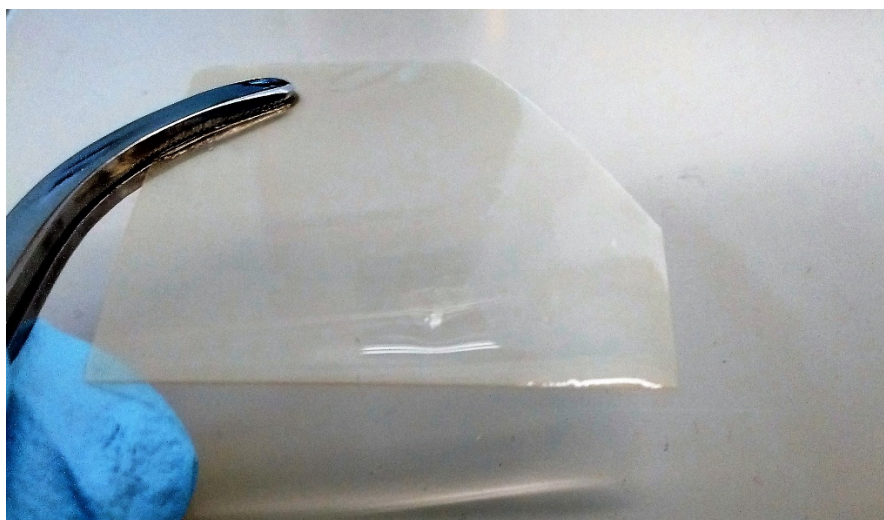
Figure 7.7. Polyethylene terephthalate covalently modified with cysteine.
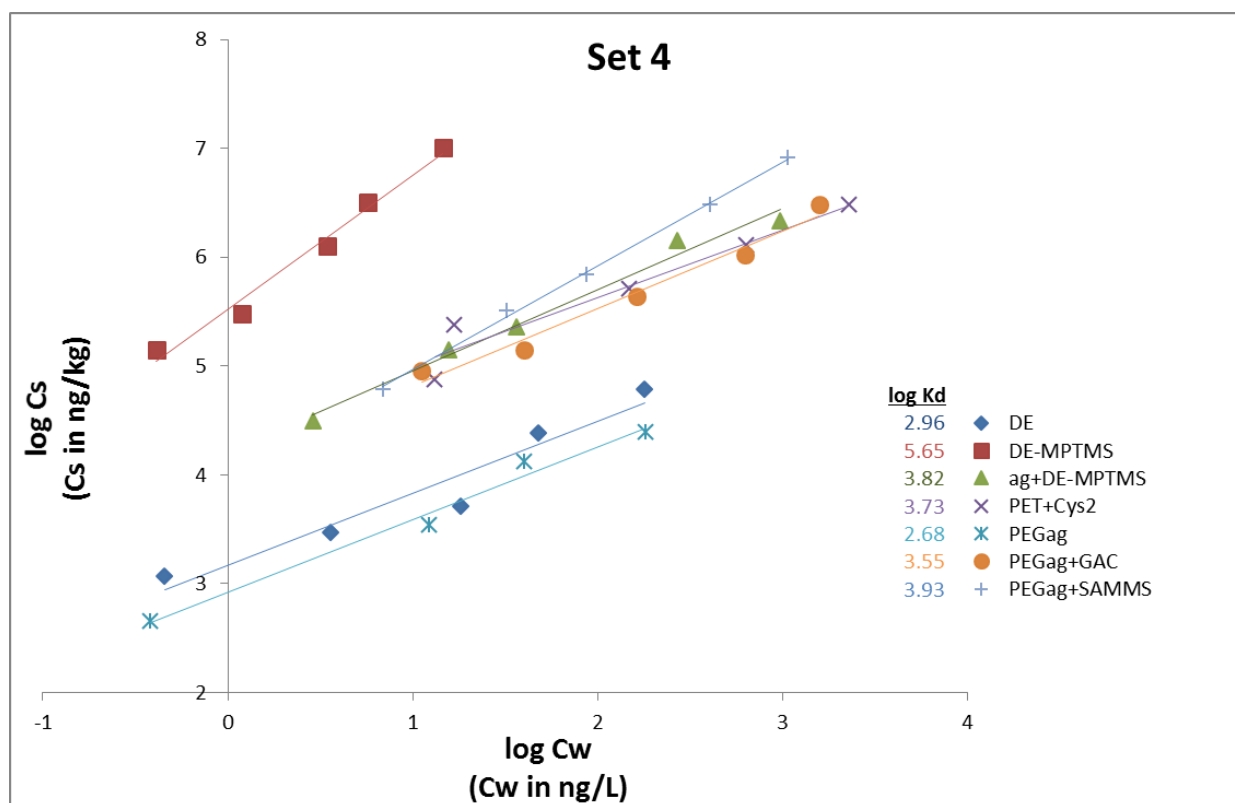
Figure 7.8. Results of fourth isotherm study. See Table 7.1 for descriptions of all materials tested.

For completeness, thiol-SAMMS and unmodified PET were tested in a final screening isotherm. The results were used in calculations of $K_{predicted}$ and are shown in Figure 7.9. As expected, partitioning by thiol-SAMMS was very strong, and comparable to that measured for DE-MPTMS, another thiolated, highly porous silica material. Refer to the attached table for a complete summary of screening isotherm results.
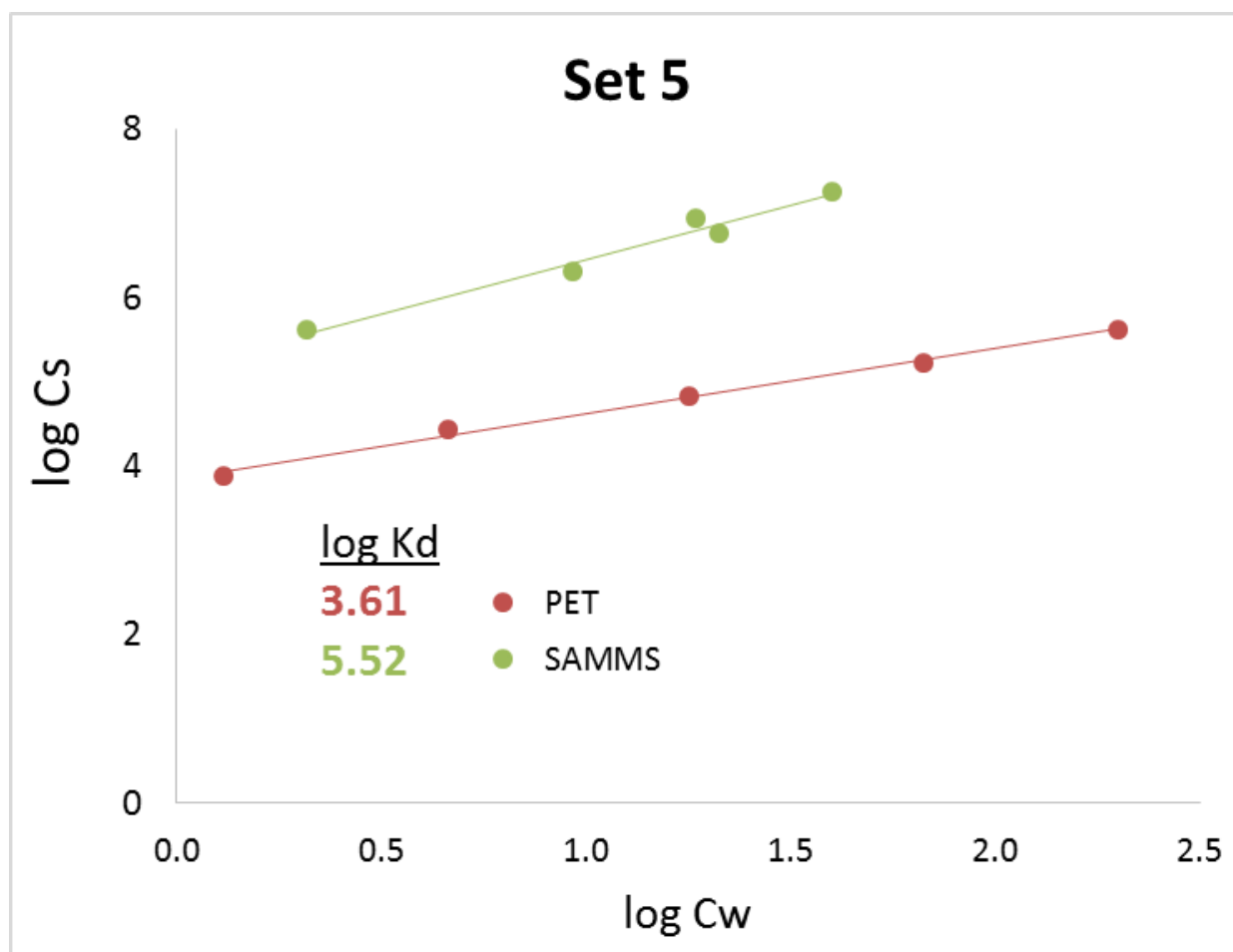
Figure 7.9. Results of fifth and final screening isotherm. See Table 7.1 for descriptions of all materials tested.

The most promising polymers in the screening phase were included in MeHg/DOM isotherms. Given the composition of the sample solutions in this experiment, the chemical speciation software MINEQL+ (v. 4.6; Environmental Research Software) predicted virtually complete complexation of MeHg by DOM prior to addition of the sorbent materials. As such, the experiment can be said to have measured the ability of the materials to partition these complexes.

All of the tested materials exhibited linear partitioning across the concentration range (Figure 7.10). However, partitioning was depressed by an average of 78% compared to the screening isotherms, in which MeHgCl was the dominant species in solution according to MINEQL+. The materials performed remarkably similarly, with an average log K_d of 3.1. As shown in Figure 7.10 below, for each of the sorption isotherms, the correlation coefficient (in log-log scale) was high with most values at 0.99 with concentration values in water spanning nearly 3 orders of magnitude. It is important to note that the aqueous concentrations were in the typical range of environmental values of a few to hundreds of ng/L.
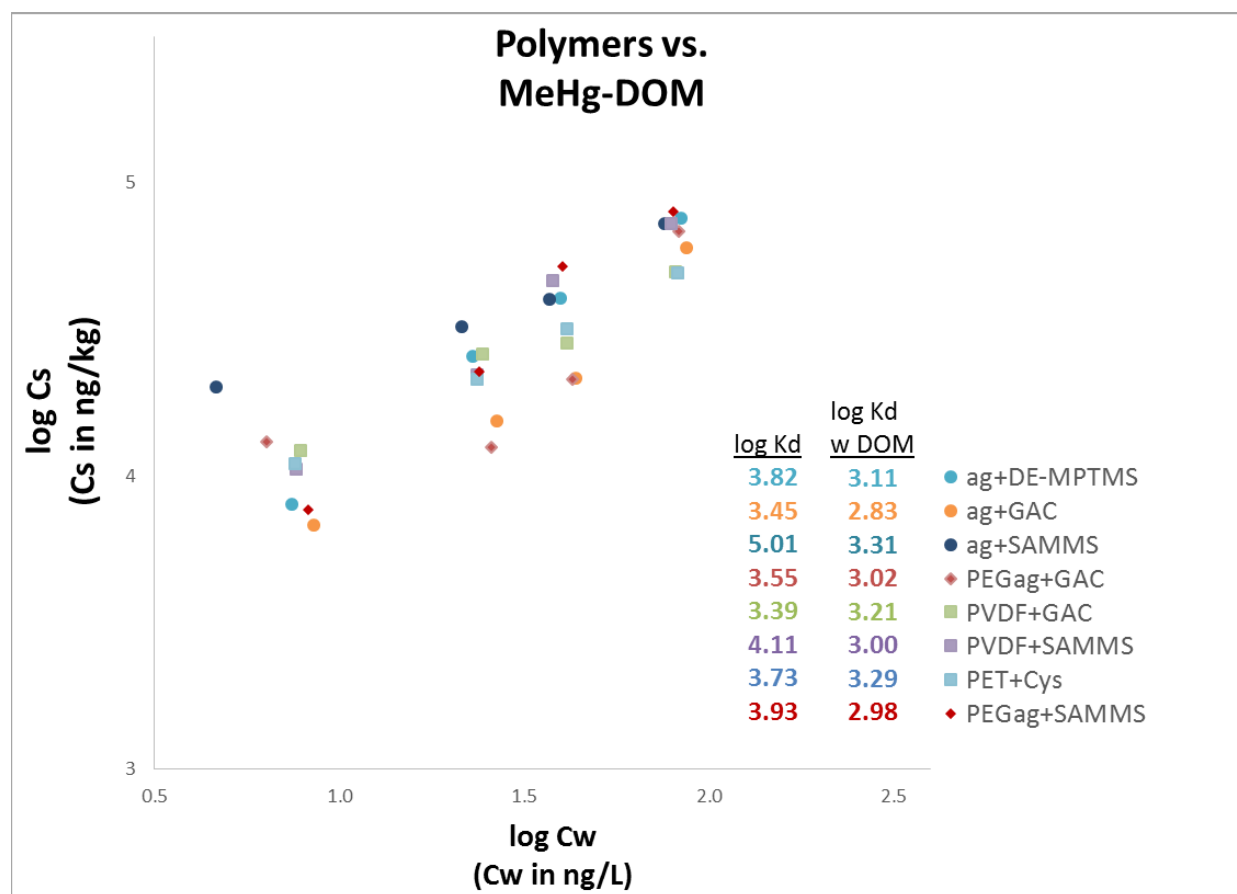
Figure 7.10. Results of MeHg-DOM isotherms. See Table 7.1 for descriptions of all materials tested.

7.4 Implications

In this research we demonstrate for the first time that a composite polymer can be synthesized that responds linearly to aqueous concentration of MeHg in water at equilibrium, in the presence of complexing ligands chloride and DOM. Thus, conceptually, we can develop an equilibrium passive sampler for MeHg in sediment porewater that is able to respond to porewater concentration of MeHg.

A material with a log K_d of 3 with respect to MeHg, exposed to an aqueous MeHg concentration of 5 ng/L (a moderate-to-low value for contaminated sediment pore water), would be capable of accumulating 500 pg of MeHg (a readily detectable amount) in a 100 mg mass of polymer. For most of the materials under consideration, this is roughly the size of a penny. Several of these materials achieved this degree of partitioning of MeHg complexed to DOM, one of the most likely ligands to dominate speciation in sediments and also one of the least diffusive. This constitutes a promising proof of concept for an equilibrium-based, polymeric passive sampling system for MeHg in sediment pore water.

Before that goal is reached, a few important questions remain to be answered. In many cases, $K_{measured}:K_{predicted}$ was significantly less than 1. This could be because MeHg did not have sufficient time to diffuse throughout the polymers in 14 d (i.e., a kinetic limitation), or because sorbent particles suspended in the polymers were permanently inaccessible to MeHg due to limitations in the effective porosity of the materials as prepared (implying that surface adsorption was the primary mechanism of accumulation). To address these questions, the kinetics of MeHg accumulation by polymers should be studied in a time series experiment. It may also be possible to devise an *in situ* calibration method for polymer equilibration, perhaps by pre-loading the sampler with isotopically-labelled MeHg as a performance reference compound. Several other practical aspects of deployment in an actual sediment will require investigation and refinement, including a method for eluting MeHg from the sampler and the physical configuration of the final device. Finally, the utility of the sampler should be validated by comparing its measurements to bioaccumulation by a relevant test organism in a side-by-side deployment.

Table 7.1. Summary of results of MeHg partitioning screening isotherms.

Material	Abbreviation	Reference	log K_d (K_d in L/kg)	log C_s/log C_w slope	log C_s/log C_w int.	log C_s/log C_w R^2	$f_{polymer}$	$f_{sorbent}$	log $K_{predict}$	$\frac{K_{measured}}{K_{predicted}}$
polyethylene	PE	n/a	2.35	0.78	2.9	0.92				
polytetrafluoroethylene (Teflon)	PTFE	n/a	2.19	0.67	2.6	0.97				
polydimethylsiloxane	PDMS	n/a	2.14	0.57	2.6	0.99				
polyoxymethylene, 38 μm thick	POM38	n/a	2.05	0.63	3.0	0.99				
cellulose acetate	CA	n/a	2.58	0.54	2.6	0.93				
cellulose nitrate	CN	n/a	2.95	0.69	3.2	0.91				
polyethersulfone	PES	n/a	2.72	0.76	2.8	0.72				
heterogeneous mixture of alkanes (paraffin)	Parafilm	n/a	2.06	1.1	1.9	0.96				
PAC suspended in PVDF; preparation was not optimized	PVDF+PAC [old]	Choi 2010	3.43	0.75	3.8	0.99	0.89	0.11	4.5	8E-02
PAC suspended in agarose; preparation was not optimized	ag+PAC [old]	Gao, et al. 2011	2.60	0.55	3.4	0.96	0.95	0.05	4.2	3E-02
powdered activated carbon	PAC	n/a	5.48	0.84	5.6	0.97				
agarose	ag	Gao, et al. 2011	2.59	0.53	3.2	0.96				
powdered activated carbon suspended in agarose	ag+PAC	Gao, et al. 2011	3.45	0.86	3.7	1.0	0.96	0.04	4.1	2E-01
poly(vinylidene fluoride) prepared with water nonsolvent	PVDF DI	Choi 2010	2.29	0.12	3.3	0.13				
coal-based granular AC suspended in poly(vinylidene fluoride)	PVDF+GAC	Choi 2010	3.39	1.0	3.3	0.84	0.89	0.11	3.9	3E-01
PAC suspended in PVDF prepared with water nonsolvent	PVDF+PAC DI	Choi 2010	3.24	0.92	3.4	0.98	0.89	0.11	4.5	5E-02
PAC suspended in PVDF prepared with 1:1 methanol:water nonsolvent	PVDF+PAC meOH	Choi 2010	3.58	0.89	3.7	0.98	0.89	0.11	4.5	1E-01
mercapto-functionalized cellulose acetate	CA+MA	Aoki, et al. 2007	2.36	1.0	2.2	0.99				
L-cysteine-functionalized polyurethane	PU+cys	Duan and Lewis 2002	1.92	0.56	2.9	0.46				
L-cysteine-functionalized polyethylene terephthalate	PET+cys	Duan and Lewis 2002	1.11	n/a	n/a	n/a				
L-cysteine-functionalized alginate suspended in agarose	alg+cys ag	Bernkop-Schnürch, et al. 2001	3.59	0.72	4.1	0.94				
mercapto-functionalized chitosan suspended in agarose	chit+MAA ag	Kast and Bernkop-Schnürch 2001	3.21	0.78	3.8	0.98				
L-cysteine-functionalized xyloglucans suspended in agarose	xylo+cys ag	Bhalekar, et al. 2013	3.45	0.73	4.0	0.95				
L-cysteine dissolved in agarose	ag+cys	Gao, et al. 2011	2.94	1.0	2.8	0.98	0.98	0.02	2.6	2E+00
L-cysteine dissolved in PVDF	PVDF+cys	Choi 2010	4.36	0.75	4.8	0.99	0.94	0.06	2.4	1E+02
thiol-SAMMS suspended in agarose	ag+SAMMS	Gao, et al. 2011	5.11	0.54	5.2	0.84	0.98	0.02	3.8	2E+01
thiol-SAMMS suspended in PVDF	PVDF+SAMMS	Choi 2010	4.11	0.82	4.4	0.98	0.947	0.053	4.2	7E-01
diatomaceous earth	DE	n/a	2.96	0.66	3.2	0.93				
mercapto-functionalized diatomaceous earth	DE-MPTMS	Yu, et al. 2012	5.65	1.2	5.5	0.98				
mercapto-functionalized diatomaceous earth suspended in agarose	ag+DE-MPTMS	Yu, et al. 2012	3.82	0.75	4.2	0.98	0.99	0.01	3.7	1E+00
L-cysteine-functionalized polyethylene terephthalate (second attempt)	PET+cys 2	Duan and Lewis 2002	3.73	0.62	4.4	0.94				
agarose doped with polyethylene glycol and glycerol	PEGag	Charlionet, et al. 1996	2.68	0.67	2.9	0.98				
granular activated carbon suspended in PEG-doped agarose	PEGag+GAC	Charlionet, et al. 1996	3.55	0.71	4.1	0.98	0.97	0.03	3.5	1E+00
hiol-SAMMS suspended in PEG-doped agarose	PEGag+SAMMS	Charlionet, et al. 1996	3.93	0.96	4.0	1.0	0.98	0.02	3.8	1E+00
polyethylene terephthalate	PET	n/a	3.64	0.76	4.0	0.99				
thiol-SAMMS	SAMMS	n/a	5.51	1.3	5.0	0.97				

7.5 Literature cited

Aiken, G. R.; Hsu-Kim, H.; Ryan, J. N., Influence of dissolved organic matter on the environmental fate of metals, nanoparticles, and colloids. Environ. Sci. Technol. 2011, 45, (8), 3196-3201.

Allen, H. E.; Fu, G. M.; Deng, B. L., Analysis of acid-volatile sulfide (AVS) and simultaneously extracted metals (SEM) for the estimation of potential toxicity in aquatic sediments. Environ. Toxicol. Chem. 1993, 12, (8), 1441-1453.

Amirbahman A, Reid AL, Haines TA, Kahl JS, Arnold C. Association of methylmercury with dissolved humic acids. Environ Sci Technol. 2002; 36:690-695.

Amirbahman, A.; Massey, D. I.; Lotufo, G.; Steenhaut, N.; Brown, L. E.; Biedenbach, J. M.; Magar, V. S., Assessment of mercury bioavailability to benthic macroinvertebrates using diffusive gradients in thin films (DGT). Environmental Science: Processes & Impacts 2013, 15, (11), 2104-2114.

Aoki D, Teramoto Y, Nishio Y. SH-containing cellulose acetate derivatives: preparation and characterization as a shape memory-recovery material. Biomacromolecules. 2007; 8(12):3749-3757.

Benoit, J. M.; Gilmour, C. C.; Mason, R. P.; Heyes, A., Sulfide controls on mercury speciation and bioavailability to methylating bacteria in sediment pore waters. Environ. Sci. Technol. **1999,** 33, (6), 951-957.

Bernkop-Schnürch A, Kast CE, Richter MF. Improvement in the mucoadhesive properties of alginate by the covalent attachment of cysteine. J Control Release. 2001; 71:277-285.

Bernkop-Schnürch A. Thiomers: a new generation of mucoadhesive polymers. Adv Drug Deliver Rev. 2005; 57:1569-1582.

Bhalekar M, Sonawane S, Shimpi S. Synthesis and characterization of a cysteine xyloglucan conjugate as mucoadhesive polymer. Braz J Pharm Sci. 2013; 49(2):285-292.

Boyd, E. S. Barkay, T., The mercury resistance operon: from an origin in a geothermal environment to an efficient detoxification machine. Front Microbiol **2012,** 3, 349.

Charlionet R, Levasseur L, J Malandain. Eliciting macroporosity in polyacrylamide and agarose gels with polyethylene glycol. Electrophoresis. 1996; 17:58-66.

Choi J. Fabrication of a carbon electrode using activated carbon powder and application to the capacitive deionization process. Sep Purif Technol. 2010; 70:362-366.

Clarisse O, Foucher D, Hintelmann H. Methylmercury speciation in the dissolved phase of a stratified lake using the diffusive gradient in thin film technique. Environ Pollut. 2009; 157:987-993.

Clarisse, O.; Dimock, B.; Hintelmann, H.; Best, E. P. H., Predicting Net Mercury Methylation in Sediments Using Diffusive Gradient in Thin Films Measurements. Environ. Sci. Technol. **2011,** 45, (4).

Clarisse, O.; Foucher, D.; Hintelmann, H., Methylmercury speciation in the dissolved phase of a stratified lake using the diffusive gradient in thin film technique. Environ. Pollut. **2009,** 157, (3), 987-993.

Clarisse, O.; Hintelmann, H., Measurements of dissolved methylmercury in natural waters using diffusive gradients in thin film (DGT). J. Environ. Monit. **2006,** 8, (12), 1242-1247.

Clarisse, O.; Lotufo, G. R.; Hintelmann, H.; Best, E., Biomonitoring and assessment of monomethylmercury exposure in aqueous systems using the DGT technique. Sci. Total Environ. **2012,** 416, 449-454.

Dahl, A. L.; Sanseverino, J.; Gaillard, J.-F., Bacterial bioreporter detects mercury in the presence of excess EDTA. Environmental Chemistry **2011,** 8, (6), 552-560.

Davison, W.; Zhang, H., Progress in understanding the use of diffusive gradients in thin films (DGT) - back to basics. Environmental Chemistry **2012,** 9, (1), 1-13.

de Maagd PG, ten Hulscher DTEM, van den Heuvel H, Opperhuizen A, Sijm DTHM. Physicochemical properties of polycyclic aromatic hydrocarbons: aqueous solubilities, n-octanol/water partition coefficients, and Henry's Law constants. Environ Toxicol Chem. 1998; 17(2):251-257.

Deonarine, A.; Lau, B. L. T.; Aiken, G. R.; Ryan, J. N.; Hsu-Kim, H., Effects of Humic Substances on Precipitation and Aggregation of Zinc Sulfide Nanoparticles. Environ. Sci. Technol. **2011,** 45, (8), 3217-3223.

Di Toro, D. M.; McGrath, J. A.; Hansen, D. J.; Berry, W. J.; Paquin, P. R.; Mathew, R.; Wu, K. B.; Santore, R. C., Predicting sediment metal toxicity using a sediment biotic ligand model: methodology and initial application. Environ. Toxicol. Chem. **2005,** 24, (10), 2410-2427.

Divis, P.; Leermakers, M.; Docekalova, H.; Gao, Y., Mercury depth profiles in river and marine sediments measured by the diffusive gradients in thin films technique with two different specific resins. Anal. Bioanal. Chem. **2005,** 382, (7), 1715-1719.

Docekalova, H.; Divis, P., Application of diffusive gradient in thin films technique (DGT) to measurement of mercury in aquatic systems. Talanta **2005,** 65, (5), 1174-1178.

Duan X, Lewis RS. Mason RP. Improved haemocompatibility of cysteine-modified polymers via endogenous nitric oxide. Biomaterials. 2002; 4:1197-1203.

Feng X, Fryxell GE, Wang L, Kim AY, Liu J, Kemner KM. Functionalized monolayers on ordered mesoporous supports. Science. 1997; 276:923-926.

Fernández-Gómez, C.; Bayona, J. M.; Díez, S., Comparison of different types of diffusive gradient in thin film samplers for measurement of dissolved methylmercury in freshwaters. Talanta **2014,** 129, 486-490.

Fernández-Gómez, C.; Bayona, J.; Díez, S., Diffusive gradients in thin films for predicting methylmercury bioavailability in freshwaters after photodegradation. Chemosphere **2015,** 131, 184-191.

Fernández-Gómez, C.; Dimock, B.; Hintelmann, H.; Diez, S., Development of the DGT technique for Hg measurement in water: Comparison of three different types of samplers in laboratory assays. Chemosphere **2011,** 85, (9), 1452-1457.

Gagnon, C.; Fisher, N. S., Bioavailability of sediment-bound methyl and inorganic mercury to a marine bivalve. Environ. Sci. Technol. **1997,** 31, (4), 993-998.

Gao Y, de Canck E, Leermakers M, Baeyens W, van der Voort P. Synthesized mercaptopropyl nanoporous resins in DGT probes for determining dissolved mercury concentrations. Talanta. 2011; 87:262-267.

Gao Y, De Craemer S, Baeyens W. A novel method for the determination of dissolved methylmercury concentrations using diffusive gradients in thin films technique. Talanta. 2014; 120:470-474.

Gilmour, C. C.; Elias, D. A.; Kucken, A. M.; Brown, S. D.; Palumbo, A. V.; Schadt, C. W.; Wall, J. D., Sulfate-reducing bacterium Desulfovibrio desulfuricans ND132 as a model for understanding bacterial mercury methylation. Appl. Environ. Microbiol. **2011,** 77, (12), 3938-3951.

Gilmour, C. C.; Podar, M.; Bullock, A. L.; Graham, A. M.; Brown, S. D.; Somenahally, A. C.; Johs, A.; Hurt Jr, R. A.; Bailey, K. L.; Elias, D. A., Mercury methylation by novel microorganisms from new environments. Environ. Sci. Technol. **2013,** 47, (20), 11810-11820.

Golding, G. R.; Kelly, C. A.; Sparling, R.; Loewen, P. C.; Rudd, J. W. M.; Barkay, T., Evidence for facilitated uptake of Hg(II) by Vibrio anguillarum and Escherichia coli under anaerobic and aerobic conditions. Limnol. Oceanogr. **2002,** 47, (4), 967-975.

Gomez-Eyles JL, Yupanqui C, Beckingham B, Riedel G, Gilmour CC, Ghosh U. Evaluation of biochars and activated carbons for *in situ* remediation of sediments impacted with organics, mercury, and methylmercury. Environ Sci Technol. 2013; 47(23):13721-13729.

Graham AM, Aiken GR, Gilmour CC. Effect of dissolved organic matter source and character on microbial mercury methylation in Hg-S-DOM solutions. Environ Sci Technol. 2013; 47:5746-5754.

Graham, A. M.; Aiken, G. R.; Gilmour, C. C., Dissolved organic matter enhances microbial mercury methylation under sulfidic conditions. Environ. Sci. Technol. **2012,** 46, (5), 2715-2723.

Haitzer M, Aiken GR, Ryan JN. Binding of mercury(II) to dissolved organic matter: the role of the mercury-to-DOM concentration ratio. Environ Sci Technol. 2002; 36:3564-3570.

Haitzer, M.; Aiken, G. R.; Ryan, J. N., Binding of mercury(II) to dissolved organic matter: The role of the mercury-to-DOM concentration ratio. Environ. Sci. Technol. **2002,** 36, (16), 3564-3570.

Han, S. H.; Gill, G. A., Determination of mercury complexation in coastal and estuarine waters using competitive ligand exchange method. Environ. Sci. Technol. **2005,** 39, (17), 6607-6615.

Hawker DW, Connell DW. Octanol-water partition coefficients of polychlorinated biphenyl congeners. Environ Sci Technol. 1988; 22:382-387.

Hollweg TA, Gilmour CC, Mason RP. Methylmercury production in sediments of Chesapeake Bay and the mid-Atlantic continental margin. Environ Sci Technol. 2009; 114:86-101.

Hollweg, TA, Gilmour CC, Mason RP. Mercury and methylmercury cycling in sediments of the mid-Atlantic continental shelf and slope. Limnol Oceanogr. 2010; 55:2703-2722.

Hsu-Kim H, Kucharzyk KH, Zhang T, Deshusses MA. Mechanisms regulating mercury bioavailability for methylating microorganisms in the aquatic environment: a critical review. Environ Sci Technol. 2013 Feb 5; 47(6):2441–2456.

Kast CE, Bernkop-Schnürch A. Thiolated polymers—thiomers: development and in vitro evaluation of chitosan-thioglycolic acid conjugates. Biomaterials. 2001; 22:2345-2352.

Lawrence, A. L.; Mason, R. P., Factors controlling the bioaccumulation of mercury and methylmercury by the estuarine amphipod Leptocheirus plumulosus. Environ. Pollut. **2001,** 111, (2), 217-231.

Le Faucheur, S.; Campbell, P. G.; Fortin, C.; Slaveykova, V. I., Interactions between mercury and phytoplankton: Speciation, bioavailability, and internal handling. Environ. Toxicol. Chem. **2014,** 33, (6), 1211-1224.

Le Faucheur, S.; Tremblay, Y.; Fortin, C.; Campbell, P. G., Acidification increases mercury uptake by a freshwater alga, Chlamydomonas reinhardtii. Environmental Chemistry **2011,** 8, (6), 612-622.

Liao W, Christman RF, Johnson JD, Millington DS, Hass JR. Structural characterization of aquatic humic material. Environ Sci Technol. 1982; 16:403-410.

Liu, J.; Feng, X.; Qiu, G.; Anderson, C. W.; Yao, H., Prediction of methyl mercury uptake by rice plants (Oryza sativa L.) using the diffusive gradient in thin films technique. Environ. Sci. Technol. **2012,** 46, (20), 11013-11020.

Luengen, A. C.; Fisher, N. S.; Bergamaschi, B. A., Dissolved organic matter reduces algal accumulation of methylmercury. Environ. Toxicol. Chem. **2012,** 31, (8).

Mason RP. The bioaccumulation of mercury, methylmercury and other toxic elements into pelagic and benthic organisms. In: Newman NC, Roberts MH Jr, Hale RC (eds). Coastal and estuarine risk assessment. Boca Raton, FL: Lewis Publishers; 2002. pp. 127-149.

Mason, R. P.; Reinfelder, J. R.; Morel, F. M. M., Uptake, toxicity, and trophic transfer of mercury in a coastal diatom. Environ. Sci. Technol. **1996,** 30, (6), 1835-1845.

Mitchell CPJ, Gilmour CC. Methylmercury production in a Chesapeake Bay salt marsh. J Geophys Res. 2008; 113. DOI: 10.1029/2008JG000765.

Mitchell CPJ, Jordan TE, Heyes A, Gilmour CC. Total mercury and methylmercury exchange between a salt marsh and a Chesapeake Bay sub-estuary. Biogeochemistry. 2012; DOI: 10.1007/s10533-011-9691-y.

Ndu, U.; Mason, R. P.; Zhang, H.; Lin, S.; Visscher, P. T., Effect of Inorganic and Organic Ligands on the Bioavailability of Methylmercury as Determined by Using a mer-lux Bioreporter. Appl. Environ. Microbiol. **2012,** 78, (20), 7276-7282.

Noh, S.; Hong, Y. S.; Han, S., Application of diffusive gradients in thin films and core centrifugation methods to determine inorganic mercury and monomethylmercury profiles in sediment porewater. Environ. Toxicol. Chem. **2015**.

Pelcová, P.; Dočekalová, H.; Kleckerová, A., Determination of mercury species by the diffusive gradient in thin film technique and liquid chromatography–atomic fluorescence spectrometry after microwave extraction. Anal. Chim. Acta **2015,** 866, 21-26.

Pham, A. L.-T.; Johnson, C.; Manley, D.; Hsu-Kim, H., Influence of Sulfide Nanoparticles on Dissolved Mercury and Zinc Quantification by Diffusive Gradient in Thin-Film Passive Samplers. Environ. Sci. Technol. **2015,** 49, (21), 12897-12903.

Pham, A. L.-T.; Morris, A.; Zhang, T.; Ticknor, J.; Levard, C.; Hsu-Kim, H., Precipitation of nanoscale mercuric sulfides in the presence of natural organic matter: Structural properties, aggregation, and biotransformation. Geochim. Cosmochim. Acta **2014,** 133, 204-215.

Pickhardt, P. C.; Fisher, N. S., Accumulation of inorganic and methylmercury by freshwater

phytoplankton in two contrasting water bodies. Environ. Sci. Technol. **2007,** 41, (1), 125-131.

Schaefer, J. K.; Morel, F. M. M., High methylation rates of mercury bound to cysteine by Geobacter sulfurreducens. Nature Geoscience **2009,** 2, (2), 123-126.

Schwarzenbach G, Schellenberg M. Die komplexchemie des methylquecksilber-kations. Helv Chim Acta. 1965; 48:28-46.

Scott, K. J., Bioavailable mercury in arctic snow determined by a light-emitting mer-lux bioreporter. Arctic **2001,** 54, (1), 92-95.

Skyllberg, U.; Bloom, P. R.; Qian, J.; Lin, C. M.; Bleam, W. F., Complexation of mercury(II) in soil organic matter: EXAFS evidence for linear two-coordination with reduced sulfur groups. Environ. Sci. Technol. **2006,** 40, (13), 4174-4180.

Skyllberg, U.; Drott, A., Competition between Disordered Iron Sulfide and Natural Organic Matter Associated Thiols for Mercury(II)-An EXAFS Study. Environ. Sci. Technol. **2010,** 44, (4), 1254-1259.

Sukitpaneenit P, Chung T. Molecular elucidation of morphology and mechanical properties of PVDF hollow fiber membranes from aspects of phase inversion, crystallization and rheology. J Membrane Sci. 2009; 340:192-205.

Sunderland, E. M., Mercury exposure from domestic and imported estuarine and marine fish in the US seafood market. Environ. Health Perspect. **2007,** 115, (2), 235-242.

Taylor, V. F.; Bugge, D.; Jackson, B. P.; Chen, C. Y., Pathways of CH3Hg and Hg ingestion in benthic organisms: an enriched isotope approach. Environ. Sci. Technol. **2014,** 48, (9), 5058-65.

Town, R. M.; Chakraborty, P.; van Leeuwen, H. P., Dynamic DGT speciation analysis and applicability to natural heterogeneous complexes. Environmental Chemistry **2009,** 6, (2), 170-177.

Vrana, B.; Allan, I. J.; Greenwood, R.; Mills, G. A.; Dominiak, E.; Svensson, K.; Knutsson, J.; Morrison, G., Passive sampling techniques for monitoring pollutants in water. TrAC Trends in Analytical Chemistry **2005,** 24, (10), 845-868.

Wang KY, Chung T, Gryta M. Hydrophobic PVDF hollow fiber membranes with narrow pore size distribution and ultra-thin skin for the fresh water production through membrane distillation. Chem Eng Sci. 2008; 63:2587-2594.

Wang Q, Wang X, Wang Z, Huang J, Wang Y. PVDF membranes with simultaneously enhanced permeability and selectivity by breaking the tradeoff effect via atomic layer deposition of TiO2. J Membrane Sci. 2013; 442:57-64.

Wang, W.-X.; Fisher, N. S., Delineating metal accumulation pathways for marine invertebrates. Sci. Total Environ. **1999,** 237, 459-472.

Williams, J. J.; Dutton, J.; Chen, C. Y.; Fisher, N. S., Metal (As, Cd, Hg, and CH_3Hg) bioaccumulation from water and food by the benthic amphipod Leptocheirus plumulosus. Environ. Toxicol. Chem. **2010,** 29, (8).

Xia K, Weesner F, Bleam WF, Bloom PR, Skyllberg UL, Helmke PA. XANES studies of oxidation states of sulfur in aquatic and soil humic substances. Soil Sci Soc Am J. 1998; 62(5):1240-1246.

Yu Y, Addai-Mensah J, Losic D. Functionalized diatom silica microparticles for removal of mercury ions. Sci Technol Adv Mater. 2012; 13(1):01500.

Zhang, T.; Kim, B.; Leyard, C.; Reinsch, B. C.; Lowry, G. V.; Deshusses, M. A.; Hsu-Kim, H., Methylation of mercury by bacteria exposed to dissolved, nanoparticulate, and microparticulate mercuric sulfides. Environ. Sci. Technol. **2012,** 46, (13), 6950-6958.

8.0 CONCLUSIONS AND RECOMMENDATIONS FOR FUTURE RESEARCH:

This 1-year SEED project advanced the field of passive sampling on two major fronts: 1) Developed an engineering approach to extend *in-situ* passive sampling to high molecular weight compounds in sediment porewater, and 2) Explored an equilibrium passive sampling approach for MeHg in sediment porewater.

In this research we demonstrate through laboratory experiments and numerical modeling that short periodic shaking of a passive sampler deployed in static sediment greatly enhances the rate of mass transfer and reduces the difference in the extent of equilibrium achieved compared to a well stirred laboratory equilibrium. The improvement over static sediment deployment is especially evident for the high molecular weight PAH compounds such as benzo(a)pyrene. We also demonstrate this method for strongly hydrophobic chlorinated organics using PCB congeners in the log Kow range of 6-8. The accuracy of measurement of porewater PCB concentrations is greatly enhanced in the vibrating passive sampler. Further work is needed to operationalize the vibrating passive sampler concept. Recommendations for future work on the vibrating passive sampler include:

1) <u>Further optimization of vibration frequency through laboratory experiments</u>. In this SEED project we introduced frequent vibrations (once every few minutes). However, our modeling results indicate that there is an optimal frequency of vibration that can be much lower (e.g. once per day). Further experimental work is needed to develop a better understanding of how the optimal frequency is impacted by compound hydrophobicity and sediment characteristics.

2) <u>Testing on strongly hydrophobic compounds such as dioxins and furans</u>. In this SEED project we tested the vibrating sampling platform using field sediments with PAHs and highly chlorinated PCBs. Ultimately, this needs to be tested in the laboratory for sediments impacted with dioxins and furans. There is very little in the current literature on the use of passive sampling for measuring freely dissolved porewater concentrations of these compounds.

3) <u>Confirmation through laboratory experiments that the concept of using freely dissolved concentrations in sediment porewater to predict biouptake can be extended to dioxins and furans</u>. Several studies have correlated the freely dissolved concentration of PAHs and PCBs to a biological endpoint, but such empirical data on dioxins and furans are lacking.

4) <u>Field testing of the sampler platform</u> along with traditional deployment of passive samplers. The prototype platforms developed in this research are ready for field deployment. These field studies should ideally target strongly hydrophobic compounds such as highly chlorinated PCBs or dioxins/furans.

This research also developed and tested polymer composites for use as equilibrium passive samplers for MeHg in sediment porewater. Several polymer composites demonstrated strong sorption characteristics and linear sorption behavior that we were seeking for use in passive sampling. These tests were also performed in the presence of two common complexing ligands in sediment porewater: chloride and dissolved organic matter. We believe that initial results presented in this report show great promise for pursuing the concept of equilibrium passive sampling for Hg and MeHg in sediment porewater.

Our study also took the first step toward demonstrating that equilibrium passive samplers for MeHg are feasible using our proposed approach, in which materials with similar partition coefficients to MeHg in sediments are deployed. Specifically, we developed several polymers with sorbent inclusions that meet our requirements for this type of passive samplers: linear uptake isotherms, and appropriate partition coefficients. Several of these materials should be able to be produced in thin films with sufficient capacity for MeHg analysis, but this will need additional testing.

Further work is needed to advance the technology development for passive sampling of MeHg and are listed below:

1) Complete testing of a suite of selected polymers prior to testing against benthic organisms, specifically:
    a. Complete kinetic testing over time with simple salts (MeHgCl) and with MeHgDOM complexes.
    b. Test equilibrium partitioning into 5-8 selected passive sampler designs, for key classes of synthesized MeHg complexes, including MeHg-thiols, MeHg-DOM complexes (with a suite of DOC compounds across a range of aromaticity and S content, see Graham et al. 2012, 2013), and colloids that contain both DOC and sulfide.
2) Empirically determine which passive sampler sorbents and pore size predict MeHg uptake by organisms.
    • We propose to use *Leptocheirus plumulosus* as a test organism because it is a mixed-type of feeder and because of our experience in developing MeHg exposure systems for this organism in collaboration with ERDC.
    • Directly test key classes of MeHg complexes for uptake by both the animals and the suite of passive samplers, using enriched stable isotope MeHg spikes in artificial sediment test matrices. We have significant experience synthesizing these complexes, included HgS nanoparticulates and colloids.
    • Use this information to narrow the set of passive samplers to 2-3.
    • Extend testing to natural sediments with the select set of passive samplers. Include measurement of total pore water MeHg, and variables needed for equilibrium modeling of MeHg complexation.
3) Develop enriched stable isotope spikes as performance reference compounds in these samplers

9.0 RESPONSE TO ACTION ITEM

Action Items Provided at Last In-Progress Review:

Please plan on considering the following comments from the Sediment Review Panel over the course of this project. Recognizing that this project is a SEED project, and is just getting underway, we are not expecting answers per se, but rather, will be interested in seeing that these items are addressed and included in the Final Report.

1. The presentation and proposal is based on mathematical modeling that suggests that uptake will be facilitated and shortened based on the vibratory disruption of the aqueous boundary layer. Empirical evidence will be needed to confirm that this is in fact the case.

Response: Yes, a major focus of this research was to perform laboratory experiments to confirm the theoretical expectation. Field sediments were used in laboratory mecosoms to test the performance of vibrating samplers and compare with static and well-mixed deployments. Chapter 5 presents the results in the form of a peer-review publication based on experimental and modeling results for PAHs in sediments. Chapter 6 presents experimental results for highly chlorinated PCBs that would fall in the range of most dioxins and furans.

2. Multiple engineering issues will need to be considered in the development of this sampler. These would include the size and construction of the sampler, effectively vibrating the sampling media across depth and width of a sampler (e.g., a 10 x 10 cm sampler), whether the vibrations will cause the sampler to come out of the sediment, weight of the sampler, this to stay in place, power source (size and longevity of the battery). We are confident that you are aware of most of these issues, and are not expecting those to be answered here, just thought about and considered in the Final Report.

Response: The engineering aspects of the development of a passive sampler were addressed in this research. As demonstrated in chapters 5 and 6, these samplers were able to function effectively for 56 h deployments in laboratory sediment mesocosms. We went through several iterations of design and settled on a final prototype shown on the right that was tested successfully in sediments. We were able to comfortably measure low aqueous concentrations of highly chlorinated PCBs with only 0.1 ppm total PCBs in sediment. We also calculated our power requirement and demonstrate in chapter 5 that the motors need to be active very infrequently (as low as once a day) and a regular AA size battery is sufficient for a 1-month deployment.
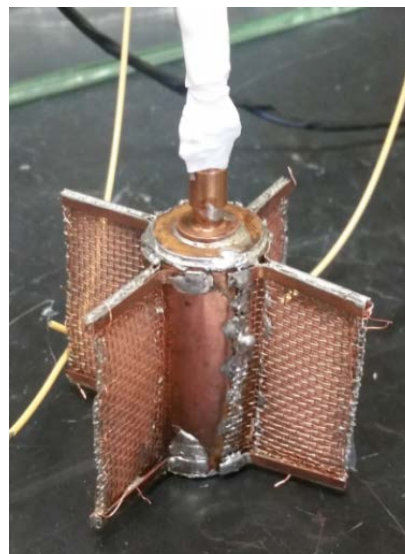
10.0 APPENDICES

10.1 Supporting information associated with section 5

Local equilibrium model for a static system

A one dimensional diffusion model, based on Fernandez et al. [1] was used to describe the mass transfer in a system containing a PE strip with the thickness of $2l_p$ and sediment with thickness of l_w on both sides. Following the Fick's second law of diffusion, for a PE strip with concentration C_{PE} and at point x and time t:

$$\frac{\partial C_{PE}}{\partial t} = D_{PE} \frac{\partial^2 C_{PE}}{\partial x^2} \qquad\qquad -l_p < x < l_p \qquad\quad \text{(S-1)}$$

Where D_{PE} is chemical diffusivity in PE (cm^2/s)

Assuming instantaneous equilibrium between pore water and sediment particles, transport equation in pore water with concentration of C_w at point x and time t will be as follows:

$$\frac{1}{R}\frac{\partial C_w}{\partial t} = D\frac{\partial^2 C_w}{\partial x^2} \qquad l_p < x < l_p + l_w \quad and \quad -l_p < x < -l_p - l_w \quad \text{(S-2)}$$

Where ρ is sediment bulk density (g/cm^3), R is retardation factor and D is the effective diffusivity (cm^2/s)

R and D are calculated as follows:

$$R = \varepsilon/(1 + \frac{\rho}{\varepsilon}K_d) \qquad\quad \text{(S-3)}$$

$$D = \frac{D_w}{1 - ln\varepsilon^2} \qquad\qquad \text{(S-4)}$$

Where D_w is chemical diffusivity in water (cm^2/s), K_d is sediment-water partition coefficient (cm^3/g) and ε is porosity (cm^3/cm^3)

The polymer is initially clean and sediment particles have initial concentration of S0.

$$C_{w0} = S_0/K_d \qquad\qquad l_p < x < l_p + l_w \quad and \quad -l_p < x < -l_p - l_w \qquad \text{(S-5)}$$

$$C_{PE} = 0 \qquad\qquad -l_p \le x \le l_p \qquad\quad \text{(S-6)}$$

At the boundary of PE-sediment, C_{PE} can be determined using the PE-water partitioning coefficient K_{PEW} and pore water concentration:

$$C_{PE} = K_{PEw}C_w \qquad\qquad x = l_p \ and \ x = -l_p \qquad \text{(S-7)}$$

Continuity of flux is also assumed at the boundary:

$$D_{PE}\frac{\partial C_{PE}}{\partial x_{PE}} = D\frac{\partial C_w}{\partial x_w} \qquad\qquad x = l_p \ and \ x = -l_p \qquad \text{(S-8)}$$

Due to symmetry the flux will be zero at the center of PE. Pore water concentration is equal to the initial concentration far away from the polymer at x=l_p+l_w and does not change by time:

$$\frac{\partial C_{PE}}{\partial x} = 0 \qquad\qquad x = 0 \qquad\qquad\qquad \text{(S-9)}$$

$$\frac{\partial C_w}{\partial t} = 0 \qquad\qquad x = l_p + l_w \quad and \quad x = -l_p - l_w \qquad \text{(S-10)}$$

Details of model simulation

Numerical solution

Explicit, finite-difference numerical modeling techniques, as described by Crank [2] were used to solve the model's equations. Briefly, the explicit method is implemented by dividing the x region with the length of L, into N intervals each of width Δx such that $x_i = i\Delta x$; i=1, 2...N and $N\Delta x = L$. In this model, polymer region with the length of l_p (half of the polymer thickness) was divided into N_p intervals. Pore water and sediment regions had the same length of l_w and were divided into N_w intervals.

C_i^j is denoted for concentration in location idx and at time jdt, or in other words C (iΔx, jΔt); j=1, 2, 3…

The numerical solution to model equations in pore water, polymer and sediment regions will be as Equations S-11, S-12 and S-13, respectively:

Pore water region:1<i<N_w

$$\frac{C_i^{j+1} - C_i^j}{\Delta t} = D\frac{C_{i-1}^j - 2C_i^j + C_{i+1}^j}{\Delta x_w^2} - \left(\frac{\rho}{\varepsilon}\right) k(K_d C_i - C_{i+N}) \qquad \text{(S-11)}$$

Polymer region: N_w+1<i<N

$$\frac{C_i^{j+1} - C_i^j}{\Delta t} = D_{PE}\frac{C_{i-1}^j - 2C_i^j + C_{i+1}^j}{\Delta x_{PE}^2} \qquad \text{(S-12)}$$

Sediment region: N+1<i<N+N_w

$$\frac{C_i^{j+1} - C_i^j}{\Delta t} = k(K_d C_{i-N} - C_i) \qquad \text{(S-13)}$$

Where N=N_w+N_p, and Δx_{PE} and Δx_w are resolutions in PE and pore water region, respectively

We added an extra point at the polymer-water boundary with the concentration of C_g in order to implement the finite difference approximation of second order derivatives:

$$\frac{C_i^{j+1} - C_i^j}{\Delta t} = D\frac{C_{i-1}^j - 2C_i^j + C_g}{\Delta x_w^2} - \left(\frac{\rho}{\varepsilon}\right) k(K_d C_i - C_{i+N}) \qquad \text{for} \quad i=N_w \qquad \text{(S-14)}$$

$$\frac{C_i^{j+1} - C_i^j}{\Delta t} = D_{PE}\frac{K_{PEw} C_g - 2C_{i+1}^j + C_{i+2}^j}{\Delta x_{PE}^2} \qquad \text{for} \quad i=N_w \qquad \text{(S-15)}$$

The concentration of the extra point can be obtained using our boundary layer condition (Equation 8):

$$D_{PE} \frac{C_{N_w+1} - K_{PEw} C_g}{\Delta x_{PE}} = D \frac{C_g - C_{N_w}}{\Delta x_w} \qquad \text{(S-16)}$$

From Equation S-16, C_g is calculated as:

$$C_g = A * C_{N_w+1} + B * C_{N_w} \qquad \text{(S-17)}$$

$$A = \frac{(\frac{D_{PE}}{dx_p})}{\frac{D_w}{\Delta x_w} + \frac{D_{PE}}{\Delta x_{PE}} K_{PEw}} \qquad \text{(S-18)}$$

$$B = \frac{(\frac{D_w}{dx_w})}{\frac{D_w}{\Delta x_w} + \frac{D_{PE}}{\Delta x_{PE}} K_{PEw}} \qquad \text{(S-19)}$$

Substituting Equation (S-17) in Equations (S-14) and (S-15), concentrations at the water-polymer boundary can be estimated as follows:

$$\frac{C_{N_w}^{j+1} - C_{N_w}^{j}}{\Delta t} = \frac{D}{\Delta x_w{}^2} \left(A * C_{N_w+1} + (B-2) * C_{N_w} + C_{N_w-1} \right) - \left(\frac{\rho k K_d}{\varepsilon} \right) * C_{N_w} + \left(\frac{\rho k}{\varepsilon} \right) * C_{N_w+N} \quad \text{(S-20)}$$

$$\frac{C_{N_w+1}^{j+1} - C_{N_w+1}^{j}}{\Delta t} = \frac{D_{PE}}{\Delta x_{PE}{}^2} \left(B * K_{PEw} * C_{N_w} + (A * K_{PEw} - 2) * C_{N_w+1} + C_{N_w+2} \right) \qquad \text{(S-21)}$$

Parameter estimation

In order to calculate the slow and fast desorption rate constants of pyrene, chrysene, and benzo(a)pyrene, Equation S-22 (Ghosh et al.[3]) was fitted with desorption kinetics data of mentioned PAHs. The desorption data were presented for manufactured gas plant site sediments in Ghosh et al.[4] (Table S1).

$$\frac{S}{S_0} = f e^{-k_f t} + (1-f) e^{-k_s t} \qquad \text{(S-22)}$$

Where f is fraction of fast desorbing pool in sediment, k_f is first-order rate constant for fast component, and k_s is first-order rate constant for slow component.

Table S5.1. Fractional loss of PAHs from Harbor point sediment measured by Ghosh et al.[4].

Time (day)	Pyrene	Chrysene	Benzo(a)pyrene
0	0	0	0
0.5	0.22	0.06	0.02
2	0.37	0.13	0.04
10	0.49	0.23	0.08

The equilibrium concentration of PAHs in PE ($C_{PE,eq}$) was determined by extracting the PE samplers after 56 days of deployment in the fully mixed PE-sediment system. Another time point measurement of PE concentration after 77 days of deployment confirmed that equilibrium had reached in PE for all PAHs in 56 days (The 77 data have been compared to 56 data in Table S3). The pore water initial (bulk) concentration (C_{w0}) and sediment-water partitioning coefficient (K_d) were calculated using the measured sediment concentration (C_{sed}) and reported values for K_{PEw} [3].

$$C_{w0} = \frac{C_{PE,eq}}{K_{PEw}}$$ (S-23)

$$K_d = \frac{C_{sed}}{C_{w0}}$$ (S-24)

Table S5.2 summarizes the parameter values used in model simulations for three PAHs.

Table S5.2. Parameter values used in model simulations

Parameter	Pyrene	Chrysene	Benzo(a)pyrene
Log D_{PE}[a] (cm^2/s)	-9.53	-10.28	-10.59
Log D_w[b] (cm^2/s)	-5.3	-5.39	-5.4
Log K_{PEw}[c] (L/kg)	4.9	5.6	6.2
Log K_d (L/kg)	3.3	4.2	4.9
Log k_f[d] (s^{-1})	-4.63	-4.76	-4.63
Log K_s[d] (s^{-1})	-6.53	-6.73	-7.2
ε (cm^3/ cm^3)	0.6		
ρ (g/ cm^3)	0.6		

a) Estimated from the correlation provided by Gschwend [5]
b) Gustafson and Dickhut [6]
c) Lohmann [7]
d) Measured by Ghosh et al. [4]

Table S5.3. Comparison of PAH concentration in PE in the fully mixed system after 56 days (C56) and 77 days (C77) of exposure. P-value is more than 0.05 for all pairs. This indicates that the difference between the 77 and 56 data is not significant at alpha level of 5% for all congeners.

Compound	C56 (ng/mg)	C77 (ng/mg)	p-value
Phenanthrene	44.5 ± 2.7	42.0 ± 1.4	0.23
Anthracene	16.2 ± 0.8	15.3 ± 0.8	0.26
Fluoranthene	51.5 ± 3.0	45.3 ± 4.8	0.12
Pyrene	57.6 ± 3.4	51.4 ± 5.5	0.17
Benz(a)anthracene	31.1 ± 1.3	30.4 ± 3.0	0.72
Chrysene	26.1 ± 1.4	26.3 ± 2.5	0.86

Benzo(b)fluoranthene	20.1 ± 1.4	19.6 ± 1.8	0.71	
Benzo(k)fluoranthene	23.2 ± 1.4	21.1 ± 1.7	0.17	
Benzo(a)pyrene	48.7 ± 1.5	45.7 ± 4.0	0.25	
Indeno(1,2,3,-cd)pyrene	42.2 ± 0.7	30.1 ± 16	0.26	
Dibenz(a,h)anthracene	4.3 ± 0.3	4.5 ± 0.5	0.76	

<u>Quantification of difference between low frequency (5 min pause) and high frequency (2min pause) vibrating data</u>

PE concentration of pyrene, chrysene, and benzo(a)pyrene in high frequency and low frequency vibrating systems at different exposure times have been shown in Table S4. Due to loss of some PE strips or low recoveries, duplicate measurements were not available for 7 day and 28 day data. Thus, only 14 day and 56 day data were compared for significance of difference. As indicated is Table S5, except for the pyrene concentration in day 14, PE concentrations in the two systems were not significantly different at alpha level of 0.05 (p-values were more than 0.05). The maximum difference between two models' predictions is for pyrene in day 7, which is only 2% (Table S6).

Table S5.4. PAH concentration in PE in high frequency and low frequency vibrating systems at different exposure times

Compound	PE concentration in low frequency vibrating system (µg/g)				PE concentration in high frequency vibrating system (µg/g)			
	7 days	14 days	28 days	56 days	7 days	14 days	28 days	56 days
Pyrene	243	279 ± 2.8	279	371 ± 0.1	303	311 ± 5	326	395 ± 24
Chrysene	69.1	75 ± 19	95	113 ± 8	99	95 ± 3	105	139 ± 8
Benzo(a)pyrene	99.8	137 ± 11	123	180 ± 2	152	142 ± 2	124	201 ± 12

Table S5.5. P-values calculated for the experimental data from high and low frequency vibrating systems.

Compound	P-value	
	14 days	56 days
Pyrene	0.014	0.28
Chrysene	0.28	0.08
Benzo(a)pyrene	0.62	0.13

Model prediction:

Table S5.6. Percent difference between high and low frequency model predictions at different exposure times.

Exposure time (day)	Pyrene	Chrysene	Benzo(a)pyrene
7	2	0.69	0.31
14	0.5	0.48	0.18
28	0.1	0.2	0.12
56	0	0	0

Quantification of difference between 2 min and 6 hour pause models

The percent differences between 2-min and 6-hour models have been indicated in Table S7 for different exposure times. The maximum difference is approximately 6%.

Table S5.7. Percent difference between 2-min and 6-hour model predictions for chrysene

Exposure time (day)	% difference
7	6.38
14	3.95
28	1.24
56	0.1

Matlab codes

Fast desorption model in static system

```matlab
outdir = 'Output_Static';
outfile = strcat(outdir,'/','Output_Static.txt');        % output file
Lw = 0.1;              % half-length of water region (cm)
Lp = 0.00125;          % half-length of polymer region (cm)
rho = 0.6;             % sediment bulk density (g/cm3)
kpew = 370000;         % PE-water partition coefficient for chrysene(cm3/cm3)
kd = 10^4.2/rho;         % sediment-water partitioning coefficient (cm3/g)
phi = 0.6;             % porosity(cm3/cm3)
Dwater = 4*10^-6;      % diffusivity in water (cm2/s)
Dw = Dwater/(1-log(phi^2));    % diffusivity in pore water (cm2/s)
Dp = 5*10^-11;         % diffusivity in PE (cm2/s)
kf = 1.7e-5;           % fast desorption rate constant (s-1)
Cw0 = 0.4;             %initial pore water concentration (ng/cm3)


Np = 5;                    % discretization number on lp
Nw = 200;                  % discretization number on lw
dxp = Lp/Np;               % resolution of water/sediment region
dxw = Lw/Nw;               % resolution of water or sediment region


A = (Dp/dxp)/((Dw/dxw)+(Dp*kpew/dxp)); %parameter
B = (Dw/dxw)/((Dw/dxw)+(Dp*kpew/dxp)); %parameter
```

```matlab
% initial condition
S0 = Cw0*kd;                            %initial sediment concentration (ng/g)
u0 = [Cw0*ones(Nw,1);zeros(Np,1);S0*ones(Nw,1)]; % Initial condition matrix

% defining the second-order differentiation operator
N = Np+Nw;
df1 = ones(Nw,1)*[1,-2,1];
Df1 = (Dw/(dxw^2))*spdiags(df1,[-1 0 1],Nw,Nw);
df2 = ones(Nw,1)*[0,(-rho*kf*kd/phi),0];
Df2 = spdiags(df2,[-1 0 1],Nw,Nw);
DfT1 = Df1+Df2;
df2_bbb = ones(Np,1)*[1,-2,1];
Df2bbbb = spdiags(df2_bbb,[-1 0 1],Np,Np);
DfT2 = [DfT1,zeros(Nw,Np);zeros(Np,Nw),Df2bbbb];
DfT2(1,:) = zeros(1,N);
DfT2(Nw,:) = [zeros(1,Nw-2),Dw/dxw^2,Dw/dxw^2*(B-2)-
rho*kf*kd/phi,Dw/dxw^2*A,zeros(1,Np-1)];
DfT2(Nw+1,:) = [zeros(1,Nw-1),B*kpew, kpew*A-2, 1,zeros(1,Np-2)];
DfT2(end,:) = [zeros(1,Nw+Np-2),2, -2];


DfT2(Nw+1:end,:) = DfT2(Nw+1:end,:)/(dxp^2)*Dp;


dfs1 = ones(Nw,1)*[0,rho*kf/phi,0];
Dfs1 = spdiags(dfs1,[-1 0 1],Nw,Nw);
Dfs1 = [Dfs1;zeros(Np,Nw)];
Dfs1(1,:) = zeros(1,Nw);


dfs2 = ones(Nw,1)*[0,kf*kd,0];
Dfs2 = spdiags(dfs2,[-1 0 1],Nw,Nw);
Dfs2(1,:) = zeros(1,Nw);
Dfs2 = [Dfs2,zeros(Nw,Np)];


dfs3 = ones(Nw,1)*[0,-kf,0];
Dfs3 = spdiags(dfs3,[-1 0 1],Nw,Nw);
Dfs3(1,:) = zeros(1,Nw);
DfT = [DfT2,Dfs1;Dfs2,Dfs3];
DfT = sparse(DfT);

Mp = @(u_current)(sum(u_current(Nw+1:N)))-((u_current(Nw+1)+u_current(N))/2);
%mass per unit area of PE (ng/cm2)

u_current (:,1) = u0;
u_inf = expm(10^14*DfT)*u0; % Equilibrium concentration (ng/cm3)
M_inf = Mp(u_inf);          % Equilibrium mass per unit area of PE (ng/cm2)

T_end = 56*24*3600;         % deployment time (s)
tvec = 10000:10000:T_end+10000;

 for jtt = 1:length(tvec)
     T_current = tvec(jtt);
     u_current (:,jtt) = expm(T_current*DfT)*u0;
     M(jtt) = Mp (u_current (:,jtt));
 end
```

```matlab
fid = fopen('Static.txt','w');
fprintf(fid,'%2.2e\n',M/M_inf);
fclose(fid);
```

Fast desorption model in high frequency vibrating system

```matlab
outdir = 'Output_Vibration';
outfile = strcat(outdir,'/','Output_Vibration.txt');          % output file
Lw = 0.1;              % half-length of water region (cm)
Lp = 0.00125;          % half-length of polymer region (cm)
rho = 0.6;             % sediment bulk density (g/cm3)
kpew = 370000;         % PE-water partition coefficient for chrysene(cm3/ cm3)
kd = 10^4.2/rho;       % sediment-water partitioning coefficient (cm3/g)
phi = 0.6;             % porosity(cm3/cm3)
Dwater = 4*10^-6;      % diffusivity in water (cm2/s)
Dw = Dwater/(1-log(phi^2));     % diffusivity in pore water (cm2/s)
Dp = 5*10^-11;         % diffusivity in PE (cm2/s)
kf = 1.4e-5;           % fast desorption rate constant (s-1)
Cw0 = 0.4;             %initial pore water concentration (ng/cm3)


Np = 5;                       % discretization number on lp
Nw = 200;                     % discretization number on lw
dxp = Lp/Np;                  % resolution of water/sediment region
dxw = Lw/Nw;                  % resolution of water or sediment region


A = (Dp/dxp)/((Dw/dxw)+(Dp*kpew/dxp)); %parameter
B = (Dw/dxw)/((Dw/dxw)+(Dp*kpew/dxp)); %parameter


% initial condition
S0 = Cw0*kd;                            %initial sediment concentration (ng/g)
u0 = [Cw0*ones(Nw,1);zeros(Np,1);S0*ones(Nw,1)]; % Initial condition matrix


% defining the second-order differentiation operator
N = Np+Nw;
df1 = ones(Nw,1)*[1,-2,1];
Df1 = (Dw/(dxw^2))*spdiags(df1,[-1 0 1],Nw,Nw);
df2 = ones(Nw,1)*[0,(-rho*kf*kd/phi),0];
Df2 = spdiags(df2,[-1 0 1],Nw,Nw);
DfT1 = Df1+Df2;
df2_bbb = ones(Np,1)*[1,-2,1];
Df2bbbb = spdiags(df2_bbb,[-1 0 1],Np,Np);
DfT2 = [DfT1,zeros(Nw,Np);zeros(Np,Nw),Df2bbbb];
DfT2(1,:) = zeros(1,N);
DfT2(Nw,:) = [zeros(1,Nw-2),Dw/dxw^2,Dw/dxw^2*(B-2)-
rho*kf*kd/phi,Dw/dxw^2*A,zeros(1,Np-1)];
DfT2(Nw+1,:) = [zeros(1,Nw-1),B*kpew, kpew*A-2, 1,zeros(1,Np-2)];
DfT2(end,:) = [zeros(1,Nw+Np-2),2, -2];


DfT2(Nw+1:end,:) = DfT2(Nw+1:end,:)/(dxp^2)*Dp;


dfs1 = ones(Nw,1)*[0,rho*kf/phi,0];
Dfs1 = spdiags(dfs1,[-1 0 1],Nw,Nw);
Dfs1 = [Dfs1;zeros(Np,Nw)];
```

```matlab
Dfs1(1,:) = zeros(1,Nw);

dfs2 = ones(Nw,1)*[0,kf*kd,0];
Dfs2 = spdiags(dfs2,[-1 0 1],Nw,Nw);
Dfs2(1,:) = zeros(1,Nw);
Dfs2 = [Dfs2,zeros(Nw,Np)];

dfs3 = ones(Nw,1)*[0,-kf,0];
Dfs3 = spdiags(dfs3,[-1 0 1],Nw,Nw);
Dfs3(1,:) = zeros(1,Nw);
DfT = [DfT2,Dfs1;Dfs2,Dfs3];
DfT = sparse(DfT);

Mp = @(u_current)(sum(u_current(Nw+1:N)))-((u_current(Nw+1)+u_current(N))/2);
%mass per unit area of PE (ng/cm2)

u_current (:,1) = u0;
u_inf = expm(10^14*DfT)*u0; % Equilibrium concentration (ng/cm3)
M_inf = Mp(u_inf);          % Equilibrium mass per unit area of PE (ng/cm2)

T_end = 120;                % pause cycle duration(s)
tvec = 60:60:T_end;
n = 2;
M(1) = 0;

for k=1:(7*24*3600)/T_end

    for jtt = 1:length(tvec)
        T_current = tvec(jtt);
        u_current (:,jtt) = expm(T_current*DfT)*u0;
        M(n) = Mp(u_current (:,jtt));
        n = n+1;
     end

    u0 = [Cw0*ones(Nw,1);u_current(Nw+1:N,length(tvec));S0*ones(Nw,1)];
    % resetting the initial condition after each pause cycle
end

fid = fopen('Vibration.txt','w');
fprintf(fid,'%2.2e\n',M/M_inf);
fclose(fid);
```

Fully mixed model

```matlab
function mixed
clc;
outdir = 'Output';
outfile = strcat(outdir,'/','Output_Mix');   % output file
m = 50;              % discretization number in time
N = 250;             % discretization number on x
L = 0.0025;          % Full-length of polymer region (cm)
rho = 0.6;           % sediment bulk density (g/cm3)
```

```matlab
kpew = 370000;        % PE-water partition coefficient for chrysene(cm3/ cm3)
kd = 10^4.2/rho;      % sediment-water partitioning coefficient (cm3/g)
dx = L/(N-1);         % resolution of polymer region
D = 5*10^-11;         % pyrene diffusivity in PE (cm2/s)
T = 56*24*3600;       % deployment time (sec)
dt = length(T)/m;     % time interval


%initial condition
C0 = 0.4;                       % initial water concentration (ng/cm3)
Cl= kpew*C0;                    % concentration at polymer-water boundary (ng/cm3)
Cp0 = [Cl;zeros(N-2,1);Cl];        % initial condition in polymer region


% defining the second-order differentiation operator
Df2 = D/dx^2*Df2_fd_gen(N);
Df2 = sparse(Df2);
Cp = Cp0;
for jtt = 2:m
Cp(:,jtt) = Cp(1:N,end)+dt*Df2* Cp(1:N,end);
M(jtt) = (sum(Cp(:,jtt))-( Cp(1,jtt)+ Cp(N,jtt))/2)*(L/(N-1));
end
fid = fopen('Output_Mix.txt','w');
fprintf(fid,'%2.2e\n',M);
fclose(fid);
end
function Df2 = Df2_fd_gen(N)
d = [-1; 0; 1];
B = ones(N,1)*[1,-2,1];
B(N-1,1) = 0;
B(2,3) = 0;
B(1,2) = 0;
B(N,2) = 0;
Df2 = spdiags(B,d,N,N);
end
```

Figures
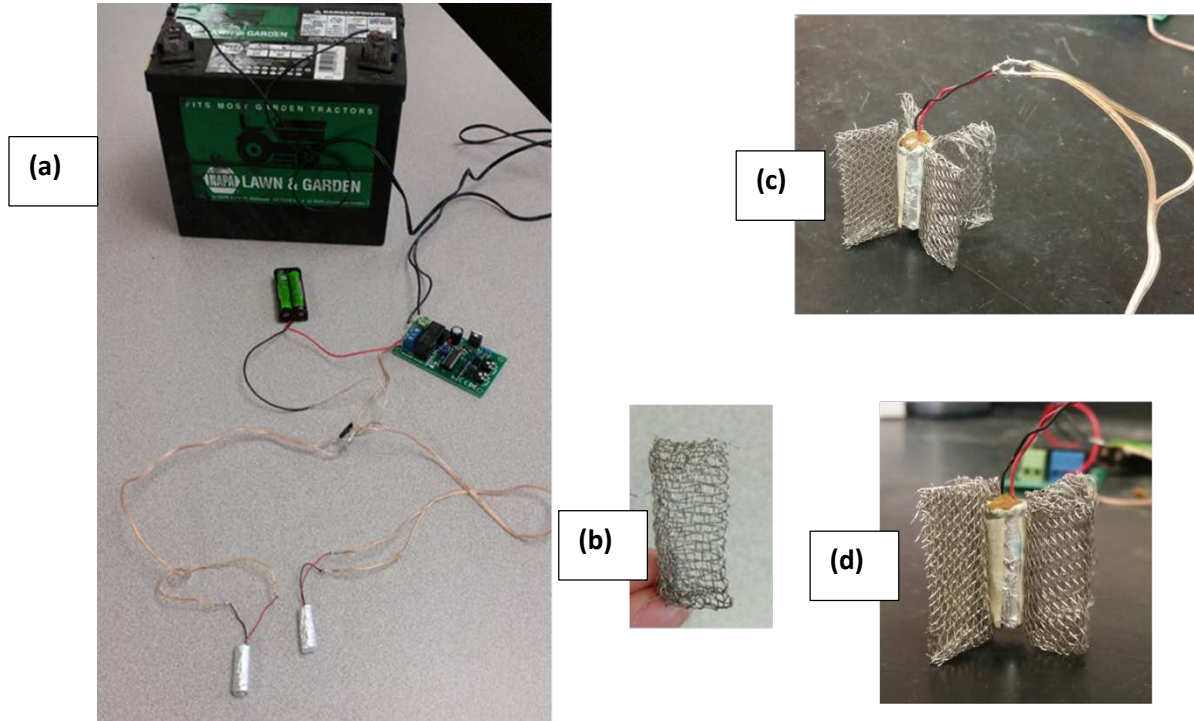
Figure S5.1- Vibrating system set up before insertion into sediment. a) Two motors were connected in parallel to a timer and a power supply (2 rechargeable batteries 1.2V each). The timers were powered by a 12 V battery. b) PE strip (6mm×20mm) closed up in stainless steel mesh. c) & d) Four meshes were attached to each motor like fins.
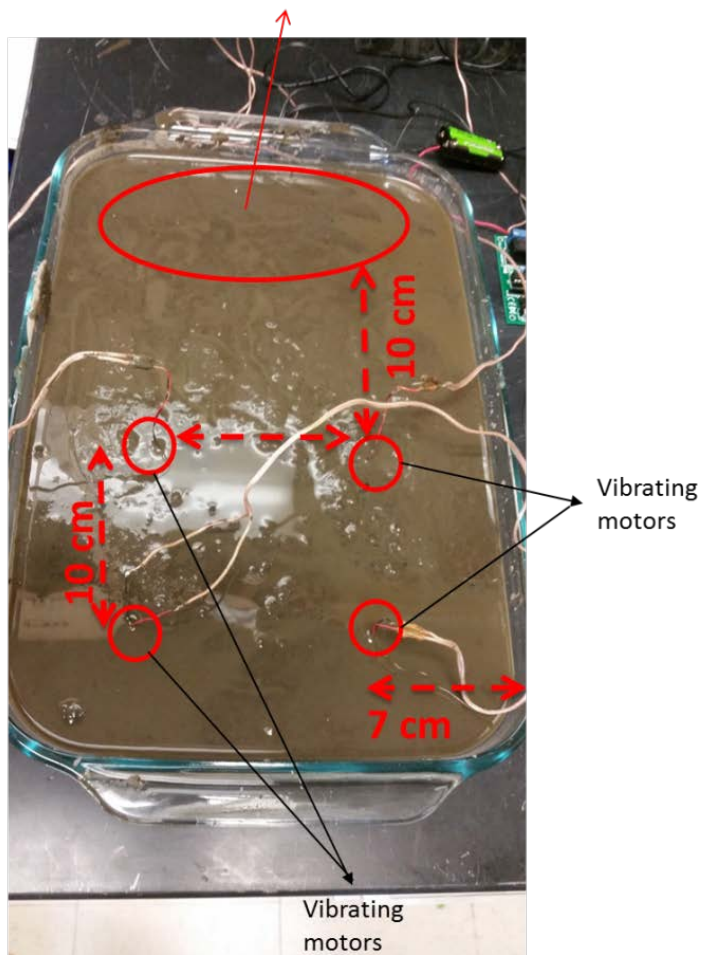
Figure S5.2- Vibrating system set up after insertion into sediment. The sediment slurry was placed in a large glass tray (25cm×35cm×6cm). Four motors were placed inside the sediment. Eight additional PE samplers, enclosed in stainless steel meshes without motors, were placed inside the same tray in a static mode far from the vibrating motors

Figure S5.3- Motor vibration in sediment. Based on our visual observation of vibration in sediment, the extent of mixing appears to extend at least 1 cm from the surface of the fins. As shown in the figure (taken with the platform slightly lifted from the sediment surface while vibrating), the vibration causes pressure waves to extend several cm away from the device, with actual fluidized mixing limited to about 1 cm around the sampler fins. The vibration effect is well beyond the thickness of the depletion layer at the end of each pause mode, which is only a few microns.
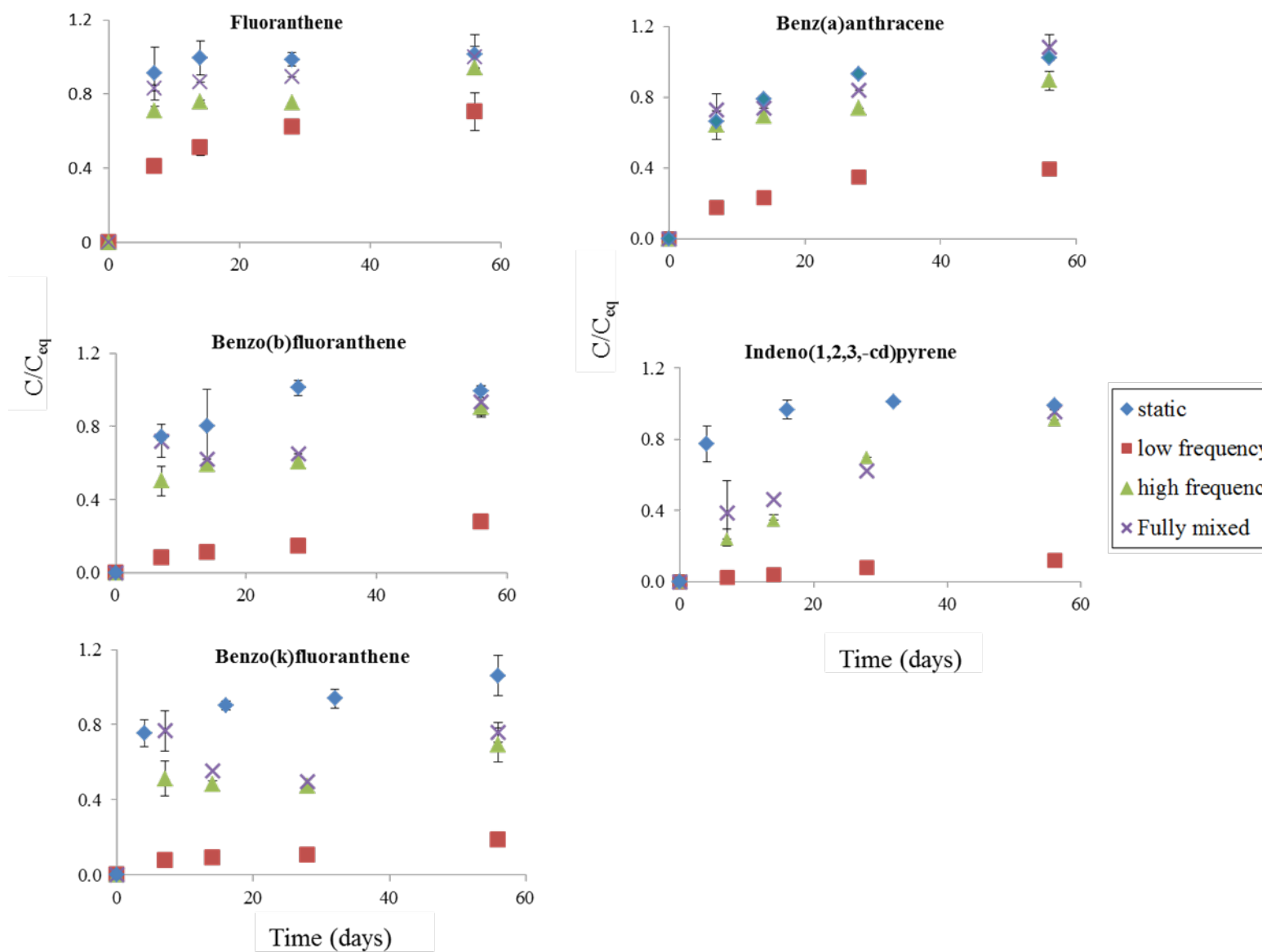
Figure S5.4- Experimental data for fractional uptake of fluoranthene and four heavy PAHs in PE passive sampler in four different systems.
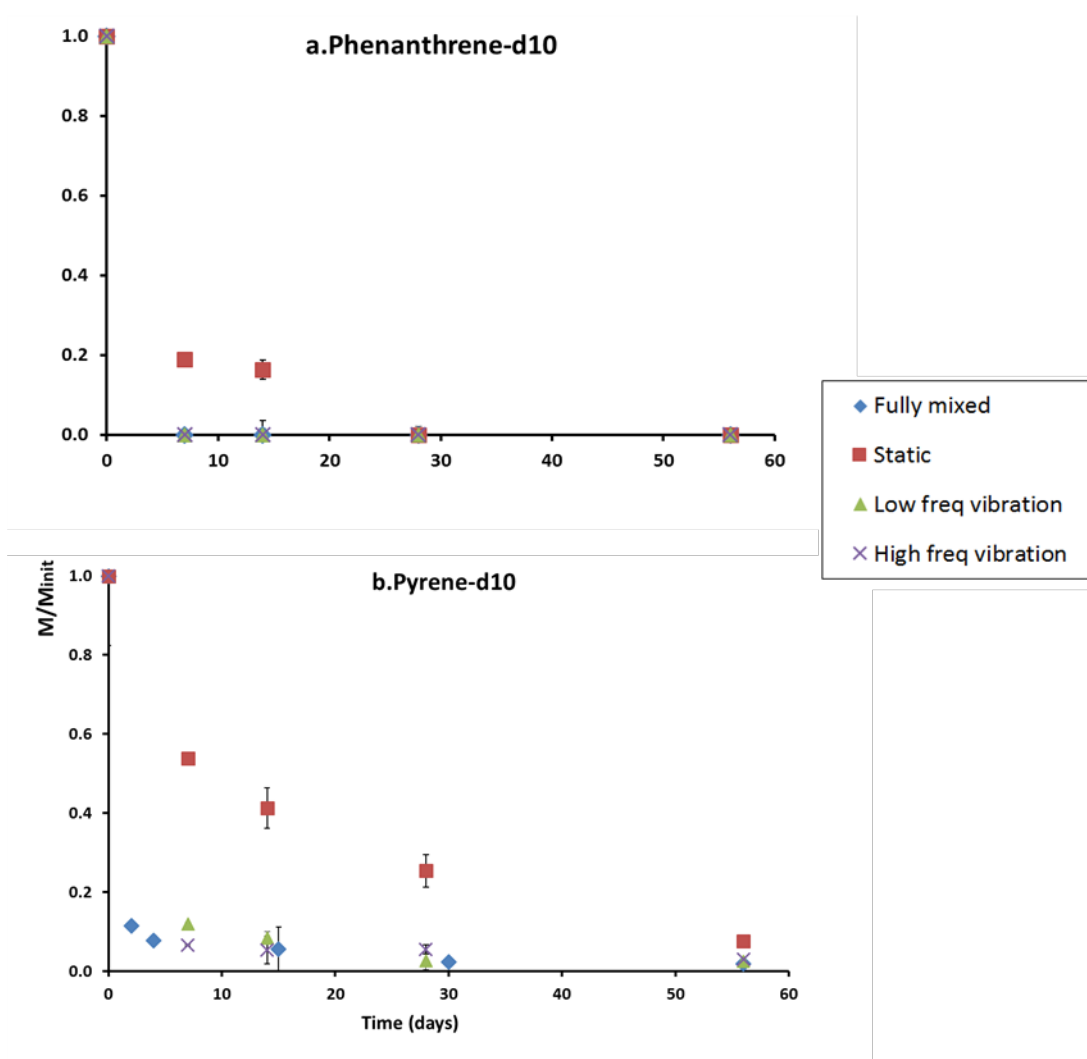
Figure S5.5. Loss profile of a) deuterated phenanthrene and b) deuterated pyrene from PE exposed to sediment under different mixing conditions.
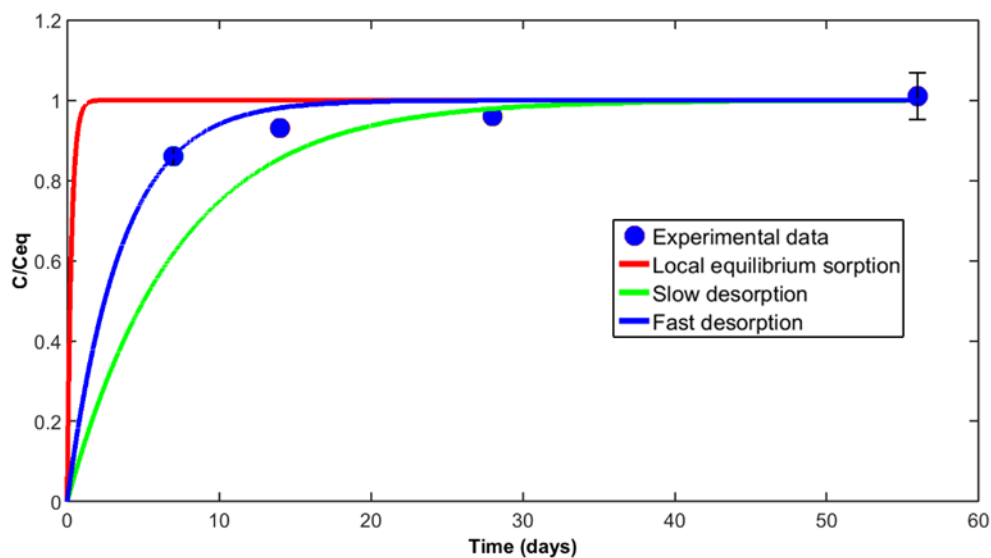
Figure S5.6- Comparison of three modeling approaches for the vibrating system for pyrene.
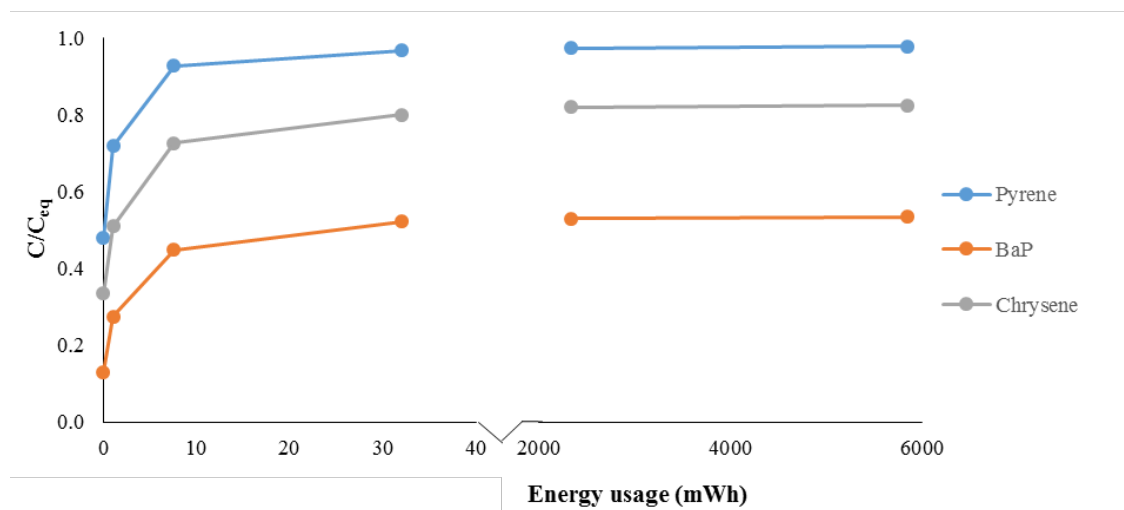
Figure S5.7. Fractional uptake of three PAHs into PE versus energy consumption of one motor after 15 days of deployment

Literature Cited

(1) Fernandez, L. A.; Harvey, C. F.; Gschwend, P. M. Using performance reference compounds in polyethylene passive samplers to deduce sediment porewater concentrations for numerous target chemicals. *Environ. Sci. Technol.* 2009, 43, 8888–8894.

(2) Crank, J. The Mathematics of Diffusion, 2nd ed.; Oxford University Press: Oxford, 1975.

(3) Ghosh, U.; Zimmerman, J. R.; Luthy, R. G. PCB and PAH Speciation among Particle Types in Contaminated Harbor Sediments and Effects on PAH Bioavailability. *Environ. Sci. Technol*. 2003, 37, 2209-2217.

(4) Ghosh, U.; Zimmerman, J. R.; Luthy, R. G. PCB and PAH Speciation among Particle Types in Contaminated Harbor Sediments and Effects on PAH Bioavailability. *Environ. Sci. Technol*. 2003, 37, 2209-2217.

(5) Gschwend, P. M. Using Passive Polyethylene Samplers to Evaluate Chemical Activities Controlling Fluxes and Bioaccumulation of Organic Contaminants in Bed Sediments, DTIC Document. 2010.

(6) Gustafson, K. E.; Dickhut, R. M.. Molecular diffusivitiy of polycyclic aromatic hydrocarbons in aqueous solution. *J. Chem. Eng. Data.*1994, 39, 281-285.

(7) Lohmann, R. Critical Review of Low-Density Polyethylene's Partitioning and Diffusion Coefficients for Trace Organic Contaminants and Implications for Its Use As a Passive Sampler. *Environ. Sci. Technol*. 2011, 46, 606-618.

10.2 Supporting information associated with section 6

Parameter estimation

PCB concentrations in PE after 56 days of deployment in the fully mixed PE-sediment system were used as the equilibrium concentration of PCBs in PE ($C_{PE,eq}$). Since no change was observed in the PE concentrations after 28 days of exposure in this system (The 28 data have been compared to 56 data in Table S5). The pore water initial (bulk) concentration (C_{w0}) and sediment-water partitioning coefficient (K_d) were calculated using the measured sediment concentration (C_{sed}) and reported values for K_{PEw}.[1]

$$C_{w0} = \frac{C_{PE,eq}}{K_{PEw}} \qquad\qquad\qquad\qquad\qquad\qquad (S\text{-}1)$$

$$K_d = \frac{C_{sed}}{C_{w0}} \qquad\qquad\qquad\qquad\qquad\qquad (S\text{-}2)$$

A two compartment model[2] was used to describe the desorption kinetics of PCBs from sediment particles into porewater:

$$\frac{S}{S_0} = f e^{-k_f t} + (1 - f) e^{-k_s t} \qquad\qquad (S\text{-}3)$$

Where S is PCB concentration in sediment, S_0 is PCB initial concentration in sediment, f is fraction of fast desorbing pool in sediment, k_f is first-order rate constant for fast component, and k_s is first-order rate constant for slow component.

The model was fitted to the normalized desorption data for PCB 128, 183, and 194 in order to determine in f, k_f, and k_s in Equation S-3 (Figure S6.6). These parameters are reported in Table S6.7.

Table S6.1 summarizes the parameter values used in model simulations for three PCBs.

Model equations

Static system

In a system containing a PE strip with the thickness of $2l_p$ and sediment/porewater with thickness of l_w on both sides, sediment concentration (S) changes following first order kinetics.[4,5]

$$\frac{\partial S}{\partial t} = k(K_d C_w - S) \qquad\qquad l_p < x < l_p + l_w \quad and \quad -l_p < x < -l_p - l_w \qquad (S\text{-}4)$$

Where t is time (s), S is chemical concentration in sediment (ng/g), K_d is sediment-water partition coefficient (cm^3/g), k is first order desorption rate constant (s^{-1}) and C_w is chemical concentration in water (ng/cm^3)

For a PE strip with concentration C_{PE} and at point x and time t:

$$\frac{\partial C_{PE}}{\partial t} = D_{PE} \frac{\partial^2 C_{PE}}{\partial x^2} \qquad\qquad -l_p < x < l_p \qquad\qquad (S\text{-}5)$$

Where C_{PE} is chemical concentration in PE (ng/cm^3) and D_{PE} is chemical diffusivity in PE (cm^2/s)

The transport equation in porewater with concentration of C_w at point x and time t will be as follows:

$$\frac{\partial C_w}{\partial t} = D \frac{\partial^2 C_w}{\partial x^2} - \left(\frac{\rho}{\varepsilon}\right) \frac{\partial S}{\partial t} \qquad l_p < x < l_p + l_w \quad and \quad -l_p < x < -l_p - l_w \quad (S-6)$$

Where ρ is sediment bulk density (g/cm^3) and ε is porosity (cm$^{3/}$ cm^3)

D is the diffusivity in water (D_w) after correction for tortuosity:

$$D = \frac{D_w}{1 - ln\varepsilon^2} \qquad (S-7)$$

Substituting Equation (1) in Equation (3), the transport equation in porewater can be re-written as:

$$\frac{\partial C_w}{\partial t} = D \frac{\partial^2 C_w}{\partial x^2} - \left(\frac{\rho}{\varepsilon}\right) k(K_d C_w - S) \qquad (S-8)$$

Initial conditions

The polymer was initially clean and porewater was assumed to be in equilibrium with sediment.

$$C_{PE} = 0 \qquad\qquad -l_p \leq x \leq l_p \qquad\qquad (S-9)$$
$$C_{w0} = S_0/K_d \qquad\qquad l_p < x < l_p + l_w \quad and \quad -l_p < x < -l_p - l_w \qquad (S-10)$$

Where S_0 is initial chemical concentration in sediment (ng/g) and C_{w0} is initial chemical concentration in water (ng/cm^3)

Boundary conditions

Continuity of flux and equilibrium condition was assumed at the PE-water boundary as done in previous work.[8]

$$D_{PE} \frac{\partial C_{PE}}{\partial x_{PE}} = D \frac{\partial C_w}{\partial x_w} \qquad\qquad x = l_p \text{ and } x = -l_p, \ t > 0 \qquad (S-11)$$

$$C_{PE} = K_{PEw} C_w \qquad\qquad x = l_p \text{ and } x = -l_p \qquad (S-12)$$

Where K_{PEw} is the PE-water partition coefficient (cm^3/cm^3)

Due to symmetry the flux will be zero at the center of the PE sheet. Porewater concentration is equal to the initial concentration far away from the polymer at $x=l_p+l_w$ and does not change over time:

$$\frac{\partial C_{PE}}{\partial x} = 0 \qquad\qquad x = 0 \qquad\qquad (S-12)$$

$$\frac{\partial C_w}{\partial t} = \frac{\partial S}{\partial t} = 0 \qquad\qquad x = l_p + l_w \quad and \quad x = -l_p - l_w \qquad (S-13)$$

Vibrating system

In the vibrating system, when the motor is in pause mode, the mass transfer is similar to the static mode and sediment and porewater concentration in the vicinity of the polymer depletes with time. Every time the motor vibrates, the sediment and porewater at the vicinity of the polymer is mixed up. We assumed that this mixing is enough to increase sediment concentration to the initial concentration in sediment (S_0). Porewater concentration right after each vibration pulse will also increase to the initial concentration:

$$C_w = C_{w0} ; \quad S = S_0 \qquad\qquad l_p < x < l_p + l_w \quad and \quad -l_p < x < -l_p - l_w, \qquad \text{(S-14)}$$

Fully mixed system

Diffusion in a polymer with thickness of $2l_p$ follows Fick's second law:

$$\frac{\partial C_{PE}}{\partial t} = D_{PE} \frac{\partial^2 C_{PE}}{\partial x^2} \qquad\qquad -l_p < x < l_p \qquad\qquad \text{(S-15)}$$

The passive sampler was assumed to be initially clean. Since the system is perfectly mixed, the porewater concentration remains constant and equal to the initial value (S_0/K_d) during the deployment time. The boundary condition is defined as:

$$C_{PE} = K_{PEw} C_{w0} \qquad\qquad x = l_p \text{ and } x = -l_p \qquad\qquad \text{(S-16)}$$

<u>Details of model simulation</u>

Numerical solution

Explicit, finite-difference numerical modeling techniques, as described by Crank [2] were used to solve the model's equations. Briefly, the explicit method is implemented by dividing the x region with the length of L, into N intervals each of width Δx such that $x_i = i\Delta x$; i=1, 2...N and $N\Delta x = L$. In this model, polymer region with the length of l_p (half of the polymer thickness) was divided into N_p intervals. Porewater and sediment regions had the same length of l_w and were divided into N_w intervals.

C_i^j is denoted for concentration in location idx and at time jdt, or in other words, C (iΔx, jΔt); j=1, 2, 3…

The numerical solution to model equations in pore water, polymer and sediment regions will be as Equations S-11, S-12 and S-13, respectively:

Porewater region: $1 < i < N_w$
$$\frac{C_i^{j+1} - C_i^j}{\Delta t} = D \frac{C_{i-1}^j - 2C_i^j + C_{i+1}^j}{\Delta x_w^2} - \left(\frac{\rho}{\varepsilon}\right) k(K_d C_i - C_{i+N}) \qquad \text{(S-17)}$$

Polymer region: $N_w + 1 < i < N$
$$\frac{C_i^{j+1} - C_i^j}{\Delta t} = D_{PE} \frac{C_{i-1}^j - 2C_i^j + C_{i+1}^j}{\Delta x_{PE}^2} \qquad\qquad\qquad \text{(S-18)}$$

Sediment region: N+1<i<N+N_w

$$\frac{C_i^{j+1}-C_i^j}{\Delta t} = k(K_d C_{i-N} - C_i)$$ (S-19)

Where N=N_w+N_p, and Δx_{PE} and Δx_w are resolutions in PE and pore water region, respectively

We added an extra point at the polymer-water boundary with the concentration of C_g in order to implement the finite difference approximation of second order derivatives:

$$\frac{C_i^{j+1}-C_i^j}{\Delta t} = D\frac{C_{i-1}^j-2C_i^j+C_g}{\Delta x_w^2} - \left(\frac{\rho}{\varepsilon}\right)k(K_d C_i - C_{i+N}) \qquad \text{for} \quad i=N_w$$ (S-20)

$$\frac{C_i^{j+1}-C_i^j}{\Delta t} = D_{PE}\frac{K_{PEw}C_g-2C_{i+1}^j+C_{i+2}^j}{\Delta x_{PE}^2} \qquad \text{for} \quad i=N_w$$ (S-21)

The concentration of the extra point can be obtained using our boundary layer condition (Equation 8):

$$D_{PE}\frac{C_{N_w+1}-K_{PEw}C_g}{\Delta x_{PE}} = D\frac{C_g-C_{N_w}}{\Delta x_w}$$ (S-22)

From Equation S-16, C_g is calculated as:

$$C_g = A * C_{N_w+1} + B * C_{N_w}$$ (S-23)

$$A = \frac{(\frac{D_{PE}}{dx_p})}{\frac{D_w}{\Delta x_w}+\frac{D_{PE}}{\Delta x_{PE}}K_{PEw}}$$ (S-24)

$$B = \frac{(\frac{D_w}{dx_w})}{\frac{D_w}{\Delta x_w}+\frac{D_{PE}}{\Delta x_{PE}}K_{PEw}}$$ (S-25)

Substituting Equation (S-17) in Equations (S-14) and (S-15), concentrations at the water-polymer boundary can be estimated as follows:

$$\frac{C_{N_w}^{j+1}-C_{N_w}^j}{\Delta t} = \frac{D}{\Delta x_w^2}\left(A * C_{N_w+1} + (B-2) * C_{N_w} + C_{N_w-1}\right) - \left(\frac{\rho k K_d}{\varepsilon}\right)* C_{N_w} + \left(\frac{\rho k}{\varepsilon}\right)* C_{N_w+N}$$ (S-26)

$$\frac{C_{N_w+1}^{j+1}-C_{N_w+1}^j}{\Delta t} = \frac{D_{PE}}{\Delta x_{PE}^2}(B * K_{PEw} * C_{N_w} + (A * K_{PEw} - 2) * C_{N_w+1} + C_{N_w+2})$$ (S-27)

Matlab codes

Fast desorption model in static system for PCB 128

```
outdir = 'Output_Static';
outfile = strcat(outdir,'/','Output_Static.txt');         % output file
Lw = 0.1;              % half-length of water region (cm)
Lp = 0.00125;          % half-length of polymer region (cm)
rho = 0.9;             % sediment bulk density (g/cm3)
kpew = 10^6.6*0.93;    % PE-water partition coefficient for chrysene(cm3/cm3)
kd = 10^5.47;          % sediment-water partitioning coefficient (cm3/g)
phi = 0.7;             % porosity(cm3/cm3)
Dwater = 10^-5.41;     % diffusivity in water (cm2/s)
Dw = Dwater/(1-log(phi^2));    % diffusivity in pore water (cm2/s)
Dp = 10^-9.35;         % diffusivity in PE (cm2/s)
kf = 3.33e-5;          % fast desorption rate constant (s-1)
Cw0 = 0.4;             %initial pore water concentration (ng/cm3)


Np = 5;                     % discretization number on lp
Nw = 200;                   % discretization number on lw
dxp = Lp/Np;                % resolution of water/sediment region
dxw = Lw/Nw;                % resolution of water or sediment region


A = (Dp/dxp)/((Dw/dxw)+(Dp*kpew/dxp)); %parameter
B = (Dw/dxw)/((Dw/dxw)+(Dp*kpew/dxp)); %parameter


% initial condition
S0 = Cw0*kd;                            %initial sediment concentration (ng/g)
u0 = [Cw0*ones(Nw,1);zeros(Np,1);S0*ones(Nw,1)]; % Initial condition matrix


% defining the second-order differentiation operator
N = Np+Nw;
df1 = ones(Nw,1)*[1,-2,1];
Df1 = (Dw/(dxw^2))*spdiags(df1,[-1 0 1],Nw,Nw);
df2 = ones(Nw,1)*[0,(-rho*kf*kd/phi),0];
Df2 = spdiags(df2,[-1 0 1],Nw,Nw);
DfT1 = Df1+Df2;
df2_bbb = ones(Np,1)*[1,-2,1];
Df2bbbb = spdiags(df2_bbb,[-1 0 1],Np,Np);
DfT2 = [DfT1,zeros(Nw,Np);zeros(Np,Nw),Df2bbbb];
DfT2(1,:) = zeros(1,N);
DfT2(Nw,:) = [zeros(1,Nw-2),Dw/dxw^2,Dw/dxw^2*(B-2)-
rho*kf*kd/phi,Dw/dxw^2*A,zeros(1,Np-1)];
DfT2(Nw+1,:) = [zeros(1,Nw-1),B*kpew, kpew*A-2, 1,zeros(1,Np-2)];
DfT2(end,:) = [zeros(1,Nw+Np-2),2, -2];


DfT2(Nw+1:end,:) = DfT2(Nw+1:end,:)/(dxp^2)*Dp;


dfs1 = ones(Nw,1)*[0,rho*kf/phi,0];
Dfs1 = spdiags(dfs1,[-1 0 1],Nw,Nw);
Dfs1 = [Dfs1;zeros(Np,Nw)];
Dfs1(1,:) = zeros(1,Nw);


dfs2 = ones(Nw,1)*[0,kf*kd,0];
Dfs2 = spdiags(dfs2,[-1 0 1],Nw,Nw);
```

```matlab
Dfs2(1,:) = zeros(1,Nw);
Dfs2 = [Dfs2,zeros(Nw,Np)];


dfs3 = ones(Nw,1)*[0,-kf,0];
Dfs3 = spdiags(dfs3,[-1 0 1],Nw,Nw);
Dfs3(1,:) = zeros(1,Nw);
DfT = [DfT2,Dfs1;Dfs2,Dfs3];
DfT = sparse(DfT);


Mp = @(u_current)(sum(u_current(Nw+1:N)))-((u_current(Nw+1)+u_current(N))/2);
%mass per unit area of PE (ng/cm2)


u_current (:,1) = u0;
u_inf = expm(10^14*DfT)*u0; % Equilibrium concentration (ng/cm3)
M_inf = Mp(u_inf);          % Equilibrium mass per unit area of PE (ng/cm2)


T_end = 56*24*3600;         % deployment time (s)
tvec = 10000:10000:T_end+10000;

 for jtt = 1:length(tvec)
     T_current = tvec(jtt);
     u_current (:,jtt) = expm(T_current*DfT)*u0;
     M(jtt) = Mp (u_current (:,jtt));
 end


fid = fopen('Static.txt','w');
fprintf(fid,'%2.2e\n',M/M_inf);
fclose(fid);
```

Fast desorption model in two min-pause vibrating system for PCB 128

```matlab
outdir = 'Output_Vibration';
outfile = strcat(outdir,'/','Output_Vibration.txt');           % output file
Lw = 0.1;              % half-length of water region (cm)
Lp = 0.00125;          % half-length of polymer region (cm)
rho = 0.6;             % sediment bulk density (g/cm3)
kpew = 10^6.6*0.93;    % PE-water partition coefficient for chrysene(cm3/cm3)
kd = 10^5.47;      % sediment-water partitioning coefficient (cm3/g)
phi = 0.7;             % porosity(cm3/cm3)
Dwater = 10^-5.41;     % diffusivity in water (cm2/s)
Dw = Dwater/(1-log(phi^2));     % diffusivity in pore water (cm2/s)
Dp = 10^-9.35;         % diffusivity in PE (cm2/s)
kf = 3.33e-5;           % fast desorption rate constant (s-1)
Cw0 = 0.4;             %initial pore water concentration (ng/cm3)


Np = 5;                    % discretization number on lp
Nw = 200;                  % discretization number on lw
dxp = Lp/Np;               % resolution of water/sediment region
dxw = Lw/Nw;               % resolution of water or sediment region


A = (Dp/dxp)/((Dw/dxw)+(Dp*kpew/dxp)); %parameter
B = (Dw/dxw)/((Dw/dxw)+(Dp*kpew/dxp)); %parameter
```

```matlab
% initial condition
S0 = Cw0*kd;                            %initial sediment concentration (ng/g)
u0 = [Cw0*ones(Nw,1);zeros(Np,1);S0*ones(Nw,1)]; % Initial condition matrix

% defining the second-order differentiation operator
N = Np+Nw;
df1 = ones(Nw,1)*[1,-2,1];
Df1 = (Dw/(dxw^2))*spdiags(df1,[-1 0 1],Nw,Nw);
df2 = ones(Nw,1)*[0,(-rho*kf*kd/phi),0];
Df2 = spdiags(df2,[-1 0 1],Nw,Nw);
DfT1 = Df1+Df2;
df2_bbb = ones(Np,1)*[1,-2,1];
Df2bbbb = spdiags(df2_bbb,[-1 0 1],Np,Np);
DfT2 = [DfT1,zeros(Nw,Np);zeros(Np,Nw),Df2bbbb];
DfT2(1,:) = zeros(1,N);
DfT2(Nw,:) = [zeros(1,Nw-2),Dw/dxw^2,Dw/dxw^2*(B-2)-
rho*kf*kd/phi,Dw/dxw^2*A,zeros(1,Np-1)];
DfT2(Nw+1,:) = [zeros(1,Nw-1),B*kpew, kpew*A-2, 1,zeros(1,Np-2)];
DfT2(end,:) = [zeros(1,Nw+Np-2),2, -2];

DfT2(Nw+1:end,:) = DfT2(Nw+1:end,:)/(dxp^2)*Dp;

dfs1 = ones(Nw,1)*[0,rho*kf/phi,0];
Dfs1 = spdiags(dfs1,[-1 0 1],Nw,Nw);
Dfs1 = [Dfs1;zeros(Np,Nw)];
Dfs1(1,:) = zeros(1,Nw);

dfs2 = ones(Nw,1)*[0,kf*kd,0];
Dfs2 = spdiags(dfs2,[-1 0 1],Nw,Nw);
Dfs2(1,:) = zeros(1,Nw);
Dfs2 = [Dfs2,zeros(Nw,Np)];

dfs3 = ones(Nw,1)*[0,-kf,0];
Dfs3 = spdiags(dfs3,[-1 0 1],Nw,Nw);
Dfs3(1,:) = zeros(1,Nw);
DfT = [DfT2,Dfs1;Dfs2,Dfs3];
DfT = sparse(DfT);

Mp = @(u_current)(sum(u_current(Nw+1:N)))-((u_current(Nw+1)+u_current(N))/2);
%mass per unit area of PE (ng/cm2)

u_current (:,1) = u0;
u_inf = expm(10^14*DfT)*u0; % Equilibrium concentration (ng/cm3)
M_inf = Mp(u_inf);          % Equilibrium mass per unit area of PE (ng/cm2)

T_end = 120;                % pause cycle duration(s)
tvec = 60:60:T_end;
n = 2;
M(1) = 0;

for k=1:(7*24*3600)/T_end

    for jtt = 1:length(tvec)
        T_current = tvec(jtt);
        u_current (:,jtt) = expm(T_current*DfT)*u0;
```

```
        M(n) = Mp(u_current (:,jtt));
        n = n+1;
     end

    u0 = [Cw0*ones(Nw,1);u_current(Nw+1:N,length(tvec));S0*ones(Nw,1)];
    % resetting the initial condition after each pause cycle
end


fid = fopen('Vibration.txt','w');
fprintf(fid,'%2.2e\n',M/M_inf);
fclose(fid);
```

Well-mixed model for PCB 128

```
function mixed
clc;
outdir = 'Output';
outfile = strcat(outdir,'/','Output_Mix');    % output file
m = 50;                  % discretization number in time
N = 250;                 % discretization number on x
L = 0.0025;              % Full-length of polymer region (cm)
rho = 0.6;               % sediment bulk density (g/cm3)
kpew = 10^6.6*0.93;   % PE-water partition coefficient for chrysene(cm3/cm3)
kd = 10^5.47;      % sediment-water partitioning coefficient (cm3/g)
dx = L/(N-1);            % resolution of polymer region
D = 10^-9.35;            % pyrene diffusivity in PE (cm2/s)
T = 56*24*3600;          % deployment time (sec)
dt = length(T)/m;     % time interval


%initial condition
C0 = 0.4;                         % initial water concentration (ng/cm3)
Cl= kpew*C0;                       % concentration at polymer-water boundary (ng/cm3)
Cp0 = [Cl;zeros(N-2,1);Cl];         % initial condition in polymer region

% defining the second-order differentiation operator
Df2 = D/dx^2*Df2_fd_gen(N);
Df2 = sparse(Df2);
Cp = Cp0;
for jtt = 2:m
Cp(:,jtt) = Cp(1:N,end)+dt*Df2* Cp(1:N,end);
M(jtt) = (sum(Cp(:,jtt))-( Cp(1,jtt)+ Cp(N,jtt))/2)*(L/(N-1));
end
fid = fopen('Output_Mix.txt','w');
fprintf(fid,'%2.2e\n',M);
fclose(fid);
end
function Df2 = Df2_fd_gen(N)
d = [-1; 0; 1];
B = ones(N,1)*[1,-2,1];
B(N-1,1) = 0;
B(2,3) = 0;
B(1,2) = 0;
B(N,2) = 0;
```

```
Df2 = spdiags(B,d,N,N);
end
```

Tables

Table S6.1. Parameter values used in model simulations

Parameter	PCB 128	PCB 183	PCB 194
Log D_{PE}[a] (cm^2/s)	-9.35	-9.53	-9.7
Log D_w[b] (cm^2/s)	-5.41	-5.44	-5.47
Log K_{PEw}[a] (L/kg)	6.6	7.1	7.3
Log K_d (L/kg)	5.47	6.13	6.75
k_f (s^{-1})	3.33×10^{-5}	3.06×10^{-5}	2.78×10^{-5}
ε (cm^3/cm^3)	0.7		
ρ (g/cm^3)	0.9		

e) Lohmann [1]
f) Gustafson and Dickhut [3]

Table S6.2. Comparison of PCB concentration in PE in the fully mixed system after 28 days (C28) and 56 days (C56) of exposure. P-value is more than 0.05 for all pairs. This indicates that the difference between the 28 and 56 data is not significant at alpha level of 5% for all congeners.

Compound	C28 (ng/g)	C56 (ng/g)	P-values
PCB 31	60.2 ± 8.3	58.4 ± 10.9	0.71
PCB 70+ 76	56.7 ± 10.1	34.9 ± 6.01	0.52
PCB 99	23.91 ± 2.8	20.5 ± 4.5	0.36
PCB 146	61.5 ± 23.8	50.8 ± 8.9	0.51
PCB 153	208.6 ± 84.6	178.7 ± 35.1	0.60
PCB 132	52.6 ± 27.9	38.0 ± 8.4	0.47
PCB 163+PCB 138	294.3 ± 156.3	221.1 ± 46.5	0.52
PCB 158	40.1 ± 31.2	26.5 ± 7.4	0.54
PCB 178+PCB 129	48.8 ± 19.9	42.7 ± 8	0.66
PCB 187+PCB 182	109.9 ± 15.3	118.3 ± 18	0.57

PCB 183	63.0 ± 15.9	62.3 ± 12.3	0.95
PCB 128	26.2 ± 20.8	16.3 ± 5.3	0.50
PCB 185	11.8 ± 1.8	12.4 ± 2.2	0.74
PCB 201	115.3 ± 17	136.6 ± 22.1	0.25
PCB 203+PCB 196	129.5 ± 22	155.8 ± 27.7	0.26
PCB 208+PCB 195	26.0 ± 5.4	30.8 ± 5.4	0.34
PCB 194	54.3 ± 9.2	64.9 ± 14.6	0.36

Table S6.3. PCB concentration in static PE at different exposure times from experiment 1 and 2.

Compound	Experiment 1				Experiment 2			
	7 d	14 d	28 d	56 d	7 d	14 d	28 d	56 d
PCB 31	19.9 ± 2.3	18.5 ± 2.4	26.1 ± 5.6	25.7 ± 4.6	15.7 ± 1.9	16.8 ± 1.8	18.5 ± 2.2	18.1 ± 2.1
PCB 70+ 76	12.1 ± 1.9	11.7 ± 1.5	16.1 ± 2.4	17.7 ± 3.1	10.3 ± 1.2	11.1 ± 1.3	12.4 ± 1.4	12.3 ± 1.4
PCB 99	3.5 ± 0.3	3.7 ± 0.6	8.1 ± 1.7	7.1 ± 1.5	3.6 ± 0.6	4.6 ± 0.5	5.4 ± 0.03	6.2 ± 0.5
PCB 146	15.4 ± 0.6	17.3 ± 1.6	22.0 ± 0.4	26.5 ± 2.7	14.9 ± 0.4	22.3 ± 1.3	21.8 ± 2.2	21.5 ± 1.1
PCB 153	31.5 ± 6.5	36.0 ± 3	45.8 ± 0.9	54.0 ± 5.8	25.7 ± 1.4	28.2 ± 3.7	42.1 ± 8.3	42.3 ± 4.6
PCB 132	6.7 ± 1.4	9.0 ± 0.9	11.3 ± 0.3	13.6 ± 1.1	4.5 ± 0.4	7.2 ± 1	10.4 ± 1.9	10.9 ± 1.1
PCB 163+PCB 138	38.6 ± 0.2	44.7 ± 4.6	56.7 ± 1	66.4 ± 6.4	34.4 ± 2.6	29.2 ± 4.8	49.9 ± 9.9	52.2 ± 5.4
PCB 158	3.1 ± 0.4	3.9 ± 0.3	5.1 ± 0.1	5.9 ± 0.7	2.6 ± 0.4	2.9 ± 0.9	4.6 ± 1.2	4.8 ± 0.4
PCB 178+PCB 129	5.2 ± 0.3	8.6 ± 0.9	11.0 ± 0.8	12.7 ± 1.7	4.3 ± 0.6	7.9 ± 5.3	8.8 ± 1.4	9.8 ± 1.3
PCB 187+PCB 182	25.4 ± 1.7	27.0 ± 2.7	33.2 ± 1.9	36.6 ± 4.5	22.7 ± 1.7	25.3 ± 2.6	31.8 ± 4.8	33.8 ± 4.8
PCB 183	8.3 ± 0.3	10.6 ± 1	17.5 ± 1	19.1 ± 2.4	7.2 ± 0.5	9.2 ± 1.3	13.9 ± 2.1	14.6 ± 2.2
PCB 128	2.5 ± 0.1	2.9 ± 0.2	3.8 ± 0.1	4.7 ± 0.5	1.5 ± 0.1	1.9 ± 0.4	3.6 ± 0.8	3.7 ± 0.4
PCB 185	3.8 ± 0.1	4.0 ± 0.4	4.7 ± 0.4	5.1 ± 0.7	2.1 ± 0.3	2.7 ± 0.4	3.8 ± 0.7	3.9 ± 0.6
PCB 201	24.4 ± 1.6	26.3 ± 3.2	41.2 ± 3.1	43.8 ± 5.7	21.5 ± 2.1	21.3 ± 3.5	35.1 ± 6.5	36.5 ± 5.9
PCB 203+PCB 196	26.4 ± 0.5	28.2 ± 3	45.5 ± 3.7	48.6 ± 5.9	23.5 ± 2.4	26.9 ± 4	39.4 ± 6.7	40.5 ± 6.5
PCB 208+PCB 195	5.7 ± 0.7	6.9 ± 0.9	8.1 ± 0.6	8.8 ± 1.1	3.5 ± 0.3	3.7 ± 0.6	6.8 ± 1.2	7.4 ± 1.1
PCB 194	12.0 ± 0.8	18.1 ± 2	21.0 ± 2.3	21.6 ± 2.2	10.0 ± 1.5	8.5 ± 0.7	17.9 ± 3.4	18.0 ± 2.9

Table S6.4. P-values calculated for the PCB concentrations in static PE from experiment 1 and experiment 2. P-value is more than 0.05 for all pairs. This indicates that the difference between PCB uptake in two experiments is not significant at alpha level of 5% for all congeners.

Compound	P-value			
	7 d	14 d	28 d	56 d
PCB 31	0.1	0.45	0.17	0.12
PCB 70+ 76	0.38	0.64	0.2	0.1
PCB 99	0.7	0.18	0.13	0.51
PCB 146	0.19	0.07	0.87	0.24
PCB 153	0.2	0.08	0.51	0.14
PCB 132	0.27	0.11	0.5	0.10
PCB 163+ 138	0.1	0.07	0.35	0.12
PCB 158	0.34	0.18	0.56	0.26
PCB 178+ 129	0.11	0.83	0.1	0.18
PCB 187+ 182	0.11	0.07	0.68	0.57
PCB 183	0.06	0.27	0.08	0.17
PCB 128	0.06	0.05	0.73	0.15
PCB 185	0.08	0.068	0.14	0.18
PCB 201	0.09	0.11	0.26	0.30
PCB 203+ 196	0.08	0.35	0.28	0.29
PCB 208+ 195	0.15	0.05	0.2	0.27
PCB 194	0.07	0.14	0.31	0.21

Table S6.5. PRC fraction remaining in PE (f_{PRC}) deployed in static system after different exposure times.

Compound	Experiment 1				Experiment 2			
	7 d	14 d	28 d	56 d	7 d	14 d	28 d	56 d
PCB 29	0.7 ± 0.04	0.6 ± 0.03	0.45 ± 0.03	0.32 ± 0.03	0.63 ± 0.02	0.60 ± 0.02	0.46 ± 0.02	0.32 ± 0.02
PCB 69	0.75 ± 0.03	0.67 ± 0.03	0.54 ± 0.02	0.39 ± 0.02	0.73 ± 0.01	0.71 ± 0.01	0.56 ± 0.00	0.39 ± 0.04

| PCB 155 | 0.89 ± 0.02 | 0.83 ± 0.04 | 0.78 ± 0.07 | 0.64 ± 0.00 | 0.82 ± 0.03 | 0.81 ± 0.01 | 0.76 ± 0.09 | 0.64 ± 0.06 |
| PCB 192 | 0.93 ± 0.05 | 0.9 ± 0.05 | 0.88 ± 0.06 | 0.74 ± 0.01 | 0.94 ± 0.01 | 0.86 ± 0.04 | 0.90 ± 0.04 | 0.74 ± 0.01 |

Table S6.6. P-values calculated for f_{PRC} in static system from experiment 1 and experiment 2. P-value is more than 0.05 for all pairs. This indicates that the difference between PRC loss in two experiments is not significant at alpha level of 5% for all congeners.

Compound	P-value			
	7 d	14 d	28 d	56 d
PCB 29	0.3	0.84	0.90	0.22
PCB 69	0.56	0.94	0.21	0.30
PCB 155	0.13	0.54	0.41	0.48
PCB 192	0.85	0.32	0.17	0.21

Table S6.7. $\log_{PEw}$ of PCB congeners. For PCB (70+76), PCB (82+151), PCB (163+138), PCB (182+187) the average log K_{PEw} of the two PCBs was used

PCB congener	$\log K_{ow}$[a]	$\log_{KPEw}$[b]
31	5.67	5.43
70+76	6.2	6.06
76	6.13	5.97
99	6.39	6.28
82+151	6.2	6.06
118	6.74	6.69
128	6.74	6.69
132	6.58	6.50
138	6.99	6.99
151	6.32	6.20
153	6.92	6.91
158	7.02	7.02
163+138	6.83	6.80
177	7.08	7.09
180	7.36	7.42
183	7.2	7.24
185	7.11	7.13
182+187	7.2	7.24
187	7.17	7.20
194	7.8	7.94

195	7.56	7.66
196	7.65	7.77
201	7.62	7.73
203	7.65	7.77
208	7.71	7.84

a) Hawker and Connell [6]

b) From the correlation provided by Ghosh et al. [8]
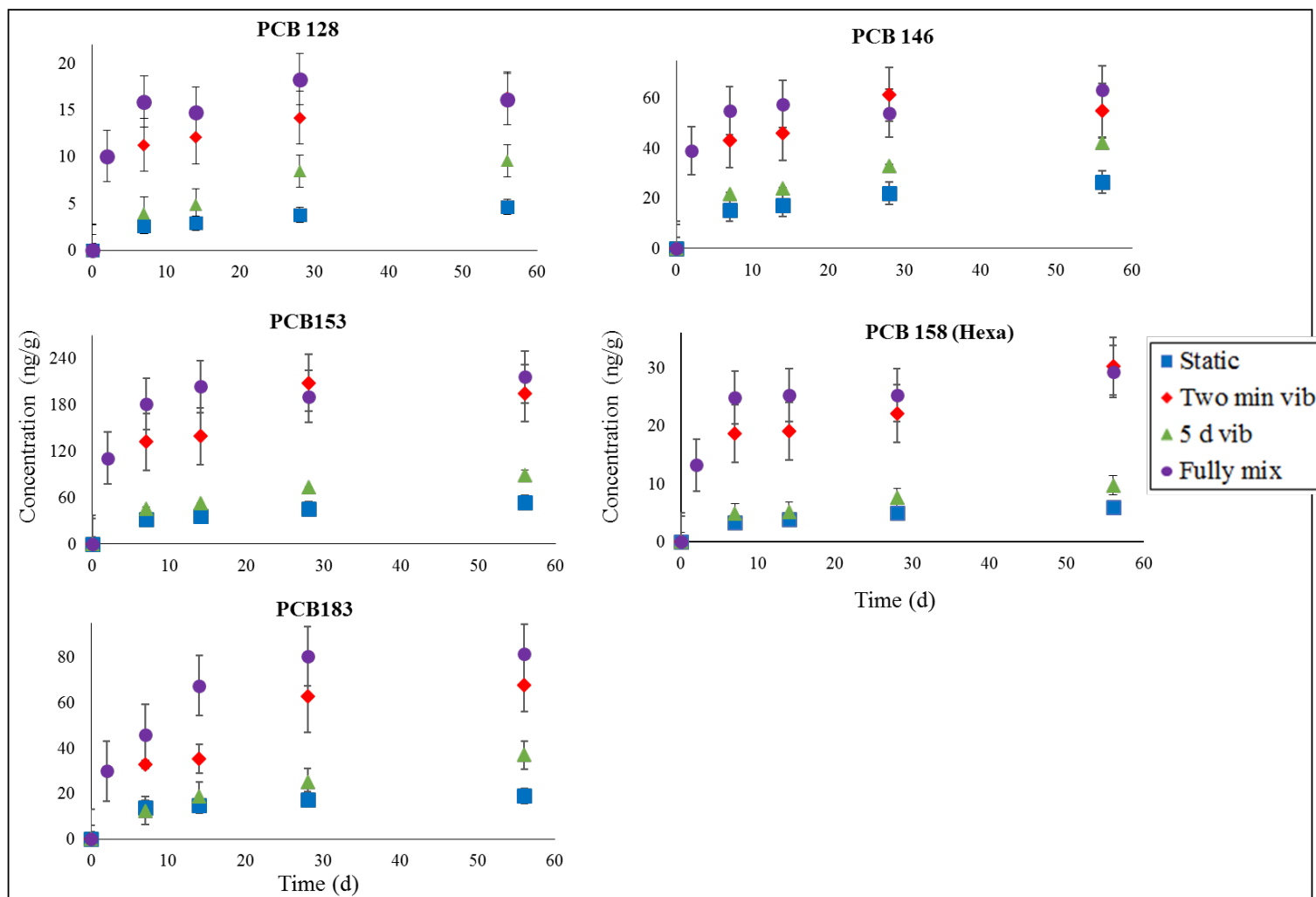
Figure S6.1. Comparison of uptake rate of hexachloro-congeners into PE in static, vibrating, and fully mixed systems
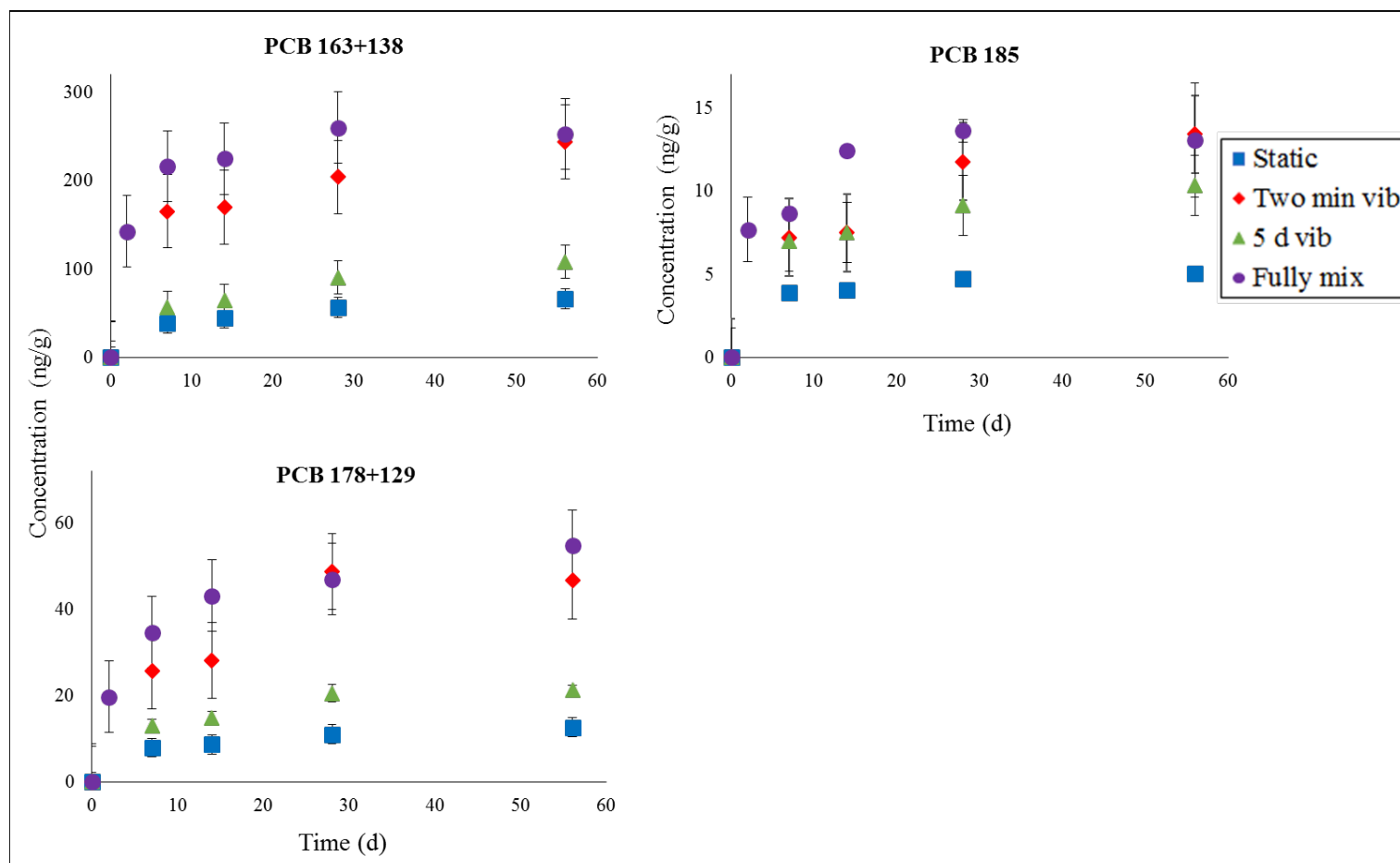
Figure S6.2. Comparison of uptake rate of heptachloro-congeners into PE in static, vibrating, and fully mixed systems
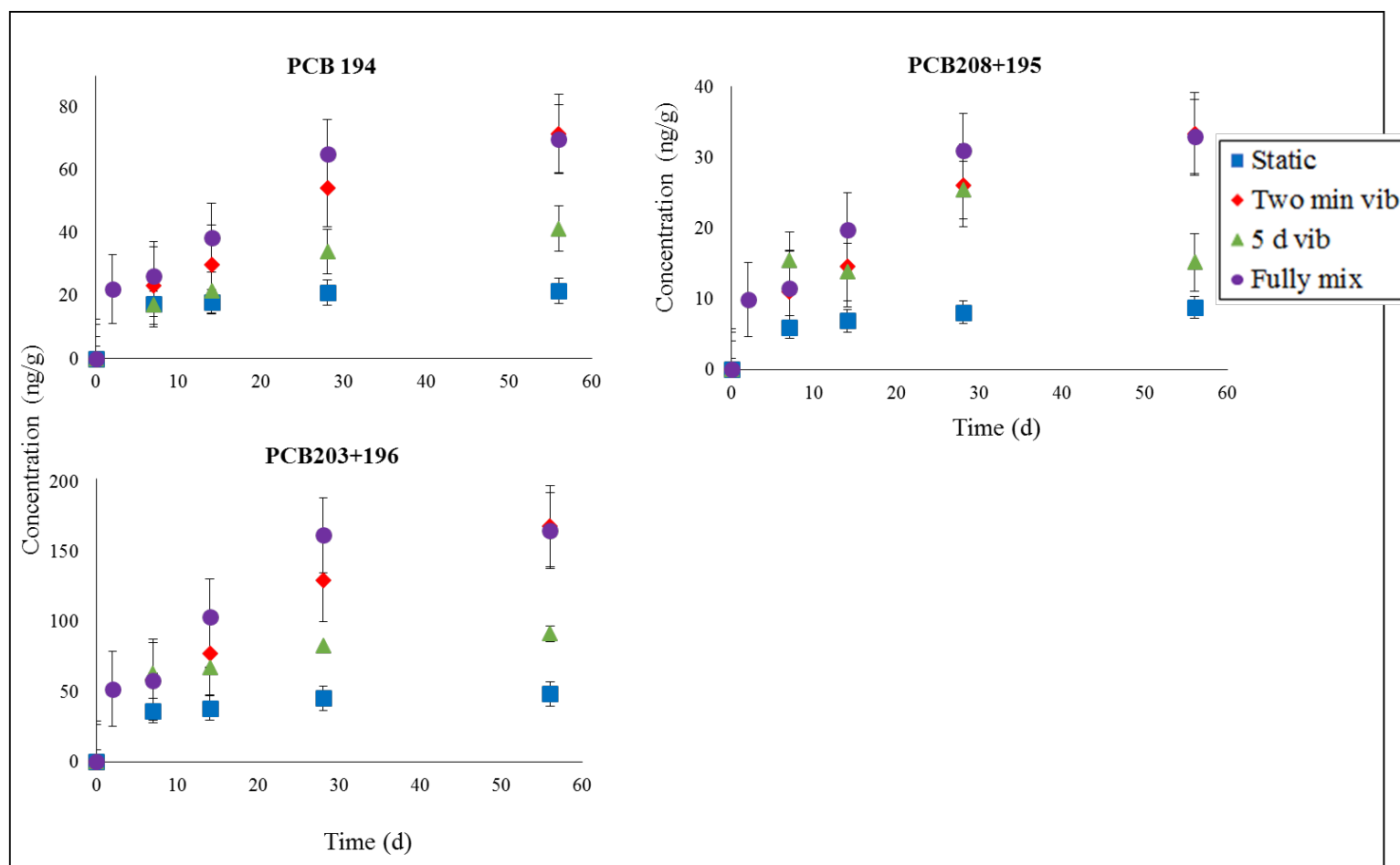
Figure S6.3. Comparison of uptake rate of octachloro-congeners into PE in static, vibrating, and fully mixed systems
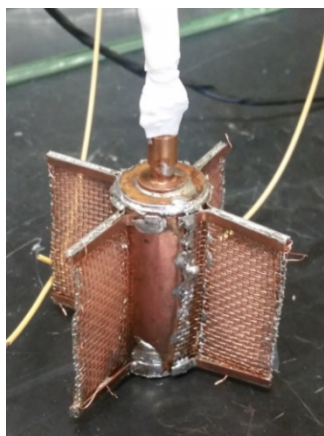
Figure S6.4. Prototype of *in situ* vibrating passive sampler built with copper casing
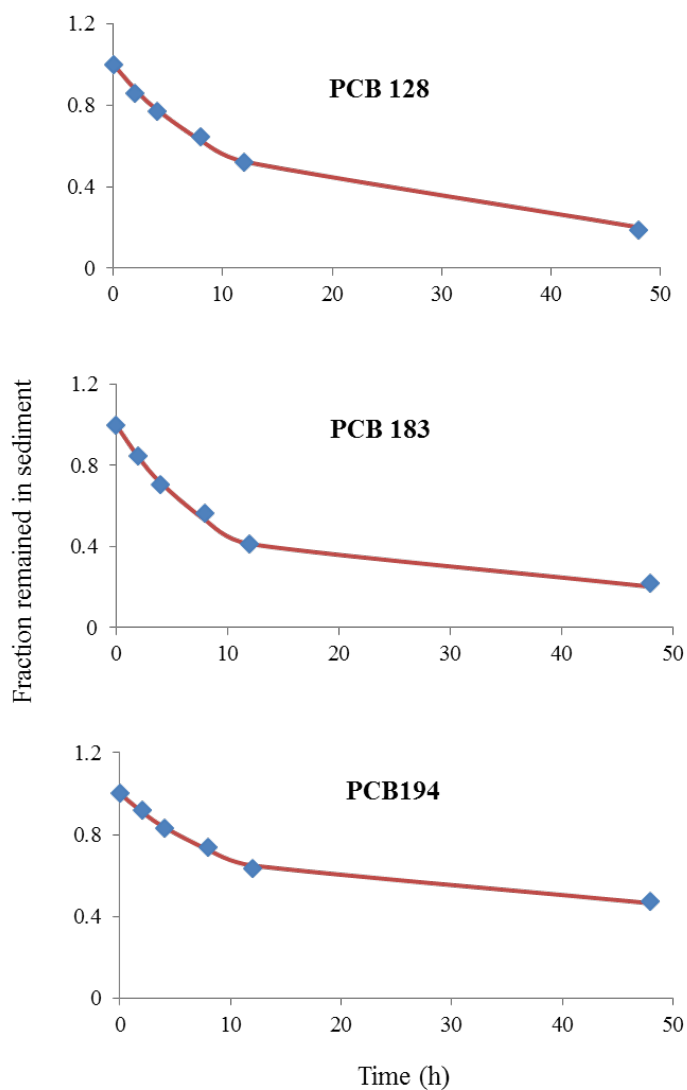
Figure S6.5. Normalized desorption data for three PCBs and dual compartment model fit

Table S6.8. Parameters estimated by fitting dual compartment model (Equation S-3) to normalized desorption data for three PCBs

Compound	f	$k_f (s^{-1})$	$k_s (s^{-1})$
PCB 128	0.48	3.33×10^{-5}	5.56×10^{-6}
PCB 183	0.8	3.06×10^{-5}	7×10^{-7}
PCB 194	0.48	2.78×10^{-5}	7×10^{-7}

Reference

1- Lohmann, R. Critical review of low-density polyethylene's partitioning and diffusion coefficients for trace organic contaminants and implications for its use as a passive sampler. *Environ. Sci. Technol.* **2011**, 46, 606-618.

2- Ghosh, U.; Talley, J. W.; Luthy, R. G. Particle-Scale Investigation of PAH Desorption Kinetics and Thermodynamics from Sediment. *Environ. Sci. Technol*. **2001**, 35, 3468-3475.

3- Gustafson, K. E.; Dickhut, R. M.. Molecular diffusivitiy of polycyclic aromatic hydrocarbons in aqueous solution. *J. Chem. Eng. Data.***1994**, 39, 281-285.

4- Lampert, D. An assessment of the design of *in situ* management approaches for contaminated sediments. Ph.D. Thesis, The University of Texas at Austin, May 2010.

5- Werner, D.; Ghosh, U.; Luthy, R. G. Modeling polychlorinated biphenyl mass transfer after amendment of contaminated sediment with activated carbon. *Environ. Sci. Technol*. **2006**, 40, 4211−4218.

6- Hawker, D. W.; Connell, D. W. Octanol-water partition coefficients of polychlorinated biphenyl congeners. *Environ. Sci. Technol.* **1988**, 22, 382-387.

7- Sacan, M.T.; Özkul, M.; Erdem, S. S. Physico-chemical properties of PCDD/Fs and phthalate esters. *SAR QSAR Environ. Res.* **2005**, 16, 443-459.

8- Ghosh, U.; Kane Driscoll, S.; Burgess, R. M.; Jonker, M. T. O.; Reible, D.; Gobas, F.; Choi, Y.; Apitz, S. E.; Maruya, K. A.; Gala, W. R.; Mortimer, M.; Beegan, C. Passive sampling methods for contaminated sediments: Practical guidance for selection, calibration, and implementation. *Integr. Environ. Assess. Manage*. **2014**, 10, 210−223.

10.3 Data associated with figures in the report.

Data for Figure 5.2

Compound	sediment conc (ug/g)	stdev	Porewater conc (ug/l)	stdev
Naphthalene	1.82	0.21	17.59	1.24
Acenaphthylene	2.17	0.18	8.45	0.77
Acenaphthene	3.71	0.30	101.17	1.33
Fluorene	2.67	0.29	27.55	0.10
Phenanthrene	19.17	0.16	52.53	0.80
Anthracene	7.04	0.13	16.02	0.09
Fluoranthene	16.00	0.93	7.49	0.25
Pyrene	16.72	0.45	7.87	0.01
Benz(a)anthracene	7.72	0.51	0.60	0.06
Chrysene	7.80	0.11	0.51	0.05
Benzo(b)fluoranthene	4.90	0.03	0.06	0.00
Benzo(k)fluoranthene	5.36	1.19	0.07	0.00
Benzo(a)pyrene	14.19	0.84	0.17	0.01
Indeno(1,2,3,-cd)pyrene	13.43	0.02	0.09	0.01
Dibenz(a,h)anthracene	2.50	0.28	0.01	0.00
Benzo(g,h,i)perylene	5.81	0.39	0.03	0.01

PE fractional uptake of PAHs into PE (C/Ceq) at different exposure times (Experimental data)

Compound	C/Ceq static					C/Ceq low frequency					C/Ceq high frequency					C/Ceq Mix				
	0	7 d	14 d	28 d	56 d	0	7 d	14 d	28 d	56 d	0	7 d	14 d	28 d	56 d	0	7 d	14 d	28 d	56 d
3) Naphthalene	0	1.14	1.71	0.93	1.13	0	0.68	0.90	0.62	0.54	0	0.49	1.25	0.76	1.15	0.00	1.84	2.74	1.07	1.00
4) Acenaphthylene	0	0.13	0.14	0.24	0.31	0	0.35	0.63	0.65	0.93	0	0.63	0.63	0.64	1.07	0.00	0.56	0.72	0.90	1.00
5) Acenaphthene	0	0.84	1.11	0.72	0.64	0	0.43	0.59	0.33	0.43	0	0.48	0.84	0.70	0.52	0.00	1.08	1.20	0.90	1.00
6) Fluorene	0	0.71	0.84	0.59	0.55	0	0.44	0.62	0.39	0.42	0	0.55	0.81	0.66	0.53	0.00	0.94	1.01	0.78	0.45
Phenanthrene	0	0.65	0.68	0.72	0.61	0	0.52	0.78	0.61	0.57	0	0.77	0.86	0.89	0.73	0.00	0.97	1.01	0.95	0.19
9) Anthracene	0	0.68		0.70	0.69	0	0.61		0.65	0.80	0	0.95	0.96	0.90	0.96	0.00	1.10	1.13	1.09	0.76
Flouranthene	0	0.41	0.51	0.62	0.71	0	0.71	0.76	0.75	0.94	0	0.83	0.86	0.89	1.00	0.00	0.88	0.95	1.11	1.07
Pyrene	0	0.33	0.42	0.53	0.62	0	0.64	0.68	0.68	0.91	0	0.74	0.77	0.80	0.93	0.00	0.77	0.84	1.00	1.00
Benz(a)anthracene	0	0.18	0.23	0.35	0.39	0	0.64	0.69	0.74	0.89	0	0.73	0.74	0.84	1.08	0.00	0.66	0.79	0.93	1.02
15) Chrysene	0	0.17	0.24	0.35	0.38	0	0.55	0.55	0.70	0.83	0	0.73	0.71	0.77	1.02	0.00	0.53	0.77	1.01	0.94
17) Benzo(b)fluoranthene	0	0.08	0.11	0.14	0.27	0	0.50	0.59	0.61	0.90	0	0.72	0.62	0.65	0.93	0.00	0.74	0.80	1.01	0.99
18) Benzo(k)fluoranthene	0	0.08	0.09	0.11	0.19	0	0.51	0.48	0.48	0.69	0	0.77	0.55	0.50	0.76	0.00	0.65	0.54	0.94	1.06
Benzo(a)pyrene	0	0.06	0.10	0.12	0.23	0	0.38	0.57	0.51	0.75	0	0.57	0.59	0.52	0.84	0.00	0.77	0.80	1.00	1.00
Indeno(1,2,3,-cd)pyrene	0	0.02	0.04	0.08	0.12	0	0.24	0.35	0.70	0.91	0	0.38	0.46	0.62	0.95	0.00	0.18	0.46	0.87	0.83
22) Dibenz(a,h)anthracene																				
23) Benzo(g,h,i)perylene	0	0.02	0.04	0.06	0.10	0	0.22	0.33	0.47	0.52	0	0.60	0.28	0.38	0.56	0.00	0.29	0.34	0.52	0.47

stdev for static data						stdev for low frequency					stdev for high frequency				
	0	7 d	14 d	28 d	56 d	0	7 d	14 d	28 d	56 d	0	7 d	14 d	28 d	56 d
	0	0.01	0.42	0	0.59	0	0.14	0.30		0.26	0	0.08		0	0.00
	0	0.03	0.18	0	0.08	0	0.22	0.05		0.03	0	0.02		0	0.03
	0	0.01	0.10	0	0.39	0	0.19	0.09		0.02	0	0.02		0	0.00
	0	0.01	0.47	0	0.33	0	0.20	0.05		0.02	0	0.02		0	0.03
	0	0.03	0.04	0	0.36	0	0.25	0.01		0.02	0	0.02		0	0.07
	0	0.03	0.00	0	0.28	0	0.28	0.00		0.00	0	0.00		0	0.08
	0	0.02	0.04	0	0.10	0	0.02	0.01		0.00	0	0.02		0	0.06
	0	0.02	0.04	0	0.08	0	0.03	0.01		0.00	0	0.02		0	0.07
	0	0.01	0.03	0	0.01	0	0.03	0.01		0.12	0	0.04		0	0.08
	0	0.01	0.03	0	0.01	0	0.03	0.14		0.06	0	0.04		0	0.06
	0	0.00	0.01	0	0.00	0	0.08	0.03		0.05	0	0.09		0	0.07
	0	0.00	0.01	0	0.01	0	0.09	0.02		0.09	0	0.11		0	0.05
	0	0.00	0.00	0	0.00	0	0.07	0.04		0.01	0	0.09		0	0.05
	0	0.00	0.00	0	0.00	0	0.06	0.03		0.06	0	0.19		0	0.01
	0	0.00	0.00	0	0.00	0	0.08	0.08		0.03	0	0.06		0	0.01

Data for Fig 5.4 and S5.4

Data for Fig 6.1

PCDD/Fs	Log Kow	PCBs	Log Kow
2,3,7,8-TCDF	6.41	PCB 128	6.74
1,2,3,7,8-PeCDF	6.74	PCB 132	6.58
2,3,4,7,8-PeCDF	6.8	PCB 146	6.89
2,3,7,8-TCDD	7.05	PCB 153	6.92
1,2,3,7,8-PeCDD	7.06	PCB 163	6.99
2,3,4,6,7,8-HxCDF	7.43	PCB 158	7.02
1,2,3,7,8,9-HxCDF 7	7.44	PCB 185	7.11
1,2,3,4,7,8-HxCDF	7.46	PCB 178	7.14
1,2,3,6,7,8-HxCDF	7.56	PCB 187	7.17
1,2,3,4,6,7,8-HpCDF	7.81	PCB 183	7.2
1,2,3,4,7,8,9-HpCDF	7.92	PCB 201	7.62
1,2,3,4,7,8-HxCDD	7.93	PCB 208	7.71
1,2,3,6,7,8-HxCDD	7.93	PCB 194	7.8

Data for Fig 6.2

PCB homolog	Conc (ng/g)	STDEV
Mono	0.00	0
Di	0.00	0.00
Tri	3.97	0.34
Tetra	8.63	0.33
Penta	7.84	1.14
Hexa	26.84	1.55
Hepta	26.07	0.37
Octa	13.85	0.14
Nona	0.60	0.01
Deca	0.52	0.06

Data for Fig 6.3; 6.4; S 6.1; S 6.2. S 6.3

PC congener	Conc in PE in Static system (ng/g)					STDEV				
	0	7 d	14 d	28 d	56 d	0	7 d	14 d	28 d	56 d
(31)	0.00	19.01	18.51	26.05	25.69	0.00	2.30	2.36	5.56	1.00
(70+76)	0.00	12.06	11.77	16.08	17.74	0.00	1.89	1.50	2.43	3.08
(99)	0.00	3.49	3.71	8.09	7.05	0.00	0.30	0.63	1.74	1.48
(146)	0.00	15.31	17.28	22.02	26.49	0.00	0.00	0.58	0.15	0.98
(153)	0.00	31.85	35.96	45.84	53.95	0.00	0.00	1.72	0.49	3.25
(132)	0.00	7.65	9.03	11.34	13.65	0.00	0.00	0.60	0.18	0.78
(163+138)	0.00	38.71	44.73	56.74	66.41	0.00	0.00	2.72	0.57	3.75
(158)	0.00	3.37	3.91	5.07	5.93	0.00	0.00	0.19	0.08	0.39
(178+129)	0.00	5.16	8.64	11.04	12.66	0.00	0.00	0.47	0.39	0.88
(187+182)	0.00	25.75	27.05	33.16	36.57	0.00	0.00	1.59	1.13	2.62
(183)	0.00	8.26	10.56	11.28	19.06	0.00	0.00	0.73	0.51	1.25
(128)	0.00	2.56	2.92	3.81	4.66	0.00	0.00	0.14	0.04	0.31
(185)	0.00	3.90	4.03	4.73	5.07	0.00	0.00	0.21	0.21	0.35
(201)	0.00	25.50	23.24	41.20	43.85	0.00	0.00	1.86	1.43	2.61
(203+196)	0.00	26.82	26.07	45.54	48.56	0.00	0.00	1.98	1.79	2.90
(208+195)	0.00	5.68	6.91	8.11	8.83	0.00	0.00	0.48	0.31	0.55
(194)	0.00	12.18	18.11	20.96	21.60	0.00	0.00	0.89	1.00	0.97

PC congener	Conc in PE in 2 min pause vibration system (ng/g)					STDEV				
	0	7 d	14 d	28 d	56 d	0	7 d	14 d	28 d	56 d
(31)	0.00	45.00	48.00	51.36	54.65	0.00	1.53	2.21	6.73	8.67
(70+76)	0.00	25.43	27.87	38.54	42.12	0.00	0.68	4.18	2.55	8.59
(99)	0.00	16.06	16.90	22.09	30.33	0.00	3.12	0.92	2.95	4.68
(146)	0.00	43.17	45.98	61.47	54.94	0.00	1.37	1.45	23.77	7.39
(153)	0.00	132.31	139.68	208.62	194.92	0.00	1.57	20.47	84.58	29.63
(132)	0.00	28.05	28.75	36.57	42.53	0.00	6.43	2.26	2.66	4.38
(163+138)	0.00	165.35	170.18	204.10	244.19	0.00	17.18	13.47	3.37	33.70
(158)	0.00	18.70	19.10	22.15	30.31	0.00	1.91	1.06	2.26	4.94
(178+129)	0.00	25.74	28.18	48.76	46.60	0.00	0.16	4.28	19.92	6.22
(187+182)	0.00	76.30	81.75	109.91	126.97	0.00	5.17	11.67	15.28	13.87
(183)	0.00	32.87	35.33	63.03	67.67	0.00	1.74	6.40	15.91	11.35
(128)	0.00	11.30	12.13	14.21	16.30	0.00	1.41	0.53	1.76	2.30
(185)	0.00	7.21	7.50	11.77	13.41	0.00	0.13	0.85	1.82	1.72
(201)	0.00	51.62	70.10	115.30	147.35	0.00	5.21	8.66	17.03	16.72
(203+196)	0.00	58.58	77.19	129.46	168.37	0.00	5.40	9.16	21.97	24.28
(208+195)	0.00	11.02	14.63	26.03	33.33	0.00	0.96	1.70	5.35	4.41
(194)	0.00	23.25	30.03	54.31	71.63	0.00	1.13	2.69	9.16	12.54

PC congener	Conc in PE in 5 d pause vibration system (ng/g)					STDEV				
	0	7 d	14 d	28 d	56 d	0	7 d	14 d	28 d	56 d
(31)	0.00	32.50	35.53	41.98	37.73	0.00	2.42	0.88	0.93	4.02
(70+76)	0.00	23.67	23.40	27.70	25.53	0.00	1.26	0.17	0.71	2.27
(99)	0.00	7.46	7.61	10.14	11.83	0.00	0.78	0.03	1.21	1.04
(146)	0.00	21.56	24.08	32.76	42.29	0.00	0.88	0.05	0.69	1.99
(153)	0.00	45.87	52.79	73.19	89.44	0.00	2.58	0.75	1.13	6.66
(132)	0.00	10.36	12.65	16.05	20.83	0.00	0.51	0.50	1.28	1.25
(163+138)	0.00	56.49	64.16	90.50	108.32	0.00	3.63	1.91	1.56	8.00
(158)	0.00	4.94	5.20	7.61	9.77	0.00	0.45	0.03	0.13	0.57
(178+129)	0.00	8.82	14.76	20.48	21.30	0.00	1.46	1.49	2.04	1.14
(187+182)	0.00	45.26	47.04	60.39	65.86	0.00	2.70	0.61	2.01	5.14
(183)	0.00	8.64	18.87	24.94	37.09	0.00	0.92	0.17	0.16	2.14
(128)	0.00	3.99	4.90	8.48	9.60	0.00	0.92	0.90	2.04	0.36
(185)	0.00	7.00	7.50	9.14	10.34	0.00	0.00	0.00	0.10	0.00
(201)	0.00	45.47	45.97	73.76	82.07	0.00	1.80	0.07	0.18	4.48
(203+196)	0.00	46.34	49.58	82.82	91.72	0.00	0.42	0.06	0.07	5.58
(208+195)	0.00	14.60	13.84	25.43	15.19	0.00	0.00	1.40	0.00	0.00
(194)	0.00	13.85	21.70	34.06	41.34	0.00	0.00	0.07	0.60	2.21

PC congener	Conc in PE in well-mixed system (ng/g)						STDEV					
	0	2 d	7 d	14 d	28 d	56 d	0	2 d	7 d	14 d	28 d	56 d
(31)	0.00	50.28	50.70	59.80	60.20	58.39	0.00	12.36	2.67	1.75	8.36	10.97
(70+76)	0.00	36.14	35.80	38.49	56.73	34.88	0.00	7.54	1.52	0.59	10.10	6.01
(99)	0.00	16.86	16.12	18.68	23.91	20.53	0.00	4.26	2.98	0.48	2.79	4.51
(146)	0.00	38.90	55.03	57.67	54.02	63.44	0.00	8.00	0.96	1.98	7.52	5.82
(153)	0.00	110.86	181.26	203.62	190.92	216.10	0.00	26.86	3.98	5.59	25.90	25.75
(132)	0.00	26.20	32.74	31.09	38.42	43.46	0.00	6.22	1.62	1.22	0.77	4.67
(163+138)	0.00	142.79	216.44	224.85	260.00	252.94	0.00	32.60	5.68	5.65	16.16	29.60
(158)	0.00	13.26	24.92	25.32	25.30	29.35	0.00	3.48	1.06	1.56	3.84	3.79
(178+129)	0.00	19.67	34.64	43.14	46.98	54.75	0.00	4.68	2.51	1.28	7.07	10.58
(187+182)	0.00	65.23	98.22	140.61	155.39	151.87	0.00	14.47	1.23	4.09	11.52	28.71
(183)	0.00	29.90	46.06	67.60	80.39	81.67	0.00	7.11	0.51	1.07	2.97	13.81
(128)	0.00	10.08	15.93	14.78	18.30	16.19	0.00	2.32	0.31	0.67	3.80	1.03
(185)	0.00	7.68	8.65	12.44	13.62	13.06	0.00	1.94	0.40	0.19	0.67	3.43
(201)	0.00	44.00	53.80	92.78	147.56	143.77	0.00	2.33	1.57	2.61	18.07	31.99
(203+196)	0.00	52.12	58.18	103.69	162.00	165.21	0.00	13.69	1.87	2.41	51.24	35.62
(208+195)	0.00	9.89	11.50	19.77	31.00	32.99	0.00	2.58	0.69	0.48	5.57	6.23
(194)	0.00	22.05	26.23	38.42	65.11	69.79	0.00	5.79	0.49	0.90	8.35	15.22

Data for Fig 6.5

Fraction of PRC remained in PE		Static system				2 min Vibration system				5 d Vibration system				Mix system			
	Initial	7 d	14 d	28 d	56 d	7 d	14 d	28 d	56 d	7 d	14 d	28 d	56 d	7 d	14 d	28 d	56 d
3) PRC-PCB29	1.00	0.70	0.60	0.45	0.35	0.06	0.04	0.00	0.00	0.59	0.45	0.29	0.12	0.00	0.00	0.00	0.00
4) PRC-PCB69	1.00	0.75	0.67	0.54	0.46	0.08	0.05	0.00	0.00	0.62	0.41	0.32	0.10	0.00	0.00	0.00	0.00
7) PRC-PCB155	1.00	0.89	0.83	0.78	0.68	0.43	0.25	0.13	0.04	0.69	0.60	0.42	0.32	0.00	0.00	0.00	0.00
9) PRC-PCB192	1.00	0.93	0.90	0.88	0.82	0.68	0.54	0.37	0.21	0.92	0.78	0.74	0.66	0.24	0.24	0.12	0.04

Data for Fig 6.6 and 6.7

	Cfree using static data (pg/L)				Cfree using 2 min-pause vibration data				Cfree using 5 d-pause vibration data				Measured Cfree	
	7 d	stdev	28 d	stdev	7 d	stdev	28 d	stdev	7 d	stdev	28 d	stdev	56 d	stdev
31	244.76	20.34	190.38	55.22	209.09	3.79	197.25	18.47	254.34	8.04	210.20	0.90	216.64	40.70
70+76	70.75	14.69	41.93	4.73	30.31	1.42	37.64	2.49	74.04	3.74	43.83	1.99	33.72	13.54
99	13.41	5.46	14.24	3.26	11.34	2.65	12.59	1.68	14.84	1.68	9.65	1.55	10.77	2.36
82+151	75.54	20.30	48.50	1.30	43.75	3.66	55.20	1.38	66.17	2.53	41.74	4.14	46.48	8.94
118	15.32	5.83	7.78	1.04	N.D	N.D	7.30	2.61	15.69	0.84	7.95	0.41	6.25	2.48
128	4.67	1.71	2.97	0.18	3.68	0.99	3.62	0.77	3.31	1.13	2.90	1.01	3.28	0.21
132	22.33	7.11	14.81	0.53	13.22	4.81	13.89	2.29	14.92	0.30	9.98	1.55	12.82	1.46
153	65.55	31.02	33.98	4.59	25.62	0.35	26.10	0.20	35.76	0.78	22.55	3.22	26.86	3.20
158	5.26	2.33	3.11	0.51	N.D	N.D	2.84	0.50	3.14	0.23	1.88	0.32	2.78	0.36
163+138	71.37	30.47	41.83	5.42	33.64	4.32	33.76	2.63	43.87	1.46	28.03	3.96	32.30	3.78
177	18.23	9.18	8.90	1.65	6.14	0.51	6.72	0.35	10.57	0.37	5.76	1.19	5.40	0.93
180	74.42	48.57	27.98	8.03	10.94	0.98	13.00	1.40	35.53	1.02	18.52	3.55	9.69	2.23
183	17.20	8.35	8.16	1.91	3.41	0.55	4.55	0.32	10.46	0.20	5.53	1.08	3.65	0.80
185	5.57	2.61	2.58	0.63	0.88	0.13	1.13	0.09	4.24	0.10	1.92	0.27	0.90	0.25
182+187	36.29	20.68	15.88	3.68	8.64	0.76	8.62	0.18	21.98	0.02	10.88	1.37	9.19	1.74
194	7.89	5.71	3.83	1.59	0.86	0.08	1.26	0.28	3.96	0.49	2.27	0.74	0.79	0.17
201	19.63	13.07	9.97	3.45	2.45	0.60	3.85	0.64	10.40	0.86	5.91	1.83	2.67	0.59
203+196	19.20	13.90	10.51	3.75	2.67	0.58	3.44	0.27	10.13	1.66	6.27	1.97	2.83	0.61
208+195	4.48	2.87	1.93	0.67	0.73	0.19	1.02	0.34	3.27	0.21	1.56	0.00	0.59	0.11

Data for Fig S5.5

Fraction of PRC remained in PE		Static system				2 min Vibration system				5 d Vibration system				Mix system			
Compound	Initial	7 d	14 d	28 d	56 d	7 d	14 d	28 d	56 d	7 d	14 d	28 d	56 d	7 d	14 d	28 d	56 d
phenanthrene_d-10	1.00	0.19	0.16	0.00	0.00	0.00	0.00	0.00	0.00	0.00	0.00	0.00	0.00	0.00	0.00	0.00	0.00
Pyrene_d10	1.00	0.42	0.38	0.21	0.08	0.01	0.00	0.00	0.00	0.01	0.00	0.01	0.00	0.01	0.00	0.01	0.00

Data for Fig S5.7

Pause time	C/Ceq	Energy usage (mWh)
2min	0.98	5849
5min	0.98	2339
6hour	0.97	32
1 day	0.93	8
5 days	0.72	1
Static	0.48	0

Data for Fig. S6.5

C/Ceq (Experimental data)						
PCB compound		2 d	4 d	8 d	12 d	48 d
128	1	0.86	0.77	0.64	0.52	0.19
183	1	0.85	0.70	0.56	0.41	0.22
194	1	0.92	0.83	0.74	0.64	0.47
C/Ceq (Model data)						
PCB compound		2 d	4 d	8 d	12 d	48 d
128	1	0.88	0.78	0.63	0.52	0.20
183	1	0.84	0.71	0.53	0.41	0.18
194	1	0.91	0.84	0.73	0.65	0.47

	material	log Cs	log Cw	log Kd	log avg Kd
Fig. 7.4					
	PTFE	2.75	0.34	2.41	
	PTFE	3.20	0.89	2.32	
	PTFE	3.64	1.38	2.26	
	PTFE	3.76	1.96	1.80	
	PTFE	4.25	2.44	1.82	**2.19**
	PDMS	2.55	0.08	2.47	
	PDMS	3.01	0.69	2.32	
	PDMS	3.31	1.33	1.98	
	PDMS	3.70	1.90	1.80	
	PDMS	3.87	2.42	1.45	**2.14**
	POM38	2.69	0.34	2.35	
	POM38	3.03	0.91	2.12	
	POM38	3.48	1.40	2.08	
	POM38	3.73	1.96	1.77	
	POM38	3.76	2.46	1.29	**2.05**
	CA	2.97	0.11	2.86	
	CA	3.45	0.72	2.73	
	CA	3.77	1.30	2.47	
	CA	4.22	1.86	2.35	
	CA	4.40	2.41	1.99	**2.58**
	CN	3.09	0.04	3.05	
	CN	3.61	0.55	3.05	
	CN	4.09	1.06	3.03	
	CN	4.58	1.60	2.98	
	CN	4.63	2.37	2.26	**2.95**
	PES	2.87	-0.26	3.13	
	PES	2.86	0.88	1.99	
	PES	3.48	1.31	2.17	
	PES	4.32	1.45	2.87	
	PES	4.62	2.21	2.42	**2.72**
	Parafilm	2.21	0.41	1.80	
	Parafilm	3.06	0.83	2.22	
	Parafilm	3.43	1.35	2.08	
	Parafilm	3.81	1.92	1.90	
	Parafilm	4.50	2.33	2.17	**2.06**
	PVDF+AC	4.05	0.47	3.59	
	PVDF+AC	4.66	1.10	3.56	
	PVDF+AC	5.04	1.54	3.50	
	PVDF+AC	5.57	2.29	3.28	
	PVDF+AC	6.01	3.05	2.96	**3.43**
	ag+AC	3.91	0.98	2.94	
	ag+AC	4.18	1.51	2.67	
	ag+AC	4.63	2.04	2.59	
	ag+AC	5.02	2.68	2.34	
	ag+AC	5.17	3.38	1.78	**2.60**

Fig. 7.5					
	material	log Cs	log Cw	log Kd	log avg Kd
	PAC	5.14	#NUM!	#DIV/0!	
	PAC	5.64	0.14	5.497795251	
	PAC	6.11	0.57	5.543732198	
	PAC	6.69	1.11	5.57996598	
	PAC	7.17	1.96	5.206737092	**5.48**
	ag	3.02	#NUM!	#DIV/0!	
	ag	3.37	0.47	2.896577369	
	ag	4.03	1.37	2.658172396	
	ag	4.13	1.80	2.324221724	
	ag	4.40	2.37	2.021792924	**2.59**
	ag+PAC	3.95	#NUM!	#DIV/0!	
	ag+PAC	4.37	0.85	3.516700727	
	ag+PAC	4.85	1.35	3.508901728	
	ag+PAC	5.45	1.99	3.457803605	
	ag+PAC	5.93	2.67	3.267268584	**3.45**
	PVDF DI	2.95	#NUM!	#DIV/0!	
	PVDF DI	3.19	0.64	2.548915092	
	PVDF DI	3.70	1.18	2.516823822	
	PVDF DI	3.79	1.89	1.90674801	
	PVDF DI	4.58	2.46	2.122157866	**2.35**
	PVDF+GAC	3.82	#NUM!	#DIV/0!	
	PVDF+GAC	4.55	1.28	3.272048906	
	PVDF+GAC	4.81	1.56	3.247481195	
	PVDF+GAC	5.16	1.54	3.610583669	
	PVDF+GAC	5.49	2.15	3.343249605	**3.39**
	PVDF+PAC DI	3.94	#NUM!	#DIV/0!	
	PVDF+PAC DI	4.53	1.18	3.343787251	
	PVDF+PAC DI	4.92	1.80	3.117051272	
	PVDF+PAC DI	5.55	2.24	3.30875689	
	PVDF+PAC DI	6.04	2.88	3.152196072	**3.24**
	PVDF+PAC meOH	3.73	#NUM!	#DIV/0!	
	PVDF+PAC meOH	4.49	0.91	3.58099527	
	PVDF+PAC meOH	5.03	1.54	3.483708501	
	PVDF+PAC meOH	5.62	1.84	3.783443739	
	PVDF+PAC meOH	5.87	2.53	3.346898687	**3.58**
	CA+MA	4.17	#NUM!	#DIV/0!	
	CA+MA	4.24	1.86	2.378467198	
	CA+MA	4.50	2.23	2.270623596	
	CA+MA	5.12	2.80	2.315642576	
	CA+MA	5.72	3.28	2.442739087	**2.36**
	PU+Cys	#NUM!	1.93	#NUM!	
	PU+Cys	3.75	1.92	1.834592946	
	PU+Cys	4.24	2.42	1.824019589	
	PU+Cys	5.04	2.78	2.264592329	
	PU+Cys	4.55	3.46	1.090452481	**1.92**
	PET+Cys	#NUM!	1.51	#NUM!	
	PET+Cys	3.09	1.98	1.106768435	
	PET+Cys	#NUM!	2.48	#NUM!	
	PET+Cys	#NUM!	3.02	#NUM!	
	PET+Cys	#NUM!	3.52	#NUM!	**1.11**

Fig. 7.6	material	log Cs	log Cw	log Kd	log avg Kd
	alg+Cys ag	4.94	0.89	4.05	
	alg+Cys ag	5.13	1.69	3.44	
	alg+Cys ag	5.66	2.32	3.35	
	alg+Cys ag	5.89	2.84	3.05	
	alg+Cys ag	6.58	3.31	3.27	
	alg+Cys ag	6.58	3.31	3.28	
	alg+Cys ag	6.58	3.31	3.28	**3.59**
	chit+MAA ag	4.50	1.30	3.20	
	chit+MAA ag	5.09	1.80	3.29	
	chit+MAA ag	5.66	2.30	3.36	
	chit+MAA ag	5.95	2.86	3.09	
	chit+MAA ag	6.35	3.35	3.00	**3.21**
	xylo+Cys ag	4.65	1.07	3.58	
	xylo+Cys ag	5.19	1.67	3.52	
	xylo+Cys ag	5.85	2.18	3.66	
	xylo+Cys ag	5.96	2.85	3.11	
	xylo+Cys ag	6.36	3.35	3.01	**3.45**
	ag+Cys	4.34	1.37	2.97	
	ag+Cys	4.75	1.91	2.84	
	ag+Cys	5.32	2.40	2.93	
	ag+Cys	5.68	2.91	2.77	
	ag+Cys	6.46	3.36	3.10	**2.94**
	ag+SAMMS	5.12	0.00	5.12	
	ag+SAMMS	5.50	0.67	4.83	
	ag+SAMMS	6.02	1.17	4.85	
	ag+SAMMS	6.48	1.66	4.82	
	ag+SAMMS	7.12	1.92	5.20	
	ag+SAMMS	7.12	1.86	5.26	
	ag+SAMMS	7.12	1.89	5.23	**5.01**
	PVDF+Cys	4.91	-0.85	5.76	
	PVDF+Cys	5.97	1.44	4.54	
	PVDF+Cys	5.83	1.42	4.41	
	PVDF+Cys	6.52	2.23	4.30	
	PVDF+Cys	6.98	2.88	4.10	**4.36**
	PVDF+SAMMS	4.96	0.62	4.34	
	PVDF+SAMMS	5.51	1.57	3.94	
	PVDF+SAMMS	5.96	1.76	4.20	
	PVDF+SAMMS	6.45	2.43	4.02	
	PVDF+SAMMS	6.88	3.04	3.84	**4.11**

	material	log Cs	log Cw	log Kd	log avg Kd
	DE	3.07	-0.34	3.42	
	DE	3.48	0.56	2.92	
	DE	3.71	1.26	2.45	
	DE	4.38	1.68	2.70	
	DE	4.79	2.25	2.54	
	DE	4.78	2.26	2.52	
	DE	4.79	2.25	2.53	**2.96**
	DE-MPTMS	5.15	-0.39	5.54	
	DE-MPTMS	5.48	0.08	5.40	
	DE-MPTMS	6.10	0.54	5.56	
	DE-MPTMS	6.50	0.76	5.75	
	DE-MPTMS	7.00	1.16	5.84	**5.65**
	ag+DE-MPTMS	4.49	0.46	4.03	
	ag+DE-MPTMS	5.14	1.19	3.95	
	ag+DE-MPTMS	5.36	1.56	3.80	
	ag+DE-MPTMS	6.15	2.43	3.72	
	ag+DE-MPTMS	6.34	2.98	3.36	
	ag+DE-MPTMS	6.33	2.99	3.33	
	ag+DE-MPTMS	6.33	2.99	3.35	**3.82**
	PET+Cys2	4.88	1.12	3.76	
	PET+Cys2	5.38	1.22	4.15	
	PET+Cys2	5.71	2.17	3.54	
	PET+Cys2	6.12	2.81	3.31	
	PET+Cys2	6.48	3.36	3.12	**3.73**
	PEGag	2.66	-0.42	3.07	
	PEGag	3.54	-0.53	4.06	
	PEGag	3.54	1.09	2.45	
	PEGag	4.12	1.60	2.52	
	PEGag	4.40	2.26	2.14	**2.68**
	PEGag+GAC	4.96	1.05	3.91	
	PEGag+GAC	5.15	1.60	3.55	
	PEGag+GAC	5.64	2.21	3.43	
	PEGag+GAC	6.02	2.80	3.23	
	PEGag+GAC	6.49	3.20	3.29	**3.55**
	PEGag+SAMMS	4.79	0.84	3.95	
	PEGag+SAMMS	5.51	1.51	4.00	
	PEGag+SAMMS	5.84	1.94	3.90	
	PEGag+SAMMS	6.49	2.61	3.88	
	PEGag+SAMMS	6.92	3.03	3.89	
	PEGag+SAMMS	6.92	3.03	3.89	
	PEGag+SAMMS	6.92	3.03	3.89	**3.93**

Fig. 7.8

Fig. 7.9

material	log Cs	log Cw	log Kd	log avg Kd
PET	3.9	0.1	3.77	
PET	4.4	0.7	3.77	
PET	4.8	1.3	3.59	
PET	5.2	1.8	3.40	
PET	5.6	2.3	3.32	3.61
SAMMS	5.6	0.3	5.30	
SAMMS	6.3	1.0	5.34	
SAMMS	6.8	1.3	5.45	
SAMMS	7.0	1.3	5.68	
SAMMS	7.3	1.6	5.66	5.52

Fig. 7.10					
	material	log Cs	log Cw	log Kd	log avg Kd
	ag+DE-MPTMS	3.2	-0.2	3.36	
	ag+DE-MPTMS	3.9	0.9	3.03	
	ag+DE-MPTMS	4.4	1.4	3.05	
	ag+DE-MPTMS	4.6	1.6	3.01	
	ag+DE-MPTMS	4.9	1.9	2.95	3.11
	ag+GAC	2.8	-0.1	2.90	
	ag+GAC	3.8	0.9	2.90	
	ag+GAC	4.2	1.4	2.76	
	ag+GAC	4.3	1.6	2.69	
	ag+GAC	4.8	1.9	2.84	2.83
	ag+SAMMS	3.2	-0.2	3.38	
	ag+SAMMS	4.3	0.7	3.64	
	ag+SAMMS	4.5	1.3	3.18	
	ag+SAMMS	4.6	1.6	3.04	
	ag+SAMMS	4.9	1.9	2.98	3.31
	PEGag+GAC	3.0	-0.1	3.14	
	PEGag+GAC	4.1	0.8	3.31	
	PEGag+GAC	4.1	1.4	2.69	
	PEGag+GAC	4.3	1.6	2.70	
	PEGag+GAC	4.8	1.9	2.91	3.02
	PEGag+SAMMS	2.7	-0.1	2.77	
	PEGag+SAMMS	3.9	0.9	2.97	
	PEGag+SAMMS	4.4	1.4	2.98	
	PEGag+SAMMS	4.7	1.6	3.11	
	PEGag+SAMMS	4.9	1.9	3.00	2.98
	PVDF+GAC	3.3	-0.3	3.62	
	PVDF+GAC	4.1	0.9	3.19	
	PVDF+GAC	4.4	1.4	3.03	
	PVDF+GAC	4.5	1.6	2.83	
	PVDF+GAC	4.7	1.9	2.78	3.21
	PVDF+SAMMS	2.7	-0.1	2.75	
	PVDF+SAMMS	4.0	0.9	3.14	
	PVDF+SAMMS	4.3	1.4	2.97	
	PVDF+SAMMS	4.7	1.6	3.09	
	PVDF+SAMMS	4.9	1.9	2.96	3.00
	PET+Cys	3.5	-0.3	3.77	
	PET+Cys	4.0	0.9	3.17	
	PET+Cys	4.3	1.4	2.96	
	PET+Cys	4.5	1.6	2.88	
	PET+Cys	4.7	1.9	2.78	3.29